SECRET
SECURITY INFORMATION
RESTRICTED DATA
This document contains Restricted Data as defined in the Atomic Energy Act of 1946. Its transmittal or the disclosure of its contents in any manner to an unauthorized person is prohibited.

CENTRAL RESEARCH LIBRARY
DOCUMENT COLLECTION

ORNL-1366
Progress
5

MARTIN MARIETTA ENERGY SYSTEMS LIBRARIES
3 4456 0360601 5

DECLASSIFIED
Classification Cancelled
By Authority of AEC 9-21-70
By: A. Goldberg 3/10/71

METALLURGY DIVISION

QUARTERLY PROGRESS REPORT

FOR PERIOD ENDING JULY 31, 1952

AEC RESEARCH AND DEVELOPMENT REPORT

OAK RIDGE NATIONAL LABORATORY
CENTRAL RESEARCH LIBRARY
CIRCULATION SECTION
4500N ROOM 175
LIBRARY LOAN COPY
DO NOT TRANSFER TO ANOTHER PERSON
If you wish someone else to see this report, send in name with report and the library will arrange a loan.
UCN-7969 (3 9-77)

OAK RIDGE NATIONAL LABORATORY
U.S. ATOMIC ENERGY COMMISSION

OAK RIDGE NATIONAL LABORATORY
OPERATED BY
CARBIDE AND CARBON CHEMICALS COMPANY
A DIVISION OF UNION CARBIDE AND CARBON CORPORATION
UCC
POST OFFICE BOX P
OAK RIDGE, TENNESSEE

SECRET
SECURITY INFORMATION

[redacted]

ORNL-1366

This document consists of 70 pages.
Copy 5 of 140 copies. Series A.

Contract No. W-7405-eng-26

METALLURGY DIVISION

QUARTERLY PROGRESS REPORT

for Period Ending July 31, 1952

J. H. Frye, Jr., Director

EDITED BY

W. H. Bridges

DATE ISSUED

NOV 25 1952

OAK RIDGE NATIONAL LABORATORY
operated by
CARBIDE AND CARBON CHEMICALS COMPANY
A Division of Union Carbide and Carbon Corporation
Post Office Box P
Oak Ridge, Tennessee

[redacted]

[redacted]

MARTIN MARIETTA ENERGY SYSTEMS LIBRARIES

3 4456 0360601 5

[redacted]

ORNL-1366
Progress

INTERNAL DISTRIBUTION

1. G. T. Felbeck (C&CCC)
2. Biology Library
3. Health Physics Library
4. Metallurgy Library
5-6. Training School Library
7. Reactor Experimental Engineering Library
8-13. Central Files
14. C. E. Center
15. C. E. Larson
16. W. B. Humes (K-25)
17. L. B. Emlet (Y-12)
18. A. M. Weinberg
19. E. H. Taylor
20. E. J. Murphy
21. E. D. Shipley
22. J. H. Frye, Jr.
23. F. C. VonderLage
24. R. C. Briant
25. J. A. Swartout
26. S. C. Lind
27. F. L. Steahly
28. A. H. Snell
29. A. Hollaender
30. M. T. Kelley
31. K. Z. Morgan
32. J. S. Felton
33. A. S. Householder
34. C. S. Harrill
35. C. E. Winters
36. D. S. Billington
37. D. W. Cardwell
38. E. M. King
39. A. J. Miller
40. D. D. Cowen
41. P. M. Reyling
42. W. H. Bridges
43. A. G. H. Andersen
44. L. K. Jetter
45. E. J. Boyle
46. W. D. Manly
47. C. D. Susano
48. W. W. Parkinson
49. R. J. Gray
50. B. S. Borie
51. D. C. Vreeland
52. E. E. Stansbury
53. G. P. Smith
54. J. E. Cunningham
55. R. S. Crouse
56. R. E. Adams
57. J. H. Erwin
58. J. O. Betterton, Jr.
59. L. D. Dyer
60. G. M. Adamson
61. E. S. Bomar
62. F. H. Eckert
63. T. W. Fulton
64. W. J. Fretague
65. R. B. Oliver
66. J. T. Howe
67. T. H. Blewitt
68. W. E. Taylor
69. J. H. Crawford, Jr.
70. J. C. Wilson
71. H. W. Savage
72. E. E. Hoffman
73. W. J. Leonard
74. J. A. Milko
75. J. M. Warde
76. E. C. Cruetz (consultant)
77. E. P. Wigner (consultant)
78. W. W. Grigorieff (consultant)

[redacted]

[redacted]

[redacted]

EXTERNAL DISTRIBUTION

79-86. Argonne National Laboratory
87-94. Atomic Energy Commission, Washington
95. Battelle Memorial Institute
96-99. Brookhaven National Laboratory
100-103. Carbide and Carbon Chemicals Company (Y-12)
104-105. Knolls Atomic Power Laboratory
106-107. General Electric Company, Richland
108-110. General Electric Company (ANPP)
111. Hanford Operations Office
112. Idaho Operations Office (Phillips Petroleum Co.)
113-116. Los Alamos
117. Massachusetts Institute of Technology (Kaufmann)
118-119. New York Operations Office
120. Patent Branch, Washington
121. Savannah River Operations Office, Wilmington
122-136. Technical Information Service, Oak Ridge
137-140. University of California Radiation Laboratory

[redacted]

[redacted]

Reports previously issued in this series are as follows:

ORNL-28	Period Ending March 1, 1948
ORNL-69	Period Ending May 31, 1948
ORNL-407	Period Ending July 31, 1949
ORNL-511	Period Ending October 31, 1949
ORNL-583	Period Ending January 31, 1950
ORNL-754	Period Ending April 30, 1950
ORNL-827	Period Ending July 31,,1950
ORNL-910	Period Ending October 31, 1950
ORNL-987	Period Ending January 31, 1951
ORNL-1033	Period Ending April 30, 1951
ORNL-1108	Period Ending July 31, 1951
ORNL-1161	Period Ending October 31, 1951
ORNL-1267	Period Ending January 31, 1952
ORNL-1302	Period Ending April 30, 1952

[redacted]

[redacted]

[redacted]

TABLE OF CONTENTS

	Page
SUMMARY	1
PHYSICAL METALLURGY OF REACTOR MATERIALS	2
Thorium Alloy Development	2
Mechanical Properties of Thorium	5
Fabrication of Thorium	5
Recrystallization of Thorium	5
Radiation Damage of Thorium	10
Electrical Resistivity and Melting Point of Thorium	10
Physical Properties of Pure Metals	10
REACTOR COMPONENT FABRICATION	11
Fuel and Control Element Fabrication	11
Zirconium Cladding of Uranium	12
Edge Welding of Zirconium-Clad Uranium Plate	13
Zirconium Cladding of Thorium	14
Aluminum Cladding of Thorium	14
Service Work	17
HOMOGENEOUS REACTOR PROGRAM	17
Welding and Fabrication Specifications	17
Titanium Fabrication	17
Titanium Riveting of Pump Impeller	18
Properties of Titanium	18
CERAMICS RESEARCH AND DEVELOPMENT	18
Ceramic Coatings for Metals	18
Radiation Damage Studies	19
Cermet Investigation	19
Hafnia Research	19
Hafnium Carbide Investigation	19
Compatibility Study of Ceramic Oxides	20
Thoria Investigation	20
Fluoride Fuel Examinations	20

[redacted]

[redacted]

FUNDAMENTAL PHYSICO-METALLURGICAL RESEARCH 21
Fundamental Principles of Alloying 21

ANP METALLURGY 29
Static Corrosion 29
Dynamic Corrosion 33
Physical Metallurgy of Liquid Metal Corrosion 40
Physical Chemistry 49
Mechanical Testing 51
Fabrication 54
Brazing and Welding 54

[redacted]

[redacted]

METALLURGY DIVISION QUARTERLY PROGRESS REPORT

SUMMARY

The mechanical properties of alloys of thorium with carbon, chromium, vanadium, and chromium and carbon continue under investigation. Tensile and impact tests on a series of specimens of virgin and remelted thorium are being run to determine the nature and extent of differences. The first phase of recrystallization experiments on cold-worked thorium has been completed with the general result that increased cold work decreased the temperature necessary for complete recrystallization. Studies of the electrical resistivity and melting point and of the radiation damage of thorium are under way.

The initial loading of MTR-type fuel units for the CP-5 reactor was fabricated according to specifications and forwarded to ANL.

The fuel concentration in the MTR fuel element has been increased 20% to offset the apparent 6% loss in Δk being experienced in operation of the reactor. Five complete loadings have been delivered to the site. Work on the sixth and seventh loading is 90 and 50% complete, respectively.

The cladding of uranium and thorium with zirconium is being attempted with modified picture-frame techniques prior to rolling. Some degree of success has been attained, with savings.

Continued support has been given to the Homogeneous Reactor Project. Considerable effort has been directed toward accumulating information on materials less subject to corrosion than austenitic stainless steels. The fabrication and properties of titanium are being investigated.

Work has continued on the application of ceramic coatings to metals for possible application in a radiator. A coating was successfully applied for the purpose of preventing adherence between zirconium-thorium compacts and the mild steel used in cladding experiments. The development of a fluoride-resistant coating was also under investigation. A program of study of ceramic-metal combinations (cermets) and an investigation of radiation effects on ceramic materials have been started. A study of the properties of hafnium oxide continues and an investigation has begun on the fabrication, synthesis, and properties of hafnium carbide. Compatibility studies of selected oxide ceramics in contact with various refractories, metals, and halides at elevated temperatures are under way. A preliminary investigation of thoria for subsequent solubility tests was commenced. Petrographic examinations have been made of several hundred fluoride fuel mixtures and a number of differential thermal analyses have been made for selected fluoride compositions; these data are being collected for the ANP fluoride fuel investigation program. Beryllium oxide moderator blocks have been fabricated for ANP at the U. S. Bureau of Mines Experiment Station at Norris.

Additions of various substances to fluorides in static corrosion tests have been made to determine the fitness of these agents as corrosion inhibitors. The corrosion of Inconel at 816°C by sodium hydroxide does not seem greatly increased by the presence of residual stresses, and the corrosion of A nickel was not at all increased.

The dynamic corrosion testing of various materials in zirconium-containing fluoride coolants has continued. In general, the zirconium-containing fluorides are less corrosive than previous fluoride mixtures, but they have the disadvantage of higher vapor pressure. Stress-rupture tests on Inconel and type 316 stainless steel in the presence of fluoride mixtures agree reasonably with expected values, but tube-burst tests give much lower than expected values.

A number of tests intended to give a better understanding of fluoride corrosion have been completed. The indications are that the subsurface voids encountered during fluoride corrosion are caused by the outward diffusion of chromium atoms, which leaves the metal enriched

with vacant lattice sites that "precipitate" to form voids. This has been repeatedly duplicated when chromium is removed from the metal lattice by either high-temperature oxidation or high-temperature vacuum treatment. Conversely, corrosion tests made with fluoride containing small amounts of chromium powder have shown that void formation can be suppressed.

The mixture of sodium with lead has possibilities as a heat transfer medium. Corrosion tests have indicated that the corrosiveness (including mass transfer) of lead is diminished with the addition of increasing amounts of sodium.

The evaluation of high-temperature brazing alloys for the joining of reactor components continues. The corrosion and oxidation resistance and tensile strength of joints made with the alloys have been tested. The behavior of basic welding variables in the cone-arc welding process is being studied to gain a better understanding of the possibilities of the process for the fabrication of tube-to-header joints in heat exchangers.

A tentative phase diagram has been determined for the zirconium-silver system. Preliminary experiments are under way in the zirconium-indium system.

PHYSICAL METALLURGY OF REACTOR MATERIALS

E. J. Boyle

THORIUM ALLOY DEVELOPMENT

J. A. Milko

Thorium-Carbon Alloys. Mechanical properties for a series of thorium-carbon alloys ranging in carbon content from 0.02 to 0.22% were given in the last quarterly report.[1] This series of alloys was studied further to obtain some indication of a suspected tendency toward precipitation hardening in the lower temperature range, that is, attempt to determine the time required for such hardening, and to make a metallographic determination of the solubility of the carbon at the higher temperatures.

Six thorium-carbon alloys were heated in a purified argon atmosphere for a definite interval of time and quenched. The test specimens selected for this investigation were removed from the grip ends of the sheet tensile bars. The sheet tensile bars were annealed for ½ hr at 650°C after a cold reduction of about 85%. Hardness measurements were made on these annealed specimens after the aging treatments listed in Table 1.

The data of Table 1 indicate that the heat treatment of 1 hr at 400°C does not increase the hardness of the 0.02, 0.05, 0.07, and 0.13% carbon alloys over that obtained in the annealed state, which suggests very little precipitation hardening. On the other hand, the 0.19 and 0.22% carbon alloys tend to develop a higher hardness after 1 hr at 400°C than in the annealed state, which indicates precipitation hardening. A microscopic examination will be made later in an attempt to correlate this increase in hardness with the suspected precipitation effects.

Further examination of the data of Table 1 indicates that the lowest hardness values are obtained on the alloys after heat treatment for 1 hr at 600 to 800°C followed by quenching. It is entirely possible that these temperatures are required for full recovery and recrystallization. (The treatment at 650°C for ½ hr may not have annealed the original sheet tensile specimens fully.) Heat treatment at increasing temperatures from 1000 to 1500°C increases the hardness of each carbon alloy and suggests solid solution hardening.

The tentative conclusions will be evaluated further by a microscopic study of the alloys. Furthermore, the hardness data suggest that

[1] J. A. Milko, *Metallurgy Division Quarterly Progress Report for Period Ending April 30, 1952*, ORNL-1302, p. 5.

TABLE 1

EFFECT OF QUENCHING TEMPERATURE ON THE HARDNESS OF PURE THORIUM*

Alloys quenched from: 400, 600, 800, 1000°C held 1 hr prior to quenching
1100, 1200, 1300°C held ½ hr prior to quenching
1400 and 1500°C held ¼ hr prior to quenching

ALLOY NUMBER	CHEMICAL COMPOSITION (%)			136° DPH HARDNESS (10-kg load, 16-mm objective)									
				Annealed at 650°C for ½ hr	After Quenching from Indicated Temperature								
	C	W	Cu		400°C	600°C	800°C	1000°C	1100°C	1200°C	1300°C	1400°C	1500°C
F-65	0.02	0.001**	0.003**	54	51	53	44	50	50	62	74	85	101
F-66	0.05	0.001	0.003	72	72	73	59	64	66	71	84		105
F-67	0.07	0.001	0.003	93	90	72	75	83	85	92	109	119	120
F-69	0.13	0.001	0.004	113	112	93	93	99	102	103	118	128	132
F-71	0.19	0.001	0.03	130	138	113	114	118	120	132	143	148	156
F-83	0.22	0.001	0.02	144	158	127	126	131	135	152	154	175	170

*Crystal bar iodide thorium.

**Probably introduced during arc melting.

additional thorium-carbon alloys should be prepared and that the precipitation effects should be studied as a function of time at the low temperatures, 200, 300, and 400°C. This study may correlate and tend to explain the creep behavior observed in Ames thorium at 300°C at several stress levels.

Thorium-Chromium Alloys. The thorium-chromium alloys are of immediate interest because of indications that they develop relatively high strength and probably a certain degree of corrosion resistance. (A tensile strength of about 50,000 psi was obtained on three alloys, as reported in the earlier progress reports. It was also observed that when the thorium-chromium alloys were left exposed to a moist laboratory atmosphere, the 2% chromium and higher alloys did not show the whitish deposit of attack that the low chromium alloys and thorium showed.) This combination of properties may become desirable for certain future applications.

Six thorium-chromium alloys were prepared by arc melting and subsequently cold rolled into a sheet with about 85% reduction in area. After a quench from 1350°C sections were removed for microscopic and hardness evaluations to obtain some information about a possible high-temperature phase and to determine the tendency toward hardening. The data obtained from this investigation are presented in Table 2.

The quench from 1350°C seems to produce an increase in hardness for the 2, 3, and 4% chromium alloys over that obtained on the annealed samples. The change in hardness will be studied later by microscopic methods.

Thorium-Chromium-Carbon Alloys. The addition of carbon and chromium to thorium was considered because both tend to strengthen thorium and because chromium appears to impart a certain degree of corrosion resistance to thorium. Such alloys have been investigated for strength, structure, and high-temperature phases.

Six thorium-chromium-carbon alloys were prepared by arc melting. The intended carbon content was maintained at 0.1%, whereas the chromium content was increased from 0.25 to 4.0%. These alloys were quenched from 1350°C and hardness

values obtained. The increase of the hardness of the thorium-chromium-carbon alloys (Table 3) over that of the thorium-chromium alloys (Table 2) can probably be attributed to the carbon. A microscopic examination will be made later in an attempt to correlate the structure, hardness, and mechanical properties.

Thorium-Vanadium Alloys. Alloys of 0.25 to 8% vanadium prepared by induction melting with the use of Ames thorium were swaged into $^5/_8$-in.-dia rounds to obtain several $^3/_8$-in. tensile test bars. The mechanical properties of these alloys have not been determined. Alloys with chromium, molybdenum, and columbium in the same range were also prepared by the same method. These are in various stages of testing and machining.

Lattice Parameter Measurements of Thorium-Carbon Alloys. Measurements of the lattice parameters of the thorium-carbon alloys were attempted after quenching from 1600 to 400°C. These measurements have not been satisfactory in all cases because of the suspected large

TABLE 2

EFFECT OF AGING TEMPERATURE ON THE HARDNESS OF THORIUM-CHROMIUM ALLOYS

ALLOY NUMBER	INTENDED CHROMIUM CONTENT (%)	136° DPH HARDNESS (10-kg load, 16-mm objective)	
		After Quenching from 1350°C*	After an Anneal at 650°C for $^1/_2$ hr
1	0	69	54
2	0.25	78	
3	0.50	78	
4	1.00	95	93
5	2.00	111	73
6	3.00	112	71
7	4.00	123	91

*The specimens, $^1/_{16}$-in.-thick sheet, were held 15 min at 1350°C prior to quenching.

TABLE 3

EFFECT OF QUENCHING TEMPERATURE ON THE HARDNESS OF THORIUM-CHROMIUM-CARBON ALLOYS

ALLOY NUMBER	INTENDED CHEMICAL COMPOSITION (%)		136° DPH HARDNESS (10-kg load, 16-mm objective) AFTER QUENCHING FROM 1350°C
	Cr	C	
1	0.25	0.1	112
2	0.50	0.1	118
3	1.00	0.1	118
4	2.00	0.1	122
5	3.00	0.1	124
6	4.00	0.1	134

grain size present. Further attempts will be made to determine the solubility of carbon in thorium at various temperatures by x-ray methods.

MECHANICAL PROPERTIES OF THORIUM

W. J. Fretague

Tensile and impact tests have been completed on a series of specimens of Ames thorium to determine the properties of virgin and remelted thorium. The results of the tensile and impact tests and the chemical analysis of the billets used are presented in Table 4. In identifying the specimens according to the billet and extrusion from which they were machined the following system was used:

1. Virgin billets are identified by the prefix A.

2. Remelted billets are identified by the prefix MX.

3. The next to the last number (in the series of letters and numbers identifying a particular specimen) denotes the type of extrusion from which the specimen was machined. The identifying number for all $^5/_8$-in. extrusions is 2, and the number 3 was used to identify 1- by 2-in. extrusions that were cold rolled to $^5/_8$ by 2 inches.

4. The letter A following the specimen number indicates that the specimen was vacuum annealed at 750°C for 30 min and furnace cooled following the machining operations.

In general remelted Ames thorium specimens exhibited higher tensile and yield strengths than virgin material of similar carbon content. This seems to be caused by the increased amounts of nitrogen, aluminum, and beryllium present in the remelted thorium.

A marked increase in tensile and yield strength was obtained by cold rolling. This increase was apparent both in the remelted and the virgin thorium. Annealing of the cold rolled material seemed to destroy any preferred orientation developed by cold rolling. Specific information is being obtained on the textures developed by extruding; extruding and cold rolling; extruding and annealing; and extruding, cold rolling, and annealing. These data should be very helpful in interpreting the results obtained from the tensile tests.

The results of Charpy V-notch impact tests are presented in Table 4. For a given analysis of thorium the extruded and annealed material has the best impact properties. The extruded materials, the extruded, cold rolled, and annealed materials, and the extruded and cold rolled materials exhibit progressively poorer impact properties, in the order listed.

There seems to be very little correlation between specific values of impact strength for different analyses of thorium even though the materials were given identical thermal and mechanical treatments prior to testing.

FABRICATION OF THORIUM

W. J. Fretague

Two $^7/_8$-in.-dia extrusions of Ames thorium billet A344B were made. Extrusion A344B1 was produced at a rate of 588 ft/min and extrusion A344B2 was produced at a rate of 2.32 ft/min; both were quenched as they left the extrusion die. Samples prepared from these two extrusions will be used to study the effect of extrusion rate on the creep properties of thorium.

RECRYSTALLIZATION OF THORIUM

F. H. Eckert

Recrystallization experiments have been completed on Ames (A349B) and iodide thorium that were cold worked 20, 40, 60, and 80%. Procedures for this investigation were outlined in the preceding quarterly report.[2]

Figures 1 and 2 show the effect of cold work on the recrystallization of Ames and iodide thorium as traced by Vickers hardness measurements.

[2] F. H. Eckert, *op. cit.*, ORNL-1302, p. 16.

TABLE 4

MECHANICAL PROPERTIES OF AMES THORIUM

SPECIMEN NUMBER	ANALYSIS (ppm)													YIELD POINT (psi)			TENSILE STRENGTH (psi)	ULTIMATE STRENGTH (psi)	ELONGATION (% in 1.4-in. gage length)	REDUCTION IN AREA (%)	PROPORTIONAL LIMIT (psi)	MODULUS OF ELASTICITY ($\times 10^6$)	IMPACT ENERGY (ft-lb)	REMARKS
	Fe	Mn	N	C	Ca	Al	Be	Si	Mg	B	Cd	Zn	Total Impurities	0.2% Offset	Upper	Lower								
MX322A821	165	<4	245	640	<50	150	200	300	<10	0.65	<0.20	<20	1784.85	30,653	31,709	30,955	37,889	76,014	46.4	70.3	18,593	7.8	16.5	As extruded
22A														28,523	28,643	28,442	36,030	69,966	58.6	70.6	23,618	7.6	18.5	Extruded and annealed
23														31,364	32,323	31,667	38,889	72,555	52.5	68.0	18,687	8.3	16.5	As extruded
24A														28,397	28,654	28,520	36,485	72,635	46.8	69.6	21,069	8.4	18.25	Extruded and annealed
MX325A921	125	<4	375	780	<50	300	225	300	<10	1.00	<0.20	<20	2190.20	37,424	38,687	37,374	43,838	84,570	48.9	66.0	25,253	7.2	9.8	As extruded
22A														30,050	30,402	30,302	38,693	72,059	50.0	65.8	23,116	7.9	13.5	Extruded and annealed
23														38,079	39,482	38,110	44,715	78,571	48.2	64.4	24,390	7.8	9.6	As extruded
24A														29,440	29,915	29,598	38,953	69,364	48.6	63.4	19,556	10.4	12.25	Extruded and annealed
31														54,121			59,799	86,207	22.9	53.4	30,151	10.1	3.5	Extruded and cold rolled
32A														30,905	31,156	30,905	39,548	67,402	51.8	59.0	24,121	9.7	15.0	Extruded, cold rolled, and annealed
33														52,980			58,736	83,503	14.3	49.5	30,832	8.2	3.4	Extruded and cold rolled
34A														30,132	30,285	29,827	38,516	67,376	44.6	57.0	23,374	11.7	10.5	Extruded, cold rolled, and annealed
A328A21	180	<3	70	325	<50	60	120	300	<40	0.45	<0.20	<20	1168.65	20,203			28,810	47,830	54.3	76.6	11,179	6.9	40.0	As extruded
22A														19,596	19,828		28,131	41,667	51.8	74.6	14,394	8.2	39.0	Extruded and annealed
23														19,187			28,600	41,340	51.8	74.2	12,703	6.8	39.5	As extruded
24A														19,168	19,404	19,270	27,235	40,179	55.4	77.0	10,534	10.5	37.5	Extruded and annealed
31														40,101			42,680	47,800	17.9	63.0	22,222	8.9	9.25	Extruded and cold rolled
32A*																							26.0	
33														39,683			41,260	43,730	19.6	65.0	25,536	8.5	8.4	Extruded and cold rolled
34A*																							25.5	
A338B21	210	<4	130	665	<50	<60	100	300	<10	0.45	<0.20	<20	1549.65	24,059	24,585	24,448	32,600	66,540	58.9	72.3	17,087	7.2	30.0	As extruded
22A														23,788	23,869	23,566	31,313	60,241	57.1	74.9	17,677	8.8	29.0	Extruded and annealed
23														23,780	24,339	23,933	32,419	63,636	51.8	72.1	15,752	7.4	28.0	As extruded
24A														24,009	24,289	24,167	31,707	59,353	60.7	71.8	18,039	8.0	29.0	Extruded and annealed
31														41,463			43,700	59,000	23.2	63.8	29,472	8.7	7.6	Extruded and cold rolled
32A														25,384	25,384	23,434	31,061	64,935	47.9	68.9	19,697	12.1	28.75	Extruded, cold rolled, and annealed
33														40,347			42,900	62,840	23.2	62.6	22,472	8.2	8.0	Extruded and cold rolled
34A														25,762	25,762	23,628	31,098	65,517	67.9	70.5	21,596	10.2	28.5	Extruded, cold rolled, and annealed
A339B21**	195	<4	80	500	~50	150	180	300	<10	0.30	<0.20	<20	1489.50	18,232			27,620	40,650	42.9	75.2	10,101	8.1	38.75	As extruded
22A														17,495			25,606	35,242	60.7	77.1	13,384	7.1	34.25	Extruded and annealed
23														16,112	16,147		27,287	34,483	50.0	75.9	10,395	7.6	41.4	As extruded
24A														17,007	17,109		25,281	31,120	50.0	75.4	13,023	7.0	34.0	Extruded and annealed
31***																	40,125	49,363	19.6	67.2			10.75	Extruded and cold rolled
32A														18,384	18,384	17,677	26,111	50,752	52.5	73.1	13,131	8.1	34.5	Extruded, cold rolled, and annealed
33														36,538			38,981	36,827	17.9	65.4	21,830	7.9	12.5	Extruded and cold rolled
34A														18,702	18,755	17,957	26,064	63,927	66.1	76.7	11,702	9.4	25.25	Extruded, cold rolled, and annealed
A343B21	105	<2	95	835	<50	60	180	300	<10	0.20	<0.20	<20	1657.40	22,610	22,867	22,610	30,730	69,200	57.1	77.0	16,444	6.9	33.0	As extruded
22A														22,298	22,472	22,298	29,980	45,662	56.4	77.6	16,088	8.0	30.5	Extruded and annealed
23														22,217	22,829		30,500	53,500	51.8	75.2	14,811	7.0	32.75	As extruded
24														22,104	22,236	22,104	29,726	48,077	47.1	73.6	16,006	9.9	29.5	Extruded and annealed
31														42,576			44,798	48,649	18.6	62.6	28,283	8.1	8.6	Extruded and cold rolled
32A														24,136	24,136	22,815	30,132	60,837	64.3	73.3	20,071	8.9	25.5	Extruded, cold rolled, and annealed
33														41,113			43,922	60,694	19.3	64.7	24,515	7.8	8.75	Extruded and cold rolled
34A														24,075	24,075	22,236	29,472	60,201	60.7	69.6	18,801	10.0	22.5	Extruded, cold rolled, and annealed

*Specimens A328A32A and A328A34A were cracked and as a result no tensile data are available.

**Billet A339B should be rechecked for carbon content. ORNL analysis gives 0.050% and 0.030% C on two arc-melted samples submitted.

***For specimen A339B31, through an oversight, the strain gage was not attached to the specimen and as a result only tensile strength, ultimate strength, per cent elongation, and per cent reduction in area were recorded.

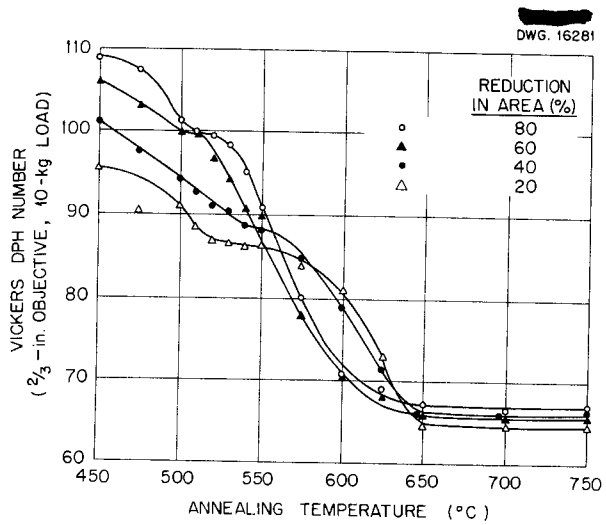

Fig. 1. Effect of Cold Work on the Recrystallization of Ames Thorium.

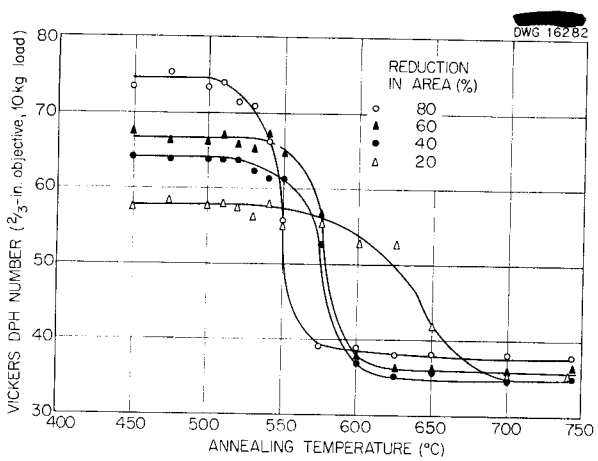

Fig. 2. Effect of Cold Work on the Recrystallization of Iodide Thorium.

Recrystallization is shown as a function of annealing temperature, with time constant at 1 hour. In general, increasing cold work decreased the temperature necessary for complete recrystallization. It has been shown in a previous report that increasing the cold work also reduced the time necessary for recrystallization to take place at any given temperature.

Table 5 shows the annealing temperature at which recrystallization starts and is completed for the various amounts of cold work. These temperatures were estimated from Figs. 1 and 2, and an attempt was made to check them by metallographic examination. However, the start of recrystallization was difficult to ascertain by metallographic means in the 20, 40, and 60% cold-worked samples, so an x-ray technique is being employed to verify the results in Table 5. By observing the line shapes of the powder diffraction pattern with a Norelco x-ray spectrometer, the strain present in the thorium samples may be measured to determine the annealing temperature at which recrystallization starts and is completed.

In all cases, the curves in Fig. 1 showed a rapid drop in hardness at the start of annealing, and microexamination revealed no evidence of recrystallization in this range. It is believed that "recovery" and/or precipitation is possibly responsible for this initial hardness drop. The higher level of impurities in the Ames metal is believed to be responsible for this action since the iodide thorium does not exhibit this "recovery" zone.

TABLE 5

EFFECT OF COLD WORK ON RECRYSTALLIZATION OF THORIUM

REDUCTION IN AREA (%)	ANNEALING TEMPERATURE AT START OF RECRYSTALLIZATION (°C)		ANNEALING TEMPERATURE AT COMPLETION OF RECRYSTALLIZATION (°C)	
	Ames Thorium	Iodide Thorium	Ames Thorium	Iodide Thorium
80	520	500	625	575
60	520	510 to 520	625	600
40	540 to 550	520	650	600
20	550 to 575	550 to 575	650	700

An investigation of the effect of carbon on the recrystallization of iodide thorium is now in progress.

RADIATION DAMAGE OF THORIUM

R. E. Adams

As part of the thorium research program, a study will be made of the physical and mechanical properties of thorium before and after irradiation and of the effects of postirradiation annealing. Duplicate test specimens will be preserved and tested while the irradiated specimens are being tested. For the nondestructive tests, the same specimens will be tested before and after irradiation.

Several thorium test specimens are scheduled to be irradiated in the LITR starting late in July. These will be exposed for six months at a neutron flux of about 0.5 to 1.0×10^{13} neutrons/cm^2 · sec. Specimens will be canned in aluminum, and it is estimated that the maximum temperature of the thorium will not exceed 400°F during irradiation.

The following test specimens will be irradiated for the purposes given:

1. three tensile specimens ($^3/_{16}$ in. in diameter, 1-in. gage length) for measurements of tensile strength, yield point, per cent reduction in area, and per cent elongation;

2. two cylindrical specimens ($^1/_4$ in. in diameter, 3 in. long) for study of possible changes in dimensional stability, density, dynamic elastic modulus, electric conductivity, and thermal conductivity;

3. four specimens (0.204 in. in diameter, $4^3/_4$ in. long), each of which can be broken in four places, for impact tests;

4. eight specimens ($^7/_{16}$ in. in diameter, $^1/_8$ in. thick) for study of changes in hardness, microstructure, and x-ray patterns; specimens clad with zirconium and aluminum will also be included to see whether changes in structure of the bond layer occur.

In addition, it is proposed to irradiate thorium specimens in the MTR to learn the effects of more intense exposure. At present these plans are contingent upon space that may be available for irradiation.

ELECTRICAL RESISTIVITY AND MELTING POINT OF THORIUM

R. E. Adams

An electric resistance furnace is being used to study the melting point and electric resistivity of thorium at high temperatures. The furnace, patterned after one used by Chiotti[3] at Ames Laboratory, contains a thorium rod $^1/_4$ in. in diameter held between two water-cooled copper electrodes $4^1/_2$ in. apart. The bar is heated by direct current in an atmosphere of purified argon. A small hole ($^1/_{32}$-in. in diameter and 0.15 in. deep) serves as a sight hole for temperature measurements. Temperatures are measured through a quartz window with a disappearing filament optical pyrometer.

Several experiments have indicated that the melting points of pure materials can be determined to within about 10°C by this method. Experiments with thorium, however, have thus far given anomalous results, and the melting point of Ames thorium bars has ranged between about 1710 and 1755°C.

Electric resistivity is found by measuring the current through the specimens and the voltage drop between two thorium wires attached $^1/_2$ in. apart at the center of the specimen. Experiments thus far indicate a sharp increase in resistivity of thorium specimens in the temperature range between 1375 and 1450°C. Work on this phase of the project is continuing.

PHYSICAL PROPERTIES OF PURE METALS

W. J. Fretague

Six melts of pure nickel were prepared by induction melting of electrolytic nickel in a

[3] P. Chiotti, *Thorium-Carbon System*, ISC-103, June 5, 1950.

zirconia crucible and casting in a graphite mold. The surface of the ingots was machined to a depth of $^1/_{16}$ in. to remove any carbon picked up from the graphite mold; and the machined ingots were swaged to $^3/_4$-in.-dia rod, vacuum-annealed at 750°C for $3^1/_2$ hr, and furnace-cooled.

Standard 0.505-in.-dia tensile specimens will be prepared and used to test experimentally the theory proposed by Taylor and Frye[4] on the application of absolute reaction-rate theory to plastic deformation.

[4] W. E. Taylor and J. H. Frye, *Application of Absolute Reaction Rate Theory to Plastic Deformation*, CF 50-10-79, Oct. 16, 1950.

REACTOR COMPONENT FABRICATION

J. E. Cunningham
R. B. Small
R. J. Beaver
J. F. Delaney
T. A. Olsen
C. C. Stone
J. H. Erwin
W. A. McNeish

FUEL AND CONTROL ELEMENT FABRICATION

MTR Fuel and Control Rod Elements. Fabrication work on the assembly of fuel and control rod elements for Arco continues at an increased and efficient pace; two units a day are now being produced.

During the quarter, the remainder of the third and all of the fourth and fifth reactor loadings were completed and shipped to Arco. A loading consists of 23 enriched fuel units and 4 cadmium control rods for the three by nine rectangular loading arrangement.

Work on the sixth loading is 90% complete. An order has been placed to procure the additional 61S aluminum alloy extrusions needed in the construction of the control rods. Delivery is expected by August 15.

It has been proposed to substitute a relatively inexpensive aluminum extrusion for the lower stainless steel section in cadmium shim safety control rods. Such a change would result in substantial saving in the cost of fabricating the control rod.

In an effort to offset the 6% loss in Δk being experienced in operation of the reactor, the fuel concentration in the uranium-aluminum alloy has either been increased 20% or the U^{235} content raised from 140 to 168 g per assembly. Other experimental work in progress in connection with this problem includes (1) tests to qualitatively determine the extent to which LiCl contained in the fuel unit by flux entrapment during brazing is influencing reactivity; (2) preparation of a mock aluminum assembly in which the aluminum side-plate thickness has been reduced 33% to improve the aluminum-to-water ratio; and (3) investigation of the possibility of further improving the aluminum-to-water ratio by lowering the thickness of the aluminum cladding on the active plates.

LITR Fuel and Control Rod Elements. Three replacement cadmium shim safety control rods and one enriched fuel unit were constructed for operation of the LITR.

Bulk Shielding Fuel Unit. The special enriched fuel unit needed to obtain more reliable data for calculating the heat release per fission of U^{235} was completed for the Bulk Shielding Facility.

CP-5 Fuel Units. The initial loading of 16 enriched uranium fuel units for the CP-5 reactor was fabricated according to specifications and shipped to ANL. The unit is similar to an MTR fuel assembly, except for thinner aluminum side plates and a wider water-gap spacing between plates, and there are only ten active plates.

ZIRCONIUM CLADDING OF URANIUM

The picture-frame technique of cladding does not lend itself readily to inexpensive, large-volume production of clad plate. Methods are being developed to roll large sheets of uranium clad on both sides with a thin layer of zirconium. The sheets will be sheared into strips of the desired size and sealed around the periphery by automatic welding. A saving would result from the decrease in the number of jacketed, exhausted, sealed, and rolled billets and from the method of jacketing itself.

The billet assembly is shown in Fig. 3. The uranium core for the present experimental work is an 0.8-in. slice cut from a 4-in. square cast ingot with a carborundum saw. The core is electropolished just prior to jacketing. The zirconium cover plates are 4-in. squares sheared from 0.09-in. sheet, which is obtained by rolling arc-melted sponge ingot in a steel jacket at 1400°F. The cover plates are rough ground to remove surface layers. The steel jacket is flame cut from $\frac{1}{2}$-in. steel plate in four pieces; two 6-in. square cover plates, one 6-in. square frame with a flame cut 4-in. square hole, and one 6-in. square

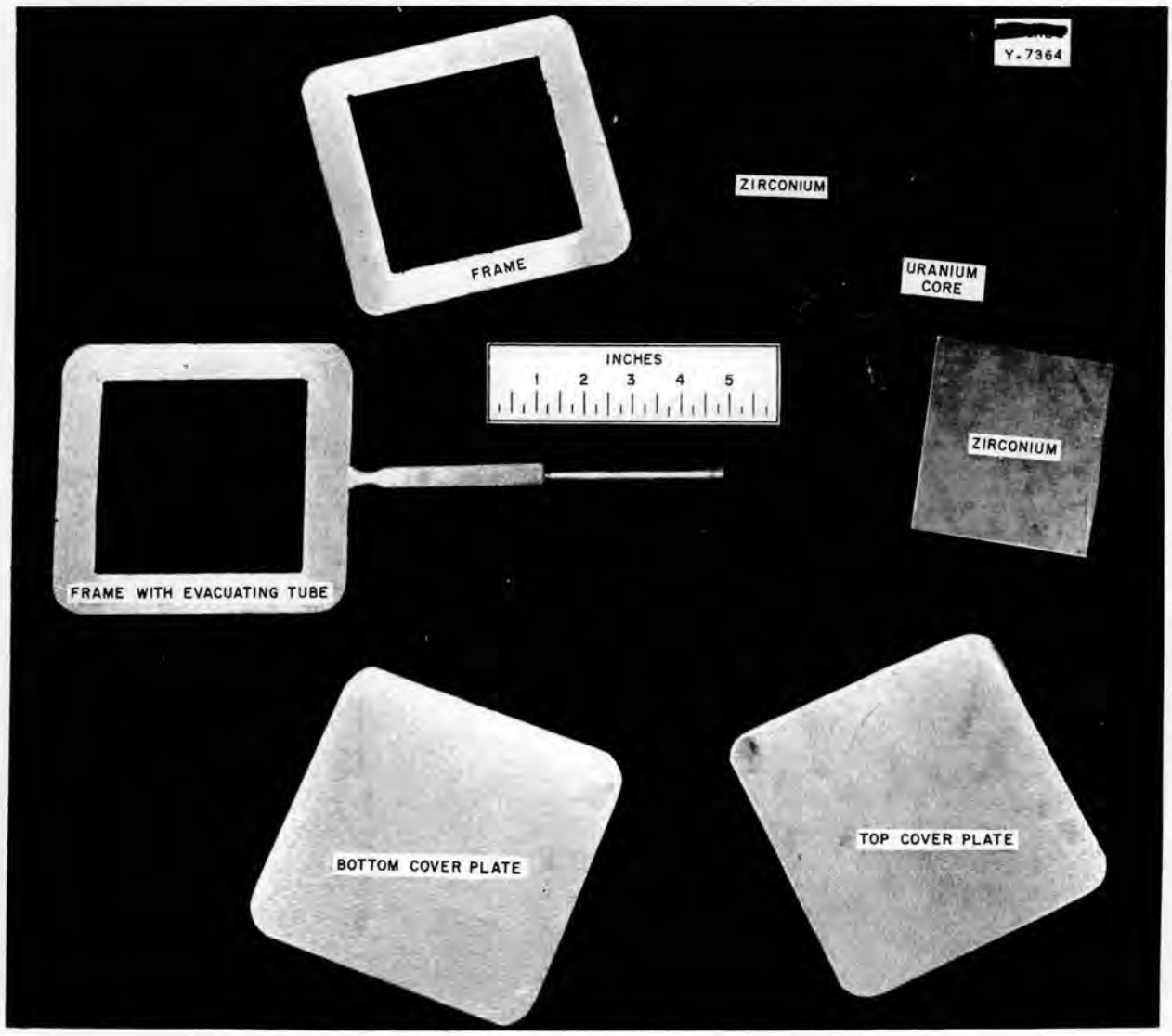

Fig. 3. Uranium Billet Assembly.

frame with a flame cut 4-in. square hole and an integral extension to be used as an exhaust tube. The extension is drilled for a $\frac{1}{4}$-in. hole and the end is internally threaded for attachment to a $\frac{1}{8}$-in. IPS nipple. All the steel jacket components are sandblasted before assembly.

The assembly is held together with C clamps, and the seams are welded with a gas-shielded torch without filler wire. A slight, positive pressure of grade XX helium is maintained within the billet to prevent oxidation of the components during welding. The welded assembly is leak checked with a Consolidated, Model 24, leak detector. The assembly is then attached to a $\frac{1}{8}$-in. nipple on a vacuum header maintained at 10^{-4} mm Hg or less. The billet is gradually heated to about 1200°F with a gas torch, the pressure is maintained at 10^{-4} mm or less, and the exhaust tube is forged shut.

The 2-in.-thick sealed billet is preheated at 1200°F for $1\frac{1}{2}$ hr and rolled to 0.130 in. by using 20% reduction per pass and reheating for 5 min between passes. The edges are sheared off and the steel is stripped from the faces to leave a clad plate about 4 in. wide and 48 in. long. The hot-rolled plate is about 0.080 in. thick and is flattened and surface finished by cold rolling to 0.065 in. in thickness.

The resultant bond shows a slight diffusion layer between the uranium core and the zirconium cladding. The core is 0.049 ± 0.004 in. thick; the cladding is 0.008 in. in average thickness and may be as thin as 0.005 in. and as thick as 0.010 inch. This high percentage of variation in cladding is believed to be caused by the method of obtaining the core, that is, slices from a cast ingot, and is expected to be reduced by using rolled or forged material for cores.

Initially, mild steel containing about 0.25% carbon was used for jacketing material. Occasional cracking during rolling, difficulty in obtaining leak-tight assemblies, and imperfect bonding led to the adoption of the 0.04% carbon titanium-killed steel that was used in the STR production with great improvement of all three difficulties.

EDGE WELDING OF ZIRCONIUM-CLAD URANIUM PLATE

The previous quarterly report outlined the method of sealing the sheared edge of zirconium-clad uranium plate. The method consists of pickling to remove the uranium core material to form a groove in which zirconium filler wire is placed. This joint is then fused with an automatic, gas-shielded welder and produces a clad edge. The defects that have been found are porosity, shrinkage cavities, crater cracks, weld metal dilution by the uranium core, and weld metal contamination by the atmosphere.

Porosity appears as small (<0.004 in.), round voids at the base metal–weld metal interface and is believed to be caused by the entrapment of either shielding gas or gas released by the clad plate during welding. By the use of heat inputs of 35 w-min/in. and slow welding speeds of 15 in./min, the porosity has been almost eliminated. In any case, the porosity is deep seated and should not affect the corrosion resistance of the joint.

Shrinkage cavities result from an insufficient heat input to completely fuse the zirconium filler wire but are eliminated in the course of reducing porosity.

Crater cracks at the end of a weld bead have been eliminated by gradually reducing the welding heat during the last $\frac{1}{8}$ in. of travel. Because of the accumulation of heat at the end of the weldment, it was possible to eliminate the crater cracks without adverse affect of the porosity.

Unfortunately, weld metal dilution by the low-melting uranium core material is increased by the method used to reduce porosity. The seriousness of this dilution is not yet known, however, since the weld metal appears unaffected by exposure in boiling water for 500 hours. The dilution is presumably reduced by the use of the lower melting zirconium–3% nickel alloy, but the resultant ductility is less and a greater tendency to surface cracking appears.

Atmospheric contamination has been greatly reduced by auxiliary shielding jets installed near

the arc. The weld metal and the heat-affected zone appear bright, and some cold rolling has been done with only a slight tendency toward surface cracking.

ZIRCONIUM CLADDING OF THORIUM

Brazing of Thorium to Zirconium Prior to Rolling. The zirconium-thorium system has a eutectic at approximately 1300°C consisting of 78% thorium and 22% zirconium. Alloys of this composition have been arc melted and rolled to 0.010-in. foil for use as a brazing alloy.

Initial efforts were confined to brazing under inert atmosphere conditions. The technique consisted of sealing the foil between the thorium and zirconium by heliarc welding around the billet circumference in a dry box. The assembled billet was protected by coating with a ceramic frit, NBS A-418, and furnace brazing at 1350°C. Although considerable alloying was accomplished, as shown in Fig. 4, porosity occurred in the brazed joint. The method was discontinued in favor of vacuum brazing.

Vacuum brazing was carried out in a pyrex bell jar by using an induction heater. A thorium billet 2 by 2 by 0.8 in., brazing foil 2 by 2 by 0.010 in., and zirconium cover plates 2 by 2 by 0.1 in. were assembled in air and placed within the glass bell jar that was evacuated to 5×10^{-5} mm Hg. Melting the alloy foil between the zirconium and thorium with the induction heater resulted in a thorium-alloy-zirconium brazed joint. When the brazed billet was sectioned, it appeared to be sound. Three billets were prepared in this manner and rolled to 0.065-in. plate at 1400°F. One plate was sectioned, and metallographic examination showed that no defects were present. The bonded interface after rolling is shown in Fig. 5. Shear tests of the as-rolled bond indicate strengths of approximately 28,000 psi.

Bond Improvement by Diffusion. Previous work has indicated that a diffusion treatment at 1800°F improves bonding between thorium and zirconium. An experiment was conducted in which zirconium cover plates 2 by 2 by 0.1 in. were welded to a thorium billet 2 by 2 by 0.8 in. under the helium atmosphere of a dry box. The assembled billet was coated with ceramics frit, NBS A-418, which protected the zirconium and thorium from eutectic formation with the steel sheath. After the billet was sheathed in steel, it was rolled at 1400°F to a 38% reduction, annealed at 1800°F for 30 min, and rolled again at 1400°F to 0.065-in. finished plate. Fairly good bonding between thorium and zirconium resulted. The metallographic appearance is shown in Fig. 6.

Roll-Cladding at 1500°F. Past experience has shown that roll-cladding zirconium to thorium by the use of conventional canning methods does not result in reliable bonding. Experiments have shown that when the billets are sheathed in steel, evacuated, heated to approximately 1000°F while under vacuum, sealed, and preheated at 1500°F for 1 hr, the core elements are visibly contaminated. The source of contamination is not yet known but is believed to be from gases released from the steel or thorium during the 1-hr preheat at 1500°F. A billet gradually heated under vacuum to 1500°F over a period of 3 hr was rolled without success. Pressure measurements made during the heating showed that little gas is released to the interior of the billet up to 1100°F but that a very large quantity appears between 1100 and 1500°F.

ALUMINUM CLADDING OF THORIUM

Thorium may be clad with aluminum by rolling evacuated sandwiches at 400°C with a 10:1 reduction. Above this temperature, an intermetallic layer is formed at the bond line; below this temperature, the degree of bonding is poor.

Samples of aluminum-clad thorium rolled at this optimum temperature were annealed for ½ hr at 350°C. An intermetallic layer had formed, and the bond strength was completely destroyed. Further annealing tests are to be made to determine the time-temperature characteristics of this intermetallic formation, which has been identified as principally $ThAl_3$.

As a result of the above tests, straight roll-cladding techniques do not appear to be promising.

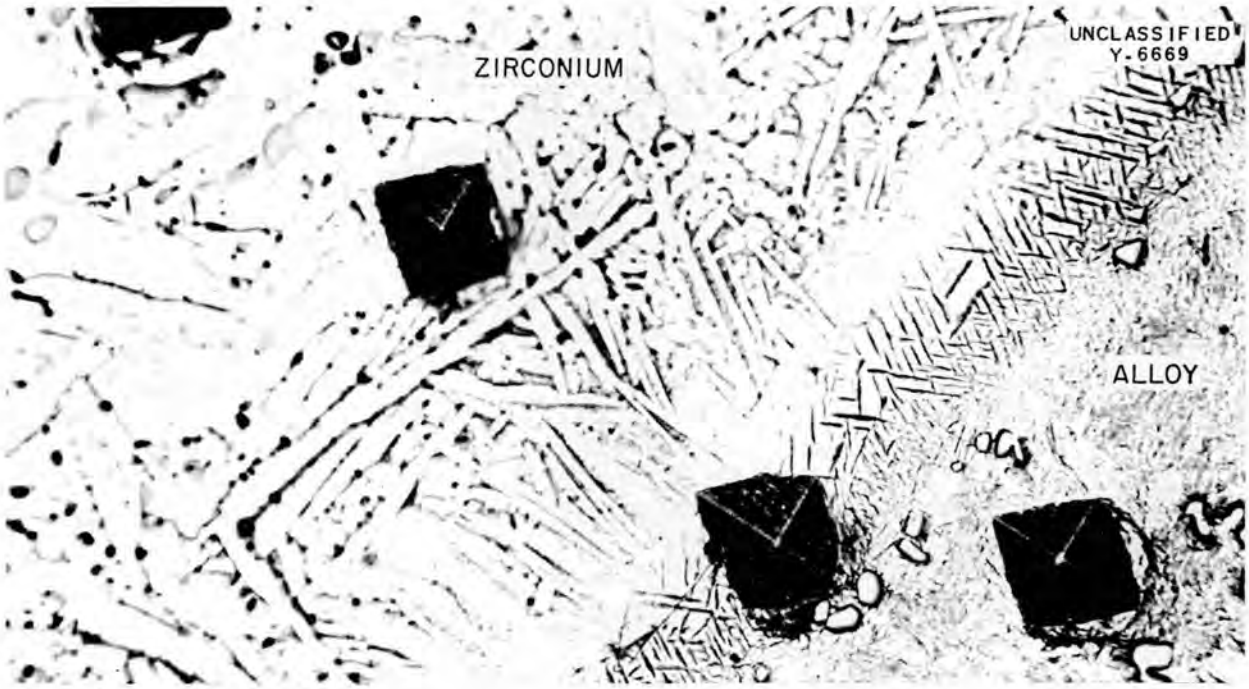

Fig. 4. As-Brazed Interfaces of Thorium Billet Brazed to Zirconium with 73% Thorium–22% Zirconium Alloy. Etched with perchloric and acetic acids. 500X

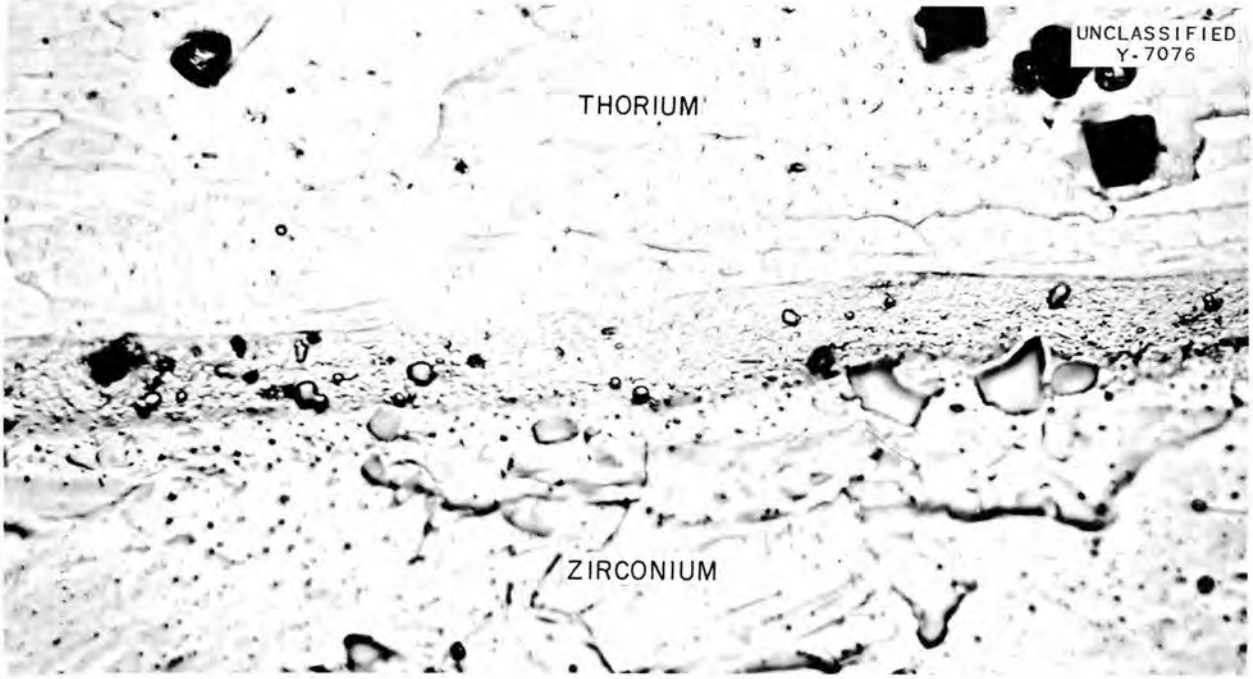

Fig. 5. Bonded Interface Between Thorium and Zirconium of Plate Produced from Brazed Billet. Etched with perchloric and acetic acids. 750X

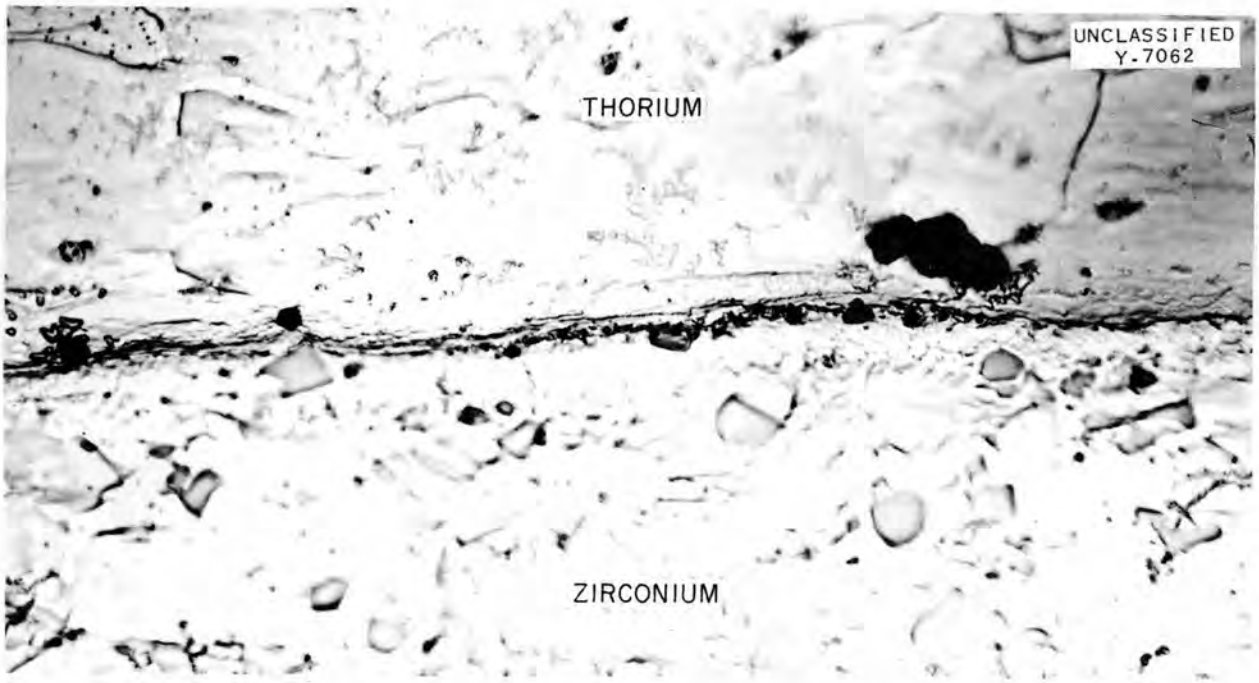

Fig. 6. Bonded Interface Between Thorium and Zirconium of Plate Subjected to Diffusion Treatment at 1800°F During Rolling Sequence. Etched with perchloric and acetic acids. 750X

A survey of possible diffusion barriers is being made.

SERVICE WORK

Casting and machining of 650 normal "J" slugs was completed. Shipment to Hanford will be made as soon as analyses are available.

Six special Chalk River fuel rods were assembled for the Westinghouse Atomic Power Division.

Preliminary work has been started for the rolling of highly enriched and depleted uranium foil.

Approximately 850 lb of $^1/_{16}$-in. uranium plate was cast and rolled for the California Research and Development Corporation.

HOMOGENEOUS REACTOR PROGRAM

E. C. Miller

The corrosion-erosion attack of austenitic stainless steels that has occurred under some conditions in dynamic corrosion loops has accelerated interest in alternate materials that may have better resistance to this type of attack. Considerable effort has been spent in accumulating available information that will permit a realistic evaluation of the engineering feasibility of such alternate materials. Titanium, which is of particular interest on the basis of corrosion-erosion behavior, is receiving much attention at this time. Unfortunately, it is relatively new as an engineering material, and the required data are frequently unavailable or uncertain. A very extensive titanium developmental program is being carried on under the sponsorship of a number of military agencies, and a considerable effort is being made here to keep pace with the current developments. In addition to titanium, similar, but less extensive, consideration is being given to modified, austenitic, chromium-nickel-iron alloys and to some of the rare metals.

WELDING AND FABRICATION SPECIFICATIONS

W. J. Leonard

Equipment used and planned for various engineering tests and the intermediate reactor design call for welding and fabrication of thick sections (up to 3 in.) of carbon steels (0.15 to 0.25% carbon) and of austenitic stainless steels, particularly type 347. Standard specifications will be used where available and acceptable, particularly in the welding of carbon steels. However, the welding of type 347 stainless steel and the welding of dissimilar metals, such as type 347 stainless steel to carbon steel, present a number of problems. Some experimental work will be done to apply available methods to present facilities and problems so that specifications and standard procedures can be established.

TITANIUM FABRICATION

A. R. Olsen P. Patriarca

The specific objective of the experimental work on the welding of titanium has been to approximate the configurations involved in making an impeller for a Westinghouse, Model 100A, pump. Tensile samples approximating the joint configurations were made with RC-70 base material and Ti-75A filler rod. Tensile tests of these welding assemblies gave maximum loads ranging from 3500 to 8300 pounds. Based on the encouraging results of these tests, it was decided to use both welding and riveting, rather than riveting alone, in assembling the actual pump impeller. Unfortunately, the available stock for machining the impeller has a carbon content higher than that generally considered suitable for welding; consequently, the additional precaution of riveting was considered advisable. The actual welding of the impeller is to be performed in the Y-12 welding shops.

The excellent corrosion-erosion resistance of titanium recommends its possible use as a valve trim; however, its tendency to gall indicated the desirability of surface hardening the material. Accordingly, a titanium poppet was hardened by a modification of the procedure that was developed by the Armour Research Foundation for surface-hardening titanium in a nitrogen atmosphere. The results are encouraging and further testing is planned.

TITANIUM RIVETING OF PUMP IMPELLER

E. S. Bomar

Because of the reputed brittleness of welds on titanium containing more than 0.25% carbon, and because of the limited knowledge of the behavior of such welds under dynamic conditions, reliance is being placed on rivets to fasten the two parts of the titanium impeller for the Westinghouse, Model 100A, pump.

In the initial tests, consideration was given to heating the rivets in a furnace, followed by upsetting in a hydraulic press. Considerable difficulty was encountered, however, in controlling the time factor and obtaining a consistently uniform upsetting. Because of this control difficulty, the procedure was modified to permit resistance heating in place by passing an electric current through the rivet and by using spot welding equipment. The results of this method of riveting give considerable promise of being satisfactory and the work is being continued.

PROPERTIES OF TITANIUM

W. J. Fretague A. R. Olsen

Modified, Izod, V-notch impact specimens of Titanium Metals Corporation, commercially pure titanium (Ti-75A) and of iodide titanium have been prepared and will be used to determine transition temperatures for commercial-purity and high-purity titanium and to study the effect of hydrogen on the impact properties and transition temperatures.

The specimens of the commercially pure titanium were prepared from annealed rod that was swaged to $\frac{1}{4}$ in. in diameter from 1-in. bar. Specimens of the high-purity titanium were prepared from annealed rods that were swaged to $\frac{1}{4}$-in. dia after arc-melting of iodide-titanium crystal bar.

The fiber textures developed in commercial titanium by swaging from 1-, $\frac{1}{2}$-, and $\frac{1}{4}$-in.-dia rods and by vacuum annealing for 1 hr at 500°C have been determined. Similar determinations were made on iodide titanium that was: arc melted and swaged; arc melted, swaged, and annealed (in the alpha range); and arc melted, swaged, and annealed (in the beta range).

CERAMICS RESEARCH AND DEVELOPMENT

J. M. Warde S. D. Fulkerson
C. E. Curtis J. R. Johnson
L. M. Doney A. J. Taylor
G. D. White

CERAMIC COATINGS FOR METALS

Radiator Coatings. Work continues on the application of ceramic coatings to metals for possible use in a radiator. Attempts were made to coat pyrometallurgical-grade nickel with National Bureau of Standards coating A-418. It was difficult to obtain satisfactory adherence because carbon in the metal formed CO_2 during the firing process. In an effort to overcome this problem, specimens of as-received nickel were annealed for 2 hr at 2000°F in an atmosphere of dry hydrogen. After this treatment, coating A-418 applied at 1700°F adhered well; however, when the specimens so coated were subjected to a 65-hr oxidation test at 1500°F, bubbles were formed under the surface of the coating. It is proposed to investigate the adherence of coating A-418 on

vacuum-melted electrolytic nickel and on nickel specimens annealed in an atmosphere of wet hydrogen.

Zirconium and Thorium Enameling. Samples of zirconium and thorium have been coated with NBS coating A-418 in connection with the thorium cladding investigation being carried out at the rolling mill.

Fluoride-Resistant Coatings. Work is proceeding on the development of a ceramic coating that could replace the present nickel metal coating in lining tanks that are used in the early separation states of the gaseous diffusion process. The coating is required to withstand fluoride attack and to be nonsusceptible to spalling. Trial compositions consisting of a phosphate glass applied to mild steel are being tested at K-25.

RADIATION DAMAGE STUDIES

A study of the effect of radiation upon various ceramic materials is in process. Test specimens of about 30 different ceramic materials are being prepared in the form of thin disks $^3/_4$ in. in diameter by 20 mils thick to be sent to Hanford for irradiation periods of three and six months. About 70% of the disks has been fabricated, and they are being given preliminary measurements by the Solid State Division.

Pyrex glass specimens that were exposed in the graphite reactor for periods of seven weeks and four months were examined. All the specimens were medium red-brown in color, similar to glasses exposed to x rays. The color disappeared on heating to 200 to 300°C. A transmission curve was made showing high absorption below 5000 Å. The color of the irradiated specimens was probably due to trapped electrons (face centers). No evidence of devitrification could be found.

CERMET INVESTIGATION

A study of ceramic metal combinations (cermets) has started; the initial phase of the investigation, comprising the design and assembly of equipment and the procurement of raw materials, is nearing completion. An investigation of the fabrication and properties of ZrC-Fe cermets has been started at the Ohio State University Engineering Experiment Station under the auspices of the ceramic laboratory. They have also undertaken the problem of joining cermets.

HAFNIA RESEARCH

Hafnia (HfO_2) received from the Chemistry Division contained the following principal impurities, according to spectroscopic analysis:

Zr	0.35%
Ti	1.00%
Fe	0.10%
Na	0.004%

It was demonstrated that this material can be changed from the monoclinic to the cubic crystal form by adding 8 mole % of CaO and firing for 1 hr at 1600°C in air. This behavior, not previously noted in the literature, is similar to that of zirconium oxide (ZrO_2), which is commercially stabilized in this manner for the purpose of increasing heat-shock resistance.

The thermal expansion behavior of hafnia from room temperature to 1300°C was determined; no inversions were found in this range.

Equimolecular mixtures of HfO_2 and SiO_2 were fired for 1 hr at 1500°C; x-ray examination indicates that hafnium silicate was synthesized by this procedure.

HAFNIUM CARBIDE INVESTIGATION

An investigation was started at the ceramic laboratory on the synthesis, fabrication, and properties of HfC. A survey of the meager available literature on the subject was made and as an initial experiment, a stochiometric mixture of HfO_2 and carbon (lampblack) was cold pressed and sintered to 2200°C by induction heating in a graphite container. At 1190°C, the burning of gases in the sight tube indicated that a reaction had apparently started. At 2200°C, volatilization of some unidentified material caused the sight tube to plug, and the test was stopped. X-ray

examination of the sinter indicated the possible presence of HfO_2 and HfN, but no recognizable pattern of HfC was observed. X-ray examination of the volatile material that had clogged the sight tube was made, but the patterns obtained were not similar to any data available. Further work is in progress.

Work on the syntheses of HfC, utilizing induction-welding equipment, has commenced at the U. S. Bureau of Mines Electrotechnical Laboratory at Norris.

COMPATIBILITY STUDY OF CERAMIC OXIDES

A study of the compatibility of selected refractory materials with various oxides, metals, carbides, and halides is in progress. Crucibles have been successfully cast of HfO_2, ThO_2, $ZrSiO_4$, and ZrO_2. It is proposed to fire the crucibles and investigate their behavior in contact with the various materials at elevated temperatures.

THORIA INVESTIGATION

A preliminary investigation of thoria for subsequent solubility tests was begun. Samples of thoria were prepared and fired to 700, 1200, and 1600 to 1630°C. The fired specimens were sent to the x-ray laboratory for determination of parameters and crystal size. Specimens have been sent to the Chemistry Division for a determination of the rate of solution.

FLUORIDE FUEL EXAMINATIONS

Petrographic Examinations. Over 300 petrographic examinations were made of fluoride mixtures during the past quarter. Several samples of fuels taken from capsules and loops were also examined. The optical properties of the following fluoride compounds have been determined; their values are not in the literature:

Li_3CrF_6
Biaxial negative
2V = about 40 deg
Alpha = 1.444
Gamma = 1.464

K_3CrF_6, cubic
n = 1.422

Na_3CrF_6, cubic
n = 1.411

KU_2F_9, orthorhombic
Biaxial negative
2V = 10 deg
Alpha = 1.544
Gamma = 1.588

UF_4, monoclinic
Biaxial negative
2V = 75 deg
Alpha = 1.500
Beta = 1.585
Gamma = 1.598
Anomalous interference colors
z = dark green
x = light green

The following systems and indices were determined by previous investigators:

Na_2BeF_4, orthorhombic
Y || C, low birefringence
Average indices = 1.303

$NaUF_5$, hexagonal
Uniaxial negative
O = 1.512

UF_3, hexagonal
Low birefringence
n = 1.73
Anamolous interference colors

BeF_2, crystallized
Anisotropic
Low birefringence
n = 1.328

All index of refraction determinations are probably accurate to about ±0.003.

In the examination of capsules containing fuel No. 21, it was found that the oxygen present will react with ZrF_4 to form well-crystallized ZrO_2.

Differential Thermal Analysis. Differential thermal analyses were made of six selected fuel mixtures. These data supplemented existing information on melting points and phases present in the fuels.

FUNDAMENTAL PHYSICO-METALLURGICAL RESEARCH

L. K. Jetter

FUNDAMENTAL PRINCIPLES OF ALLOYING

Silver-Zirconium System (J. O. Betterton, T. M. Kegley, Jr.). The silver-zirconium system is of interest in that it shows the effect of alloying silver, with a filled *d* band and one *s* electron in the free atom, with zirconium with a free atom containing two *d* electrons and two *s* electrons. The two elements are on the same row of the periodic table, and the atoms are of approximately the same size, the silver atom being only 7.7% smaller on the basis of the closest distances of approach in the element crystal structures. The system is of further interest because of a martensitic type of transformation of the beta phase that, upon cooling, results in hardness effects in silver-zirconium. These effects are similar to those encountered in many other zirconium and titanium systems involving a eutectoid on the solvent-rich end of the phase diagram. Vickers hardness values of alloys cast on the water-cooled copper plate are shown as a function of composition in Fig. 7. The hardness maximum occurs within the beta solid-solution region.

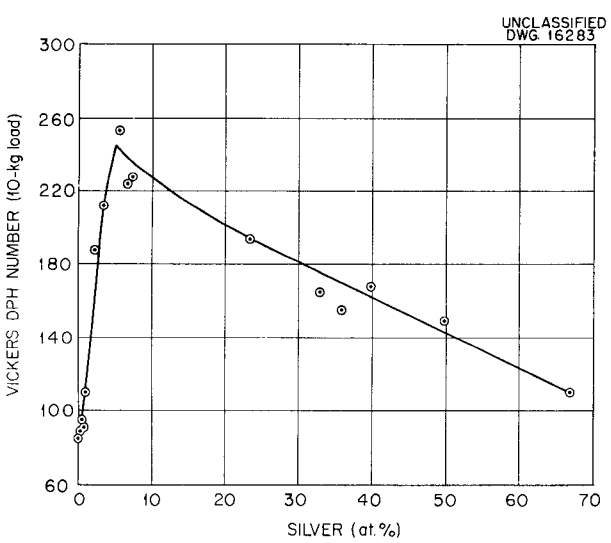

Fig. 7. Vickers Hardness of Silver-Zirconium Alloy After Arc-Casting.

The results of quenching experiments on small specimens of arc-melted, iodide zirconium alloys are shown in the tentative silver-zirconium phase diagram of Fig. 8. These alloys had been annealed for periods of time varying from 1 day at 1150°C to 29 days at 523°C. The alloys were carefully weighed, and the compositions shown are based on the changes in weight during the casting and annealing. The critical specimens will be analyzed chemically, although these results have not yet been obtained. Since pure zirconium specimens did not appreciably change in weight during similar casting and annealing, for the drawing of Fig. 8 it was felt justified to assume that the whole weight loss in the alloys was entirely silver.

The eutectoid decomposition temperature of the beta phase has been investigated by observing the temperature at which the transformation structure is replaced by a structure of isothermal alpha grains. On this basis, the eutectoid temperature has been shown in Fig. 8 as being somewhat less than 703°C. For example, after the alloy 2.1[1] was annealed for 22 days at 702.9°C, it contained transformed beta phase after quenching. On the other hand, after the alloy 5.4 was annealed for 29 days at 523°C, it still showed a transformed beta structure; it may be that the grain boundaries resulting from the transition $\alpha \leftrightarrows \beta$ are changed to isothermal alpha boundaries only very slowly at this temperature. In the first place, it is not thought probable that the eutectoid temperature could be so low as 523°C on the basis of the slope of the β/β + compound boundary. If grain boundaries of the transformed beta phase are so persistent at 523°C, there is question concerning the interpretation of the transformed structures observed in the 703°C anneal. A new method of heat treatment would seem to be advantageous.

Experiments are now being done in which alloys of 3 to 5 at. % silver are heat treated at 1000°C and then slowly cooled to avoid the formation of

[1] The alloy number is the atomic per cent of the solute.

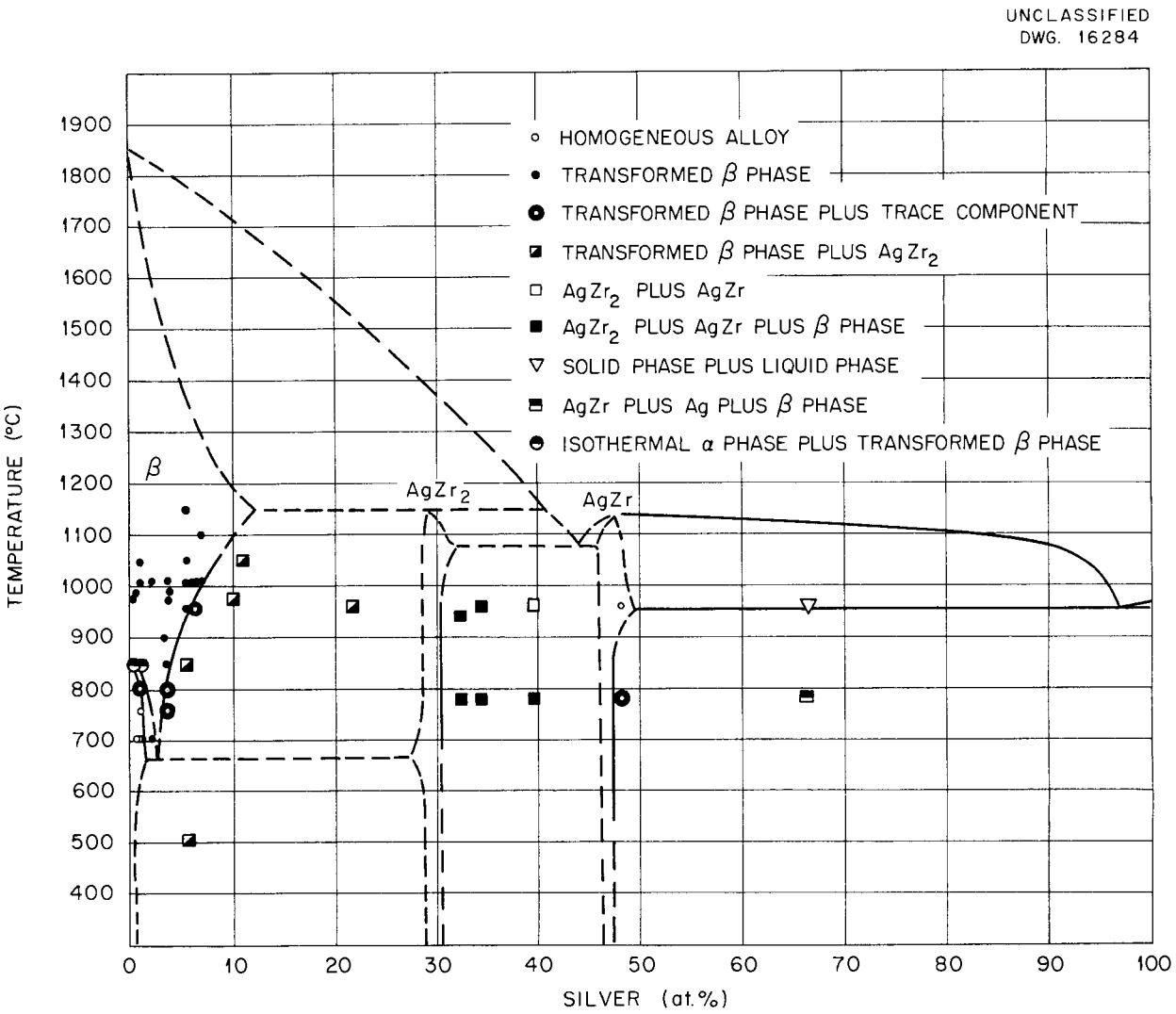

Fig. 8. Tentative Phase Diagram of the Silver-Zirconium System.

the transposed beta structure. It may be that equilibrium can then be more easily attained by annealing at 500 to 700°C the alloys that contain the eutectoid rather than the transposed beta phase. Some evidence in support of the sluggishness of the change of transformed beta grain boundaries to the isothermal alpha grain boundaries is the slowness found by McPherson and Hansen[2] in the change from transposed beta structure to isothermal alpha structure in pure zirconium annealed near the transition temperature. For example, an anneal of 24 hr at 852°C still contained some transformed beta structure, although this temperature is 10 to 11°C under the transformation temperature of pure zirconium given in the literature. This effect could also be explained by slight impurities in the iodide zirconium, as McPherson and Hansen pointed out; but if the present explanation is accepted instead, the results agree with that observed at 523°C.

Investigation of the phase boundaries between the alpha and beta regions has shown that when the beta phase is quenched in a two-phase ($\alpha + \beta$) alloy, the phase appears to undergo the eutectoid reaction during quenching. Figure 9 shows the

[2] D. J. McPherson and M. Hansen, *The Phase Diagrams of Binary Zirconium Base Alloys*, COO-89, Armour Research Foundation, March 31, 1952.

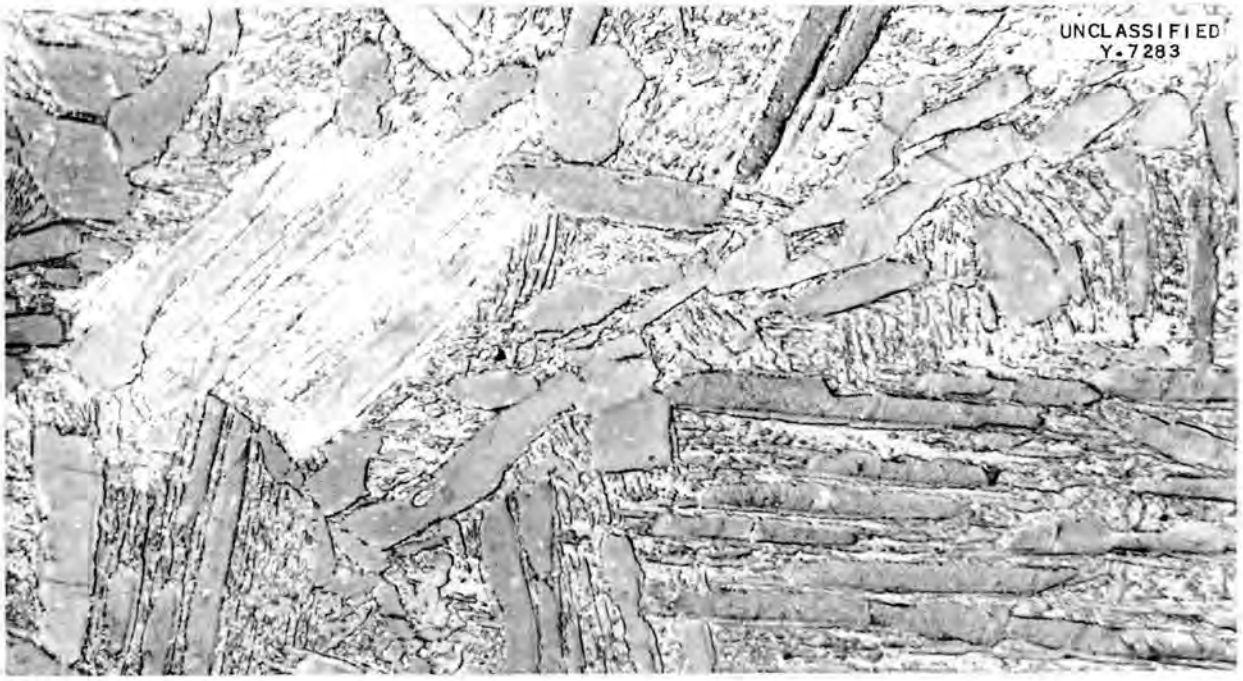

Fig. 9. Alloy 0.51 Quenched from 857.4°C Showing the Two-Phase Microstructure with Large Grains of Alpha Phase in a Matrix of Decomposed Beta Phase. Etched with 0.5% HF–50% alcohol–49.5% glycerine mixture; polarized light. 250X

microstructure of the alloy 0.51 quenched from 857.4°C in this region. A similar effect was found in alloy 0.78 annealed at 802°C, but in the alloys annealed at 703°C no structures of this type were observed; the alloys 0.52, 0.71, and 0.78 were isothermal alpha plus a small amount of a second phase, although in alloy 0.71 some residual, coarse, transformed beta (apparently from the homogenization quenching) remained evident. The alloys 1.08 and 2.09 were of transposed beta structure with very small particles of second phase. If the transformed beta structure is regarded, as suggested earlier, as being unaffected by 22 days at 703°C, then the presence of very small particles of second phase in these alloys would be consistent with placing them in the alpha plus compound region; and the eutectoid reaction would, in this case, be between 762 and 703°C. This may be better understood after new experiments involving slow cooling have been performed, and the diagram of Fig. 8 has been left with the eutectoid temperature less than 703°C.

The microstructure of the alloy 21.4 in the as-cast condition is shown in Fig. 10. This photograph shows the white phase, tentatively called $AgZr_2$, surrounding large primary beta grains, which have since decomposed eutectoidally. The reaction between the liquid and the beta phase did not go to completion, and a small residue of chilled eutectic may be seen inside the $AgZr_2$ phase. After alloy 21.4 was annealed for 9 days at 963°C, the microstructure shown in Fig. 11 was observed. If the white grains in the photograph of Fig. 11 are observed carefully, graduations in color, which indicate the presence in $AgZr_2$ of alloy gradients from the peritectic reaction, may be seen. These gradients indicate that the $AgZr_2$ phase exists over a definite range of composition, as has been indicated very roughly by the dashed lines around this phase in Fig. 8.

Other alloys in the (β + $AgZr_2$) region were heated as high as 1050°C, and in the beta region as high as 1150°C, but without incipient melting; therefore future quenching experiments will be

Fig. 10. Microstructure of Alloy 21.4 in the As-Cast Condition Illustrating the Peritectic Formation of $AgZr_2$. The eutectoid areas were formerly beta-phase primary grains that reacted with liquid in the grain boundaries to form the white phase. The third phase in the middle of the white areas is a eutectic. Etched electrolytically with perchloric and acetic acids very briefly and then swabbed with acetic acid. 1000X

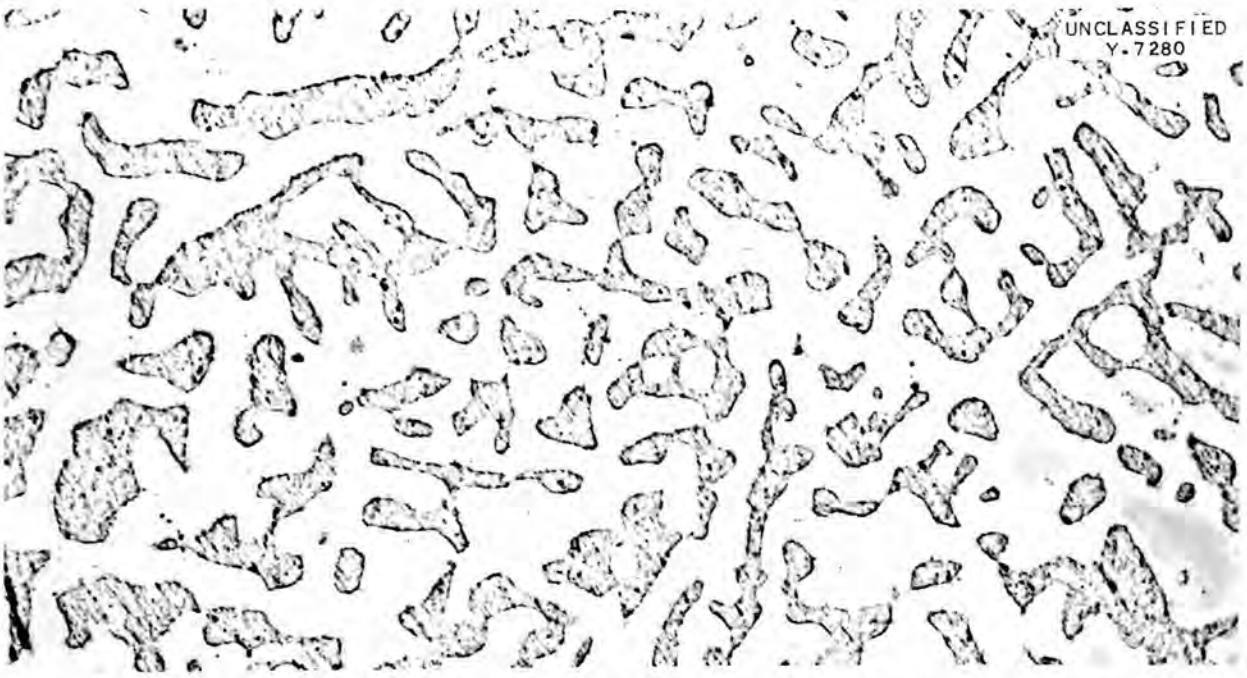

Fig. 11. Alloy 21.4 Annealed Nine Days at 963°C Showing Transformed Beta Phase in Matrix of $AgZr_2$ Phase. Hand polished without etching. 250X

required to determine the temperature of the peritectic horizontal. The alloy 32.4 annealed for five days at 951.5°C consists of mostly $AgZr_2$ phase with a small amount of the AgZr phase as shown in Fig. 12. The actual composition of this phase is therefore slightly lower in silver than that given by the formula $AgZr_2$.

Alloys 34.2 and 39.7 were found to be in the two-phase region ($AgZr_2$ + AgZr) after annealing for seven days at 963°C, whereas alloy 48.3 was found to be within the homogeneous region of the phase, which is tentatively called AgZr, after annealing for eight days at 963°C. The microstructure of this alloy is shown in Fig. 13. This phase appears gray-white in bright-field illumination and in various shades of blue during rotation in polarized light. The polished surfaces of the microscopic specimens have frequently shown in this phase a needle-like deformation twin that appears as bright blue in polarized light and as a yellow-gray in bright-field illumination. At lower temperatures, the alloy 48.3 is not homogeneous but contains a trace amount of the silver solid solution. This is illustrated by the photograph of alloy 48.3 annealed for ten days at 779°C, shown in Fig. 14. Tentatively then, it would appear that the AgZr region is somewhat displaced toward the zirconium side from the composition represented by AgZr.

A minor third phase was observed, in addition to the $AgZr_2$ and AgZr phases, in the alloys 33.1, 35.8, and 39.7 in the as-cast condition and in the specimens that were annealed for ten days at 779°C. This constituent appears to be dendrites of a primary beta phase that crystallized during casting and remained in the alloys as a consequence of an incomplete peritectic reaction, $\beta + \text{liquid} \leftrightarrows AgZr_2$. The tentative phase diagram has been sketched with this in mind, and the formation of primary beta grains is shown up to about 40 at. % silver. An alternate interpretation, not shown on the diagram, would be that the beta phase formed a eutectic with the AgZr phase, and a peritectoid formation of $AgZr_2$ therefore would occur at a slightly lower temperature. This interpretation is favored by the tendency for the minor third phase to occur in conjunction with the AgZr phase rather than with the $AgZr_2$ phase

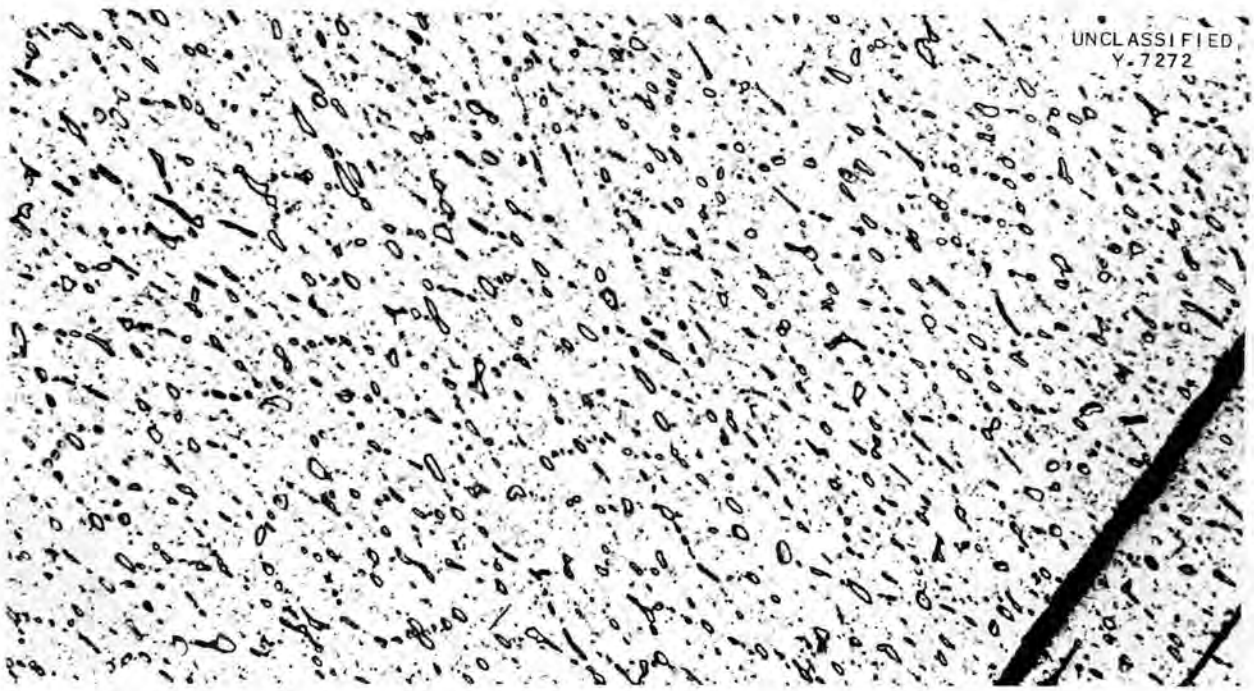

Fig. 12. Alloy 32.4 Annealed Five Days at 951.5°C Showing the Phase Tentatively Called $AgZr_2$ Plus a Small Amount of AgZr Phase. Etched 30 sec with 2% HF–48% HNO_3–50% glycerin mixture; bright field. 250X

Fig. 13. Alloy 48.3 Annealed Eight Days at 963°C Showing Homogeneous AgZr Phase. Hand polished; polarized light. 250X

Fig. 14. Alloy 48.3 Annealed Ten Days at 779°C Showing the AgZr Phase with a Small Amount of Silver Solid Solution. Etched briefly in 1% HF–49% acetic acid–50% glycerine; bright field. 250X

in the alloys 35.8 and 39.7 annealed at 779°C. Additional experiments at 779°C are planned in order to make certain that the minor phase disappears when equilibrium conditions are obtained.

Etching of the silver-zirconium alloys by electrolytic means has been highly satisfactory in the regions of the zirconium-rich solid solutions, but this method pits and stains the surface badly as the silver content is increased. The best method found for preparing alloys that contain the $AgZr_2$ or AgZr phases is to polish by hand and to chemically etch the surface with one of the following reagents:

1% HF + 49% glycerine + 50% HNO_3,

1% HF + 49% glycerine + 50% alcohol,

1% HF + 49% glycerine + 50% acetic acid.

The use of an acetic acid swabbing during and after etching reduces the amount of general staining.

Because of the uncertainty about the beta eutectoid temperature, preparations are now being made to run a series of heating and cooling curves in this region. The thermal analysis ingots will be arc melted a number of times and then heated for long periods of time to make them uniform in composition. This uniformity will be tested by chemical analysis of the center and surface of the ingots. The thermal analysis will then be conducted with a sensitive potentiometer by the method of Hume-Rothery and Raynor.[3]

A quenching arrangement using silicone diffusion pump oil as the quenching medium has been made for the continuously pumped, mullite, tube furnace. Provisions have also been made to supply the furnace with purified argon. Unfortunately, a defective mullite tube that leaked slightly has prevented the use of the furnace for the determination of the solidus curves. A preliminary trial of the silicone oil quenching bath was quite satisfactory, and the mullite tube is now being replaced with a leak-tight tube.

[3] W. Hume-Rothery and G. V. Raynor, *J. Inst. Metals* 61, 208 (1937).

Indium-Zirconium System (G. W. Boyd, J. O. Betterton). The indium-zirconium system occurs between the silver-zirconium and tin-zirconium systems when these binary systems are arranged in the order of their solutes on the second long period of the periodic table. In the silver-zirconium system the beta phase decomposes eutectoidally, that is, the addition of silver to zirconium depresses the close-packed hexagonal phase at the expense of the body-centered cubic phase. In the tin-zirconium system the opposite is true, and the alpha phase forms by a peritectoid reaction, that is, the addition of tin to zirconium expands the close-packed hexagonal phase region at the expense of the body-centered cubic phase. Since the indium-zirconium system is intermediate in the solute position on the periodic table, it might reasonably be expected to be either a peritectoid type similar to tin-zirconium or at least a system where the α/β boundaries were not depressed so rapidly as in the silver-zirconium system. The atomic size factor of the indium-zirconium system is –5.9%; consequently, there is no reason to expect restricted solid solution.

The preliminary annealing experiments were done with the alloy 9.6[4] that was annealed at the temperatures 1007, 972, 847, and 523°C. The times of annealing varied between 6 and 23 days, and the alloy was cold worked before the anneals. Two results for this alloy, pictured in Figs. 15 and 16, show that at 847°C the alloy consists of isothermal alpha phase, whereas after quenching from 972°C the alloy contains isothermal alpha phase plus transformed beta phase. There is a strong suggestion here that the alpha phase forms peritectoidally from the beta phase and an intermediate phase. This result is of particular interest since it not only fits the general trend of the silver-zirconium and tin-zirconium systems but also agrees with the occurrence of peritectoid alpha phases in the titanium-aluminum and the zirconium-aluminum systems, suggesting that Group III elements may, in general, show this tendency when alloyed with Group IVa elements.

The indium-zirconium alloys containing 2.5, 5, 7.5, 9.6, 12.5, 15, 19.3, 21, 23, 26, 28, and

[4] As in the silver-zirconium system, the indium-zirconium alloys are numbered according to their atomic per cent of solute.

33 at. % indium have been made successfully by arc melting. Certain arc-melting experiments were tried with higher indium contents but were unsuccessful because the indium metal boiled before the temperature that was needed to melt the zirconium was reached. For the present, attention will be given mainly to the higher zirconium alloys, and only occasional experiments with diffusion cans or with master alloys will be attempted to find a satisfactory method of making alloys with more than 35 at. % indium. The as-cast microstructures of these alloys showed beta to be the primary phase up to 19.3 at. %, with areas of what might be a eutectic between the grains of beta phase increasing with indium content. Between 19.3 and 23 at. % indium, the cast structures show a new primary phase that, from the proportion present, is probably near the composition $InZr_4$. Although only preliminary observations have been made on annealed specimens of alloys other than 9.6 at. % indium, there appears to be a homogeneous phase in this system of the tenative composition $InZr_3$, which at 1007°C includes alloys 26 and 28 within its homogeneity region. There appears to be another intermediate phase of composition near $InZr_4$ and another of still higher indium content than 33 at. %.

In the investigation of these alloys it has been found more satisfactory to use hand polishing followed by brief etching in 20% HF–20% HNO_3–60% glycerine than to use electrolytic etching, which appears to pit the specimens badly. All the alloys will be annealed at various temperatures between 850 to 1200°C in order to determine whether the complete constitution of the α/β boundaries confirm a peritectoid formation of the hexagonal, alpha phase.

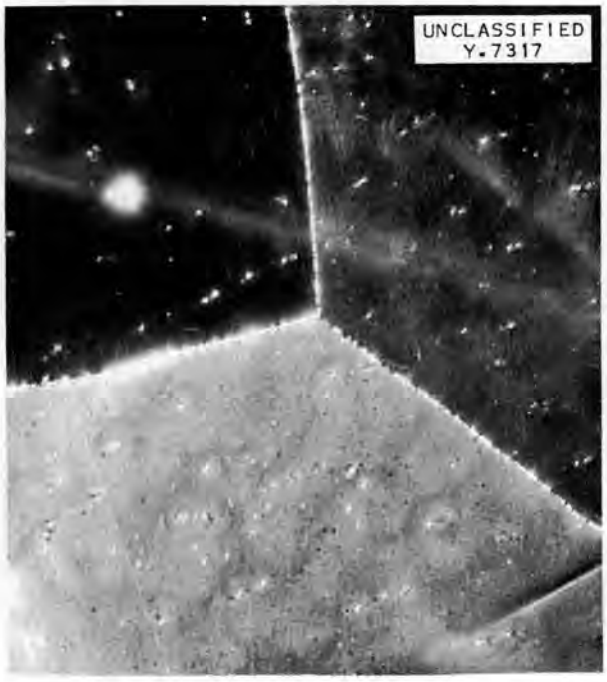

Fig. 15. Indium-Zirconium Alloy 9.6 Annealed for 96 hr at 972°C Followed by Annealing for Nine Days at 847°C Showing Isothermal Alpha Phase. Etched with 20% HF–20% HNO_3–60% glycerine; polarized light. 250X

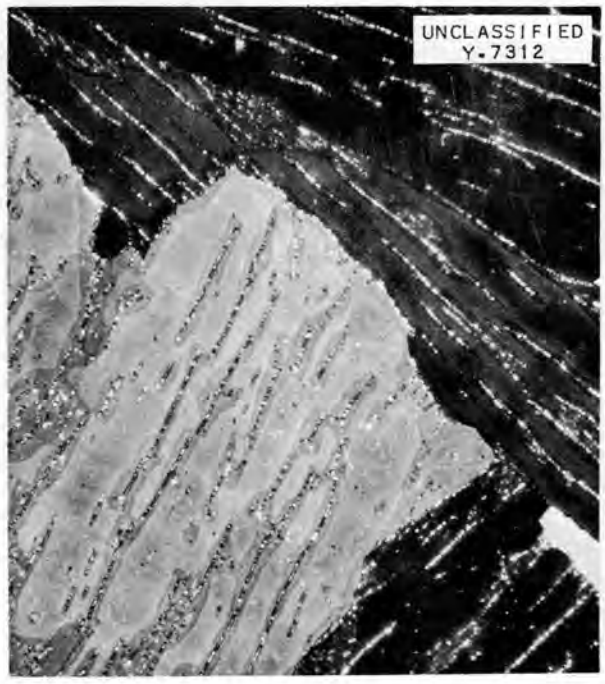

Fig. 16. Indium-Zirconium Alloy 9.6 Annealed for 96 hr at 972°C Showing Isothermal Alpha Grains Surrounded by Transformed Beta Matrix. Etched with 20% HF–20% HNO_3–60% glycerine; polarized light. 250X

ANP METALLURGY

W. D. Manly

STATIC CORROSION

D. C. Vreeland
R. B. Day
L. D. Dyer
E. E. Hoffman

Corrosion by Fluorides. Static corrosion tests at 816°C for 100 hr in fluorides with various addition agents have been continued to check the possibility that the additions act as corrosion inhibitors. Some of the additions appeared to have some effect in inhibiting corrosion. Tests have been run with additions of lower percentages of sodium (previous sodium tests were with 10% additions), lithium, potassium, calcium, titanium, manganese, MnO_2, CrF_2, NiF_2, and FeF_3.

In the case of the sodium, lithium, potassium, calcium, titanium, and manganese additions, it was thought that these elements might possibly act as "getters" to reduce the available amount of oxygen in the system and thus help to reduce corrosion.

Manganese dioxide additions were made to determine whether the addition of oxygen in this form would increase corrosion. Positive results were obtained.

The metal fluorides (also sodium, lithium, and potassium) were added to test the possibility that a reaction of the following type might be the corrosion mechanism:

$$2aF + \beta \rightleftharpoons \beta F_2 + 2a$$

where a would represent sodium, lithium, or potassium and β would represent iron, nickel, or chromium. If this were the case, then additions of metal fluorides and also sodium, lithium, or potassium should tend to drive the reaction to the left and help reduce the corrosion. However, additions of the iron, nickel, and chromium fluorides had no effect in reducing corrosion (the purity of these salts is not known). Sodium, lithium, and potassium did reduce corrosion, but as was mentioned, their action may be that of "getters" rather than that of taking part in the reaction.

Classified in Table 6 are the various additions according to the results obtained in the tests. The classification is based on tests that were run with the addition percentages given in Table 7. It is conceivable that different amounts of the addition agents might result in different corrosion results. In Fig. 17 is shown the type of attack on Inconel that resulted in the test with the CrF_2 addition.

Table 7 shows the results obtained in using additions in corrosion tests.

TABLE 6

RELATIVE EFFECTS OF ADDITION AGENTS ON CORROSION BY FLUORIDES

ADDITION AGENTS REDUCING CORROSION	ADDITION AGENTS INCREASING CORROSION	ADDITION AGENTS WITH LITTLE OR NO EFFECT ON CORROSION
Sodium	MnO_2	CrF_2
Lithium	NiF_2	$NiF_2 + CrF_2 + FeF_3$
Potassium	FeF_3	
Calcium		
Titanium		
Manganese		

TABLE 7

EFFECTS OF VARIOUS ADDITIONS TO FLUORIDE NO. 14* IN STATIC CORROSION TESTS FOR 100 hr AT 816°C IN VACUUM

MATERIAL	ADDITION	DEPTH OF METAL AFFECTED (mils)	METALLOGRAPHIC NOTES
Inconel	1% Na	½	Specimen and tube have a few subsurface voids
	5% Li	½	One-mil surface layer
	5% K		No attack
	5% Ca		One-half-mil surface layer, no attack beneath surface layer
	5% Ti		One-half-mil surface layer, no attack beneath surface layer
	5% Mn		No attack
Type 321 stainless steel	1% Na		No attack
	5% Li		No attack
	5% K		No attack
	5% Ca	½	One-half-mil surface layer, attack to ½ mil beneath surface layer
	5% Ti		No attack
	5% Mn	1	Subsurface voids, ½ to 1 mil
Inconel	10% CrF_2	4	Subsurface voids
	10% NiF_2	7	Subsurface voids
	10% FeF_3	9	Subsurface voids
	3⅓% CrF_2, 3⅓% NiF_2, 3⅓% FeF_3	2	Subsurface voids
	10% MnO_2	9	Subsurface voids and intergranular penetration
Type 309 stainless steel	10% MnO_2	4	Subsurface voids and intergranular penetration

*Fluoride No. 14 composition: 10.9 mole % NaF, 1.1 mole % UF_4, 44.5 mole % LiF, 43.5 mole % KF.

Tests have been run on Inconel, type 321 stainless steel, and A nickel exposed to fluoride No. 14 that was treated by bubbling hydrogen through it for 2 hr while the molten fluoride was held at a temperature of approximately 980°C. There appeared to be no significant reduction in corrosion when the hydrogen pretreated fluoride was used. The results of the tests are listed in Table 8.

Hydroxide Corrosion. A series of temperature-dependence tests of Inconel in sodium hydroxide has been completed. From the results listed in Table 9, it would appear that in a 100-hr test corrosion of Inconel is negligible until the test temperature is raised to some point above 450°C.

Tests have been run to check the effect of residual stresses on the corrosion resistance

Fig. 17. Attack on Inconel Resulting from Exposure to Fluoride No. 14 Plus 10% CrF_2 for 100 hr at 816°C in Vacuum. 200X

TABLE 8

EFFECT OF HYDROGEN PRETREATMENT OF FLUORIDE NO. 14 IN TESTS FOR 100 hr AT 816°C

MATERIAL	HYDROGEN TREATED	METALLOGRAPHIC NOTES
Inconel	No	One to 2 mils of subsurface voids
	Yes	One to 2 mils of subsurface voids
Type 321 stainless steel	No	One-half mil of subsurface voids
	Yes	One-half mil of subsurface voids
A nickel	No	No attack
	Yes	No attack

of Inconel in sodium hydroxide at 816°C. The stresses were induced by cold rolling. The tests were first run for 50 hr, but all the specimens were corroded throughout their entire thickness. The time was then cut to 8 hours. The results of the 8-hr tests are listed in Table 10 and would seem to indicate that residual stresses of this nature do have a deleterious effect on the corrosion resistance of Inconel in sodium hydroxide.

Similar tests were run on A nickel for 50 hr, but there was no evidence of attack even on the most severely cold worked (71%) specimens tested.

TABLE 9

TEMPERATURE-DEPENDENCE TESTS OF INCONEL IN SODIUM HYDROXIDE FOR 100 HOURS

TEMPERATURE OF TEST (°C)	WEIGHT CHANGE (g/in.^{2})	METALLOGRAPHIC NOTES
350	None	No attack
450	None	No attack
550	+0.0050	Three to 4 mils of intergranular penetration
593	+0.0060	Three to 4 mils of intergranular penetration

TABLE 10

EFFECT OF RESIDUAL STRESSES ON CORROSION OF INCONEL IN SODIUM HYDROXIDE FOR 8 hr AT 816°C

REDUCTION IN THICKNESS (%)	ORIGINAL THICKNESS (mils)	WEIGHT CHANGE (g/in.^{2})	METALLOGRAPHIC NOTES
71	10	−0.0011	Attacked throughout
50	17.5	+0.0088	Nine mils of penetration, 2 to 3 mils of unattacked material
26	26	+0.0188	Seven to 8 mils of penetration, 12 mils of unattacked material
11	31	+0.0171	Four to 5 mils of penetration, 23 mils of unattacked material
6	33	+0.0203	Three to 5 mils of penetration, 25 mils of unattacked material
0	35	+0.0210	Three to 5 mils of penetration, 27 mils of unattacked material

Liquid Metal Corrosion. Tests of type 1020, chromized steel have been run in various low-melting-point alloys. In some cases it was difficult to estimate the exact extent of attack because of the adherence of bath metal to the specimen. In all tests, however, attack appeared to be severe enough so that type 1020, chromized steel could not be recommended as a container material for the low-melting-point alloys tested. Tests were for 100 hr at 816°C; except in one case, both specimens and tubes were chromized. Results are presented in Table 11, and Fig. 18 shows the type of attack that occurred.

Vanadium that was tested in molten zinc and lead for 100 hr at 760°C was apparently unattacked in lead, whereas in zinc, attack was so heavy that the container tube was completely penetrated.

Temperature-dependence tests of several materials in molten lead have been run. The only attack that was noted in these tests was at 700°C and above. Tests were of 100-hr duration, and details are listed in Table 12.

TABLE 11

RESULTS OF TESTS OF TYPE 1020, CHROMIZED STEEL IN VARIOUS LOW-MELTING-POINT ALLOYS FOR 100 hr AT 816°C

BATH	METALLOGRAPHIC NOTES
67.8% Sn–32.2% Cd	(Test of chromized specimen in Inconel tube.) Specimen apparently unattacked; however, it was only partially covered by bath metal
67.8% Sn–32.2% Cd	Both specimen and tube attacked; in places the specimen is completely penetrated
43% Sn–57% Bi	Erratic attack to 10 mils in depth
60% Bi–40% Cd	Erratic attack to 8 mils in depth

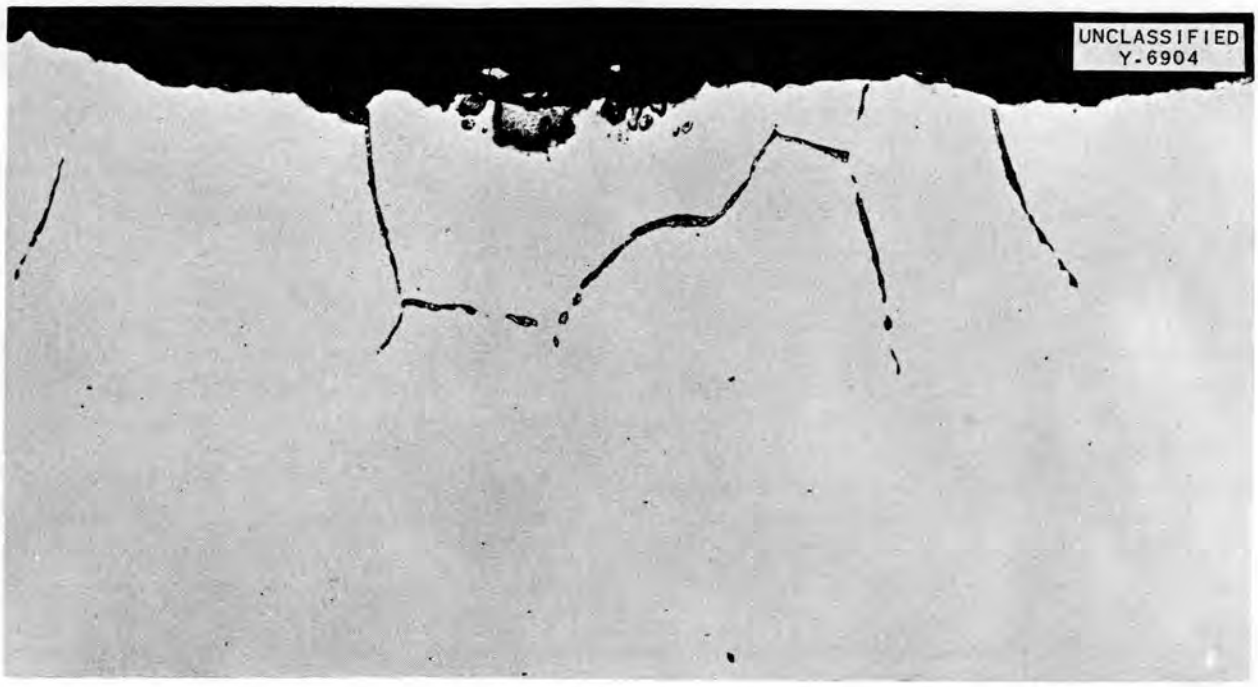

Fig. 18. Attack on Type 1020 Chromized Steel Resulting from Exposure to Molten 60% Bismuth–40% Cadmium Alloy for 100 hr at 816°C in Vacuum. 200X

DYNAMIC CORROSION

G. M. Adamson, Jr. K. W. Reber

Thermal Convection Loops. Emphasis in the dynamic corrosion testing program has shifted from testing Fulinak No. 14 to the testing of various coolants containing zirconium fluoride. Owing to the way the zirconium fluoride coolants are prepared, they are not so corrosive to Inconel as Fulinak No. 14. They do have the disadvantage of high vapor pressure, which results in the subliming of zirconium fluoride in the expansion pots of the loops. Since it is more readily available, some work is still being done with Fulinak No. 14.

TABLE 12

TEMPERATURE-DEPENDENCE TESTS OF VARIOUS MATERIALS IN MOLTEN LEAD FOR 100 HOURS

MATERIAL	TEMPERATURE (°C)	METALLOGRAPHIC NOTES
Inconel	400	No attack
Type 446 stainless steel	400	No attack
Type 309 stainless steel	400	No attack
Inconel	500	No attack
Type 446 stainless steel	500	No attack
Type 309 stainless steel	500	No attack
Inconel	600	No attack
Type 446 stainless steel	600	No attack
Type 309 stainless steel	600	No attack
Inconel	700	Specimen attacked to about ½ mil
Type 446 stainless steel	700	No attack
Type 309 stainless steel	700	No attack
Inconel	816	Specimen attacked 5 to 9 mils
Type 446 stainless steel	816	Slight roughening of surface

Tables 13, 14, and 15, which are continuations of tables presented in the last report,[1] summarize the results from the thermal convection loops operated during this period. Data for the new Inconel loops are listed in Table 13, for the 300 series stainless steel loops in Table 14, and for the remaining loop materials in Table 15. The types of coolants used are also listed, and their compositions are given in Table 16.

Four different coolants containing zirconium fluoride were tested in Inconel loops. Loop 236 showed the most attack, but the attack was still below the average measured with Fulinak No. 14. Loop 234, which was the only one not cleaned with hydrogen, produced a maximum attack of only 5 mils. This loop should be more nearly comparable to those operated with Fulinak No. 14 that gave attacks of 10 to 15 mils. Figures 19 and 20 are typical hot- and cold-leg sections of loop 234. These should be compared with similar photomicrographs of the attack of Fulinak No. 14 presented in the last report.[2] Although not so much attack is found with the zirconium fuels, the mechanism of attack presented in the last report seems to hold for the zirconium fuels also.

In the expansion pot of the two loops in which Fuzrna No. 27 was circulated, over 200 g of zirconium fluoride was sublimed. The material was found both on the insulated sides and the exposed top of this chamber. It was present as both large and small crystals. The pots have an internal cross-sectional area of 7.4 in.^{2}, and the temperature of the interface is about 1300°F.

If loop 234 is compared with the other Inconel loops in which zirconium fluoride fuels have been circulated, or the degreased loops in which Fulinak No. 14 has been circulated are compared with those cleaned by hydrogen, it appears that the hydrogen treatment does more harm than good. It may cut down the total amount of attack, but the attack is concentrated in a few grain boundaries.

[1] G. M. Adamson and K. W. Reber, *Metallurgy Division Quarterly Progress Report for Period Ending April 30, 1950*, ORNL-1302, p. 52-54.

[2] *Ibid*, Fig. 71, p. 107.

TABLE 13

INCONEL LOOPS

LOOP NO.	CLEANING PROCEDURE	COOLANT	TIME OF CIRCULATION (hr)	REASON FOR TERMINATION	HOT LEG TEMPERATURE (°F)	METALLOGRAPHIC NOTES		CHEMICAL NOTES
						Hot Leg*	Cold Leg	
216	Degreased	Fubena 17	574	Scheduled	1500	Heavy to moderate intergranular attack, 6 to 13 mils; in hot horizontal leg, attack only on one side	No attack; some nonmetallic particles on wall	Large increase in chromium, decrease in iron, slight decrease in uranium
217	Degreased	Fubena 17	500	Scheduled	1500	Heavy to moderate intergranular attack, up to 13 mils	No attack; light metal deposit as layer and crystals	Increase in chromium, decrease in iron and uranium
220	Degreased	Fulinak 14	2	Scheduled	1500	Light pitting, 2 to 4.5 mils	Scattered crystal deposit	Chromium decreased slightly in cold leg and considerably in hot leg; iron decreased slightly in both legs
221	Degreased	Funazrk 21	500	Scheduled	1500	Light to moderate intergranular pitting, 3 to 7 mils	Rough surface; thin non-metallic layer	Some increase in chromium, decrease in nickel, small increase in iron, and decrease in uranium
222	Degreased	Fulinak 14	500	Scheduled	1650	Intergranular attack up to 18 mils; pitting, 6 mils	Thin deposit	Chromium and iron both decreased; no systematic variations
228	Hydrogen	Funazrk 21	500	Scheduled	1500	Light intergranular pitting, 3 to 13 mils	Rough surface; thin deposited layer	Small increase in chromium, decrease in nickel; uranium variable
224	Degreased	Fulinak 14 and NaK	500	Scheduled	1500	Intergranular pitting, up to 10 mils	Thin surface layer with some adhering nonmetallic particles	
230	Hydrogen	Fnazrk 24	500	Scheduled	1500	Light intergranular pitting, average 4 mils with maximum 7 mils; grains not outlined	No deposited layer	
226	Hydrogen	Funazrk 26	500	Scheduled	1500	Widely scattered intergranular pitting, average 7 mils with maximum of 10 mils	Both metallic and nonmetallic deposits	
229	Degreased	Fulinak 14 not treated	500	Scheduled	1500			
227	Degreased	Fulinak 14	500	Scheduled	1500	Moderate to heavy pitting, 6 to 16 mils, mainly intergranular	Very thin metallic layer	
234	Degreased	Fuzrna 27	480	Power failure	1500	Lightly scattered intergranular pitting, up to 5 mils, average 2 mils; dirty Inconel used	Both metallic and nonmetallic crystals on walls	
236	Hydrogen	Fuzrna 27	462	Power failure	1500	Moderate intergranular pitting, average 8 mils with maximum of 10 mils; some pits in grains	Both metallic and nonmetallic particles on wall	
225	Degreased	Fulinak 14 + ½ % Zr	500	Scheduled	1500			
231	NaK	Fuzrna 27	500	Scheduled	1500			

*Hot leg annealed ½ hr at 1750°F.

TABLE 14

STAINLESS STEEL LOOPS

LOOP NO.	TYPE OF STAINLESS STEEL*	COOLANT	TIME OF CIRCULATION (hr)	REASON FOR TERMINATION	HOT LEG TEMPERATURE (°F)	METALLOGRAPHIC NOTES		CHEMICAL NOTES
						Hot Leg	Cold Leg**	
252	310	Fulinak 14	368	Plug and instrument failure	1500	Very heavy intergranular pitting, up to 20 mils	Thin deposited layer; large crystals attached to surface	Chemical analyses irregular and no definite trends discernible
122	316	Fulinak 14	87	Leak	1700	Heavy intergranular attack, 3 to 7 mils; some grains removed	Metallic layer 2 mils thick	All coolant leaked out
123	316	Fulinak 14	500	Scheduled	1650	Intergranular attack, up to 13 mils; some grains removed	Metallic layer 1 mil thick	Iron, chromium, and uranium all decreased; hot leg highest with all
126	316	Fulinak 14 H_2 treated	309	Plug	1500	Heavy intergranular attack, up to 14 mils; some grains removed	Nonuniform metallic deposit; few nonmetallic crystals in top portion	Chromium increased, iron decreased; uranium varied, but little change; nickel same
124	316	Funazrk 21	199	Leak	1500	Intergranular attack, usually 5 mils but occasionally up to 11 mils	Some evidence of a thin metallic deposit	Chromium up slightly; nickel decreased; iron varied but was unchanged; uranium lower
120	316	Fulinak 14 not treated	62	Plug	1500	Heavy intergranular attack, up to 12 mils; some grains removed	Thin surface deposit with both metallic and nonmetallic crystals adhering	
125	316	Fulinak 14	91	Plug	1650			
128	316	Fuzrna 27	500	Scheduled	1500			

***Hydrogen fired, hydrogen atmosphere.**
****Metallic plug found in lower cold leg.**

TABLE 15

MISCELLANEOUS LOOPS

LOOP NO.	MATERIAL	COOLANT	TIME OF CIRCULATION (hr)	REASON FOR TERMINATION	HOT LEG TEMPERATURE (°F)	METALLOGRAPHIC NOTES		CHEMICAL NOTES
						Hot Leg	Cold Leg	
341	Monel	Fulinak 14	31	Leak	1500	No pitting or intergranular attack, up to 14 mils removed	No attack; no deposit	No hot leg samples; no change in iron or chromium; nickel up slightly
44	Iron	Fulinak 14	25	Plug	1350	Rough surface with no large attack evident; possibly some even removal	Rough surface with no attack or deposit	Chromium decreased; iron varied but averaged same; uranium lower
375	Hastelloy B	Fulinak 14	60	Plug	1500	Subsurface pitting, 2 mils, mainly in particles of a second phase	Surface deposit which appears to be same second phase	Iron decreased slightly; uranium slightly lower; nickel and molybdenum varied
107	Nickel	Fulinak 14	1000	Scheduled	1500	Surface polished; no pitting or intergranular attack; from 8 to 10 mils removed; large grains	Crystal deposit	Nickel up 30 ppm; iron and chromium both down

TABLE 16

COMPOSITION OF COOLANTS

COMPONENTS	FULINAK 14		FUBENA 17		FLINAK 12		FUNAZRK 21		FUNAZRK 26		FUZRNA 27		FNAZRK 24	
	wt %	mole %	wt %	mole %	wt %	mole %	wt %	mole %	wt %	mole %	wt %	mole %	wt %	mole %
UF_4	7.8	1.1	12.6	2.0			10.7	3.8	10.7	3.8	10.9	4.0		
NaF	10.3	10.9	39.4	37.0	11.7	11.5	1.8	4.8	13.8	36.6	16.7	46.0	14.8	36.0
KF	56.1	43.5			59.1	42.0	25.9	50.1	7.3	14.0			10.2	18.0
LiF	25.8	44.5			29.2	46.5								
BeF_2			48.0	51.0										
ZrF_4							61.6	41.3	68.3	45.6	72.4	50.0	75.0	46.0

The attack in these few foundaries actually extends deeper than attack that is spread out. It has not been determined whether this effect is caused by the concentration of impurities; a more likely supposition is that fewer grain boundaries result from the large grains. During the hydrogen cleaning, temperatures as high as 1900 to 1950°F result in considerable grain growth.

The other special material tested in the loops was Fubena No. 17. These loops had been operated previously but the metallographic report was not received until this period. Two Inconel loops had circulated this coolant at 1500°F for 500 hours. The hot-leg attack varied from heavy to moderate and was typical intergranular pitting. The pitting varied in depth from 6 to 13 mils. A thin deposited layer was present in the cold leg of both loops. The uranium analyses after termination were lower in every section than in the two original samples, which may be an indication that some uranium was precipitated from the coolant.

The results, reported in the last report, obtained from drilling successive layers from the inside of loop 210 were confirmed by similar examination of loop 219, as shown by the data in Table 17. The chromium was leached out but not so much as with loop 210. The systematic increase in total percentages of iron, chromium, and nickel is also not so definite.

The second part of Table 17 presents similar results from Inconel loop 78, and Table 18 presents results from type 316 stainless steel loop 121. Flinak No. 12 was circulated for 1000 hr at 1500°F in loop 78, whereas Fulinak No. 14 was circulated 500 hr in loop 121. With Inconel loop 78, the variations appear to be the same as that found with Fulinak No. 14 but the changes are much smaller. Even in the layer 25 mils deep the chromium is not so high as originally. The fluorides are very low and constant and show practically no penetration. With the type 316 stainless steel loop 121, chromium is only reduced slightly, and iron is the major material leached out. Nickel and molybdenum are essentially unchanged. With this loop, the fluorides are much higher than in the others and decrease gradually with depth, which is evidence that they are entrapped in crevices. A loop in which zirconium fluoride coolants were circulated has been drilled, but no chemical results are yet available.

To determine the effect of temperature on corrosion, Inconel loops 218 and 222 were run at 1300° and 1650°F, respectively. The attack increased slightly with temperature but remained of the same general type. Type 316 stainless steel loop 123 was then operated at 1650°F and was the first loop of 300 series stainless steel to operate 500 hr without plugging. The test was repeated with loop 125 but this loop plugged in only 91 hours. The only difference found so far

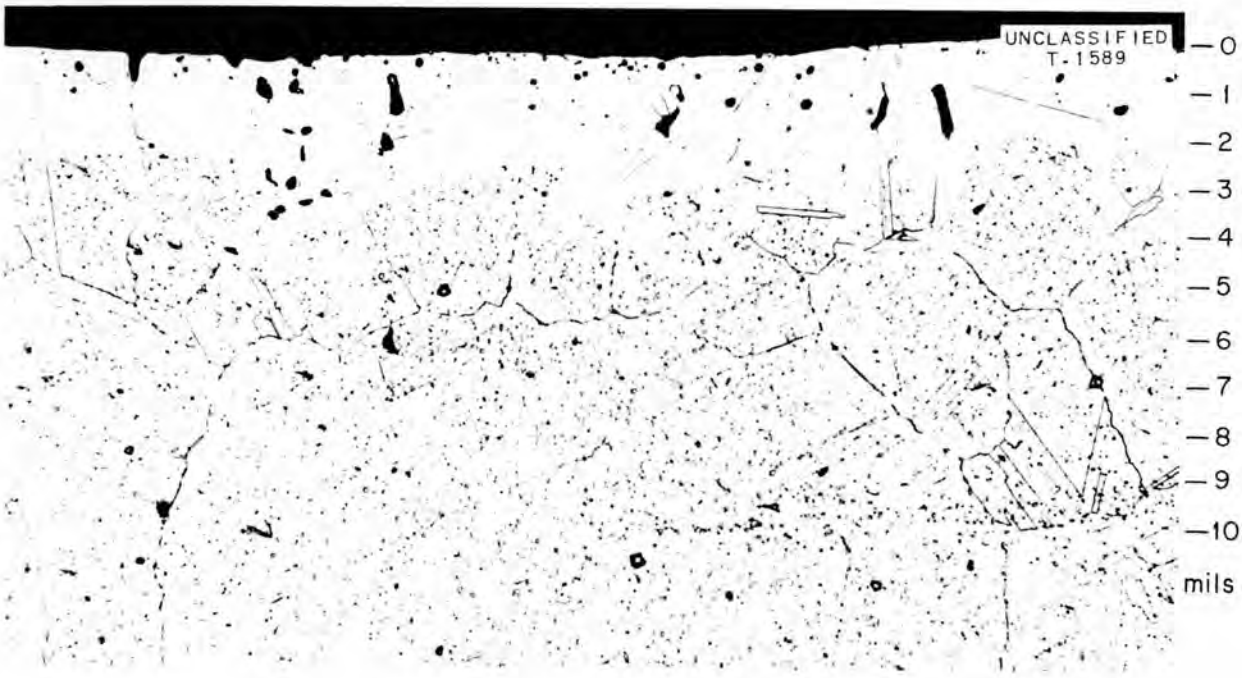

Fig. 19. Hot Leg Section of Inconel Thermal Convection Loop in Which Fuzrna No. 27 Was Circulated for 500 hr at 1500° F. Etched with aqua regia. 250X

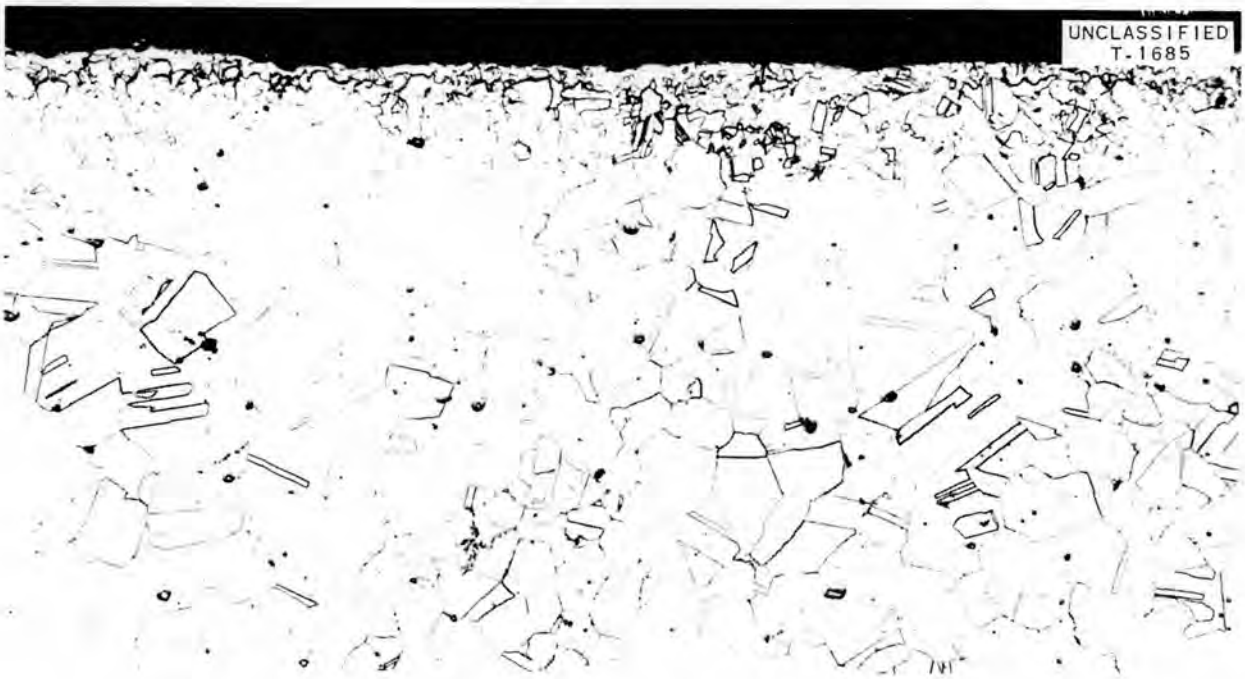

Fig. 20. Cold Leg Section of Inconel Thermal Convection Loop Shown in Fig. 19.

TABLE 17

ANALYSES OF WALLS OF LOOPS 219 AND 78

DEPTH OF LAYER (mils)	COMPOSITION (%)									
	Fe	Ni	Cr	Fe/Ni	KF*	LiF*	NaF*	Other	Total Fe, Ni, and Cr	Total
Loop 219										
2	7.33	80.84	8.74	0.091	0.45	0.55	0.2	Average 0.7 Co, Cu, Si, and Mn	96.91	98.8
5	7.42	80.42	8.73	0.092	1.5	0.55	0.4		96.57	99.7
10	7.46	79.60	9.39	0.094	1.2	0.55	0.4		96.45	99.3
15	7.60	79.98	10.63	0.095	0.3	0.3	0.2		98.21	99.7
20	7.48	79.88	11.08	0.095	0.3	0.3	0.2		98.44	99.9
25	7.15	77.57	13.18	0.092	0.15	0.15	0.1		98.90	99.0
30	7.20	76.90	14.15	0.094	0.15	0.15	0.1		98.25	99.3
Exterior	7.08	76.46	15.85	0.093					99.39	100.1
Loop 78										
5	7.03	78.3	12.0	0.089	0.09	0.3	0.07	1.68**	97.4	99.5
10	8.66	77.5	11.8	0.112	0.03	0.15	0.02	1.46	98.0	99.6
15	6.93	77.6	13.6	0.090	0.02	0.1	0.02	1.18	98.1	99.4
20	6.81	77.7	13.7	0.088	0.02	0.1	0.02	1.30	98.3	99.6
25	6.66	77.9	14.3	0.086	0.06	0.2	0.07	1.78	98.9	101.0
Exterior	7.15	77.4	15.2	0.092				1.48***	99.8	101.0

*These values calculated from spectrographic analysis of metal.

**Total of spectrographic analysis for Al, Co, Cu, Mn, Mo, Si, and Ti.

***Average of those above values.

TABLE 18

ANALYSES OF WALLS OF LOOP 121

DEPTH OF LAYER (mils)	COMPOSITION (%)									
	Fe	Ni	Cr	Mo	KF*	LiF*	NaF*	Other	Total Fe, Ni, Cr, and Mo	Total
2	60.4	16.9	14.5	2.8	1.5	3.7	1.1	Average 1.6 Co, Cu, Mn, Si	94.6	102.5
5	60.8	16.1	14.7	2.7	0.9	3.7	1.1		95.2	101.6
10	63.5	14.8	15.1	2.5	0.5	2.2	0.5		95.9	100.7
15	64.1	14.6	15.7	2.5	0.3	1.1	0.5		96.9	100.4
20	65.2	14.3	16.2	2.5	0.2	0.7	0.5		98.2	101.1
25	65.1	14.0	16.8	2.4	0.3	0.7	0.5		99.3	101.4
Exterior	66.0	13.3	16.8	2.4					98.5	100.1

*These values calculated from spectrographic analysis of metal.

in these loops is that the chromium content of the fluoride increased with loop 125 and decreased with loop 123.

The other variable investigated during this period was a small addition of NaK to Fulinak No. 14. Eight cubic centimeters of NaK was added to Inconel loop 224, which circulated for 500 hr at 1500°F. The attack in the hot leg of this loop measured a maximum of 10 mils and was of the usual type. It is obvious that no large improvement in corrosion resistance was obtained. Since the attack is on the low side but still within the spread previously found with Fulinak No. 14, it is impossible to say whether a small improvement was obtained. The impurities in the fluoride after termination were not so high as usual, which may indicate that some improvement was obtained.

Mechanical Testing in Fluorides. The stress-rupture and tube-burst tests with Fulinak No. 14 were continued. Because of their unfavorable vapor pressures, it will not be possible to test zirconium fluoride coolants in the present apparatus. Results obtained from stress-rupture tests check the expected values quite well, but those in the tube-burst tests are much lower than expected.

In the stress-rupture tests at 1500°F, stresses of 6000 and 7000 psi resulted in rupture times of 131 and 94 hr with Inconel. Stresses of 4000 and 5000 psi were attempted but resulted in failure through mechanical troubles in 661 and 575 hr, respectively. These stress-rupture times agree very well with values obtained previously. One type 316 stainless steel sample ruptured in 25 hr under a stress of 8000 psi.

Table 19 lists the rupture times obtained at 1500°F with Fulinak No. 14 in the tube-burst tests. These figures are much lower than would be expected from the stress-rupture data. No explanation is available for this discrepancy. A type 316 stainless steel sample now under test has survived 69 hours.

The first photomicrographs were received for the tube-burst and stress-rupture specimens that had been run in fluorides. In every case a deposited layer was found on the Inconel samples.

TABLE 19

TUBE-BURST TEST

STRESS (psi)	RUPTURE TIME (hr)	
	Inconel	Type 316 Stainless Steel
2000		880
2400		634
2500	128	
2900	73	

All the samples had been run in type 316 stainless steel pots with type 316 stainless steel holders. The original specimens had been destroyed; so the nature of the mass-transferred layer is not yet known. New equipment is now on order in the shop so that Inconel may be tested in an all-Inconel apparatus.

PHYSICAL METALLURGY OF LIQUID METAL CORROSION

A. deS. Brasunas L. S. Richardson

Nature of Fluoride Corrosion. The nature of subsurface voids observed in most corrosion test specimens exposed to molten fluoride has been quite puzzling. Careful study of the specimens and a number of critical experiments have indicated that the voids are true vacancies caused by the diffusion of chromium from the metal into the fluoride bath. The basis for this conclusion may be briefly summarized as follows:

1. Careful nonaqueous polishing has never enabled retention of any particles in the porous surface region.

2. Chemical analysis of the attacked metal surface has revealed a substantial loss in chromium (from 15 to less than 5%).[3]

3. The abnormally high chromium content of the fluoride in comparison with nickel and iron content

[3] A. D. Brasunas and L. S. Richardson, *ANP Project Quarterly Progress Report for Period Ending March 10, 1952*, ORNL-1227, p. 124.

indicates a preferential solution of chromium from the alloy.

4. Calculations of void area anticipated from change in chromium content are in accord with observations.

5. Depth of void formation bears a direct relationship to the amount of chromium in the bath.

6. Attacked specimens show weight losses but no dimensional changes.

7. The loss of chromium from the alloy, caused by either high-temperature oxidation or high-temperature vacuum treatment, has also resulted in similar void formation. Such voids have been observed previously[4,5] in diffusion experiments where diffusion in one direction exceeded the extent of diffusion in the opposite direction.

8. The addition of small amounts of chromium powder to saturate the fluoride bath with chromium has prevented void formation under conditions that otherwise favor void development.

9. Fluorine is not detected below the metal surface.

The porous surface region of an Inconel metal specimen previously exposed to molten fluoride is shown in Fig. 21. Many of the voids, especially those not in grain boundaries, have a definite shape that bears a relationship to the metal lattice. Figure 22 shows a similar area prior to fluoride attack. The inclusions shown in Fig. 22 are convenient sites for the deposition of vacancies; two such sites may be seen in Fig. 21.

The corrosion of Inconel by air is known to form a chromium-rich oxide layer at elevated temperatures. In a 200-hr exposure to air at 1200°C, the region beneath the oxide layer of an Inconel specimen was found to contain voids similar to those observed in fluoride-attacked Inconel. This is illustrated by Fig. 23.

[4] L. C. C. da Silva and R. H. Mehl, *Journal of Metals* 191, 155 (1951).

[5] *Monthly Technical Progress Report for October 20 to November 20, 1951*, SEP-82, Sylvania Electric Products Co.

The high vapor pressure of chromium relative to that of iron or nickel suggests that high-temperature vacuum treatment would also be a suitable means of removing chromium. Inconel and an 80% nickel–20% chromium alloy were exposed to a vacuum of 0.1 mm for 42 hr at 1375°C. Both samples showed many subsurface voids; those in Inconel appeared to be spherical, whereas those in the nickel–chromium alloy were angular, as shown in Figs. 24 and 25.

Chemical analysis of the entire Inconel specimen shown in Fig. 26 indicated a drop in chromium content from about the usual 15 to 9.2%.

The mechanism of void formation in Inconel is therefore believed to occur in two stages. The first involves a loss of chromium atoms by diffusion to the metal surface and then into the fluoride bath. The resulting large number of vacant lattice sites is reduced to a more stable number by precipitation, as illustrated in Fig. 27. For ease of illustration, only six vacancies are shown to constitute a void. The number of vacant atoms involved in the voids shown in previous photomicrographs is of the order of 10^{12} atoms.

Effect of Chromium Addition to Fluoride No. 14. The addition of $^1/_4$% chromium powder to fluoride No. 14 was effective in suppressing subsurface void formation in Inconel in static tests and in thermal gradient, seesaw tests. Tests that were made under identical conditions with no chromium addition resulted in void formation to a depth of about 4 mils. The test conditions are given in Table 20.

The hot zones of the test specimens are shown in Fig. 28. The cold zone of specimen SSF-37 is shown in Fig. 29. The absence of voids when chromium is added is in agreement with the current theory that subsurface voids are the result of chromium depletion of the metal surface region by the molten fluoride. Chemical analyses ordinarily do indicate a relatively high chromium content in the fluoride bath. Hence, the chromium powder addition serves to saturate the fluoride with this constituent, and the Inconel container therefore suffers little, if any, attack.

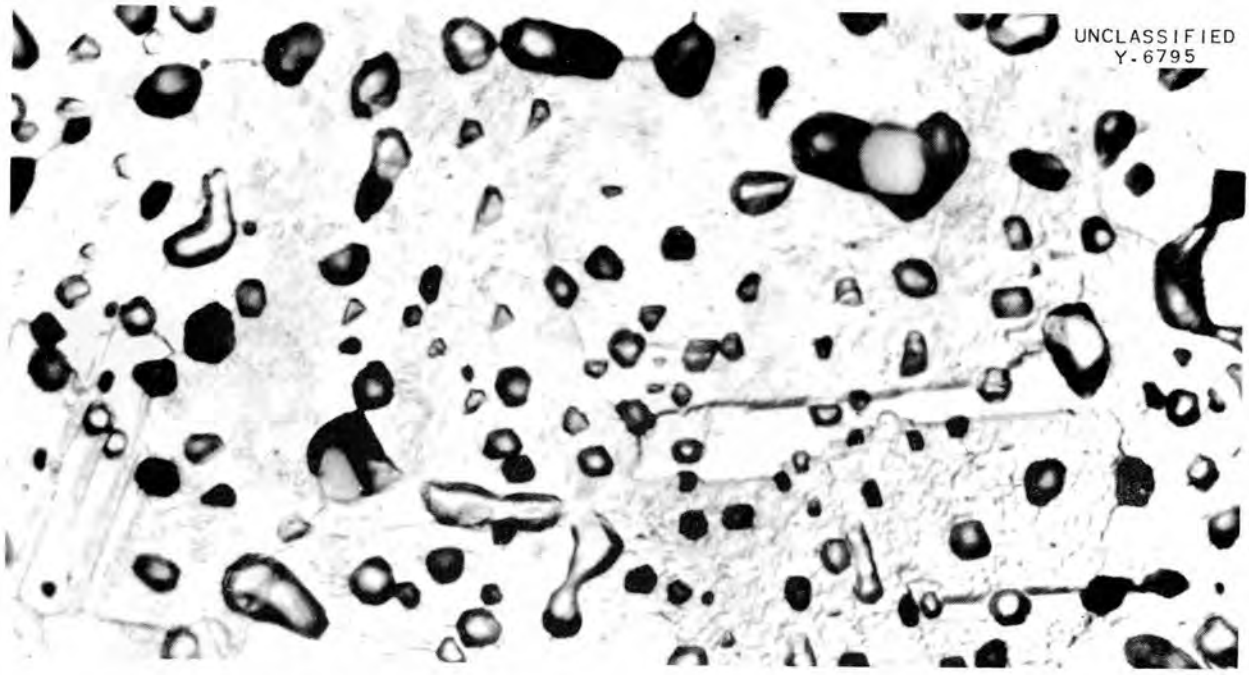

Fig. 21. Porous Surface Region of Fluoride-Attacked Inconel Showing Geometric-Shaped Voids and Larger Irregularly Shaped Voids in Grain Boundaries and Around Inclusions. Etched with aqua regia. 2000X

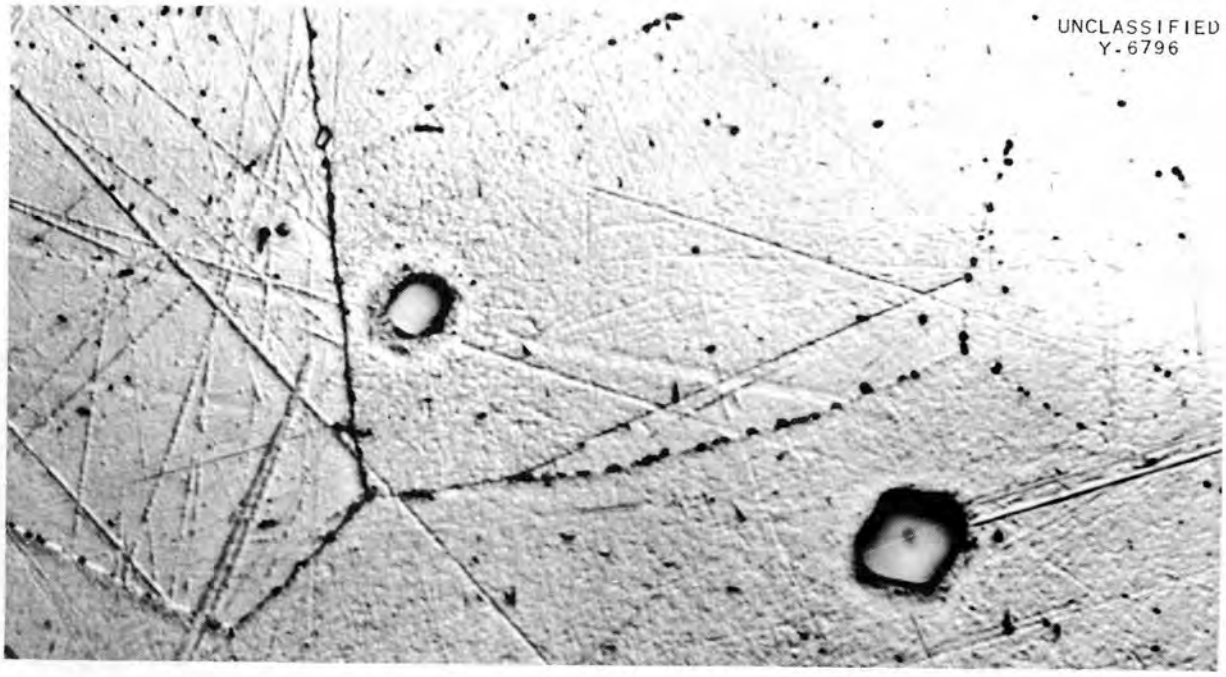

Fig. 22. Area Similar to That Shown in Fig. 21 Prior to Fluoride Attack. Etched with aqua regia. 2000X

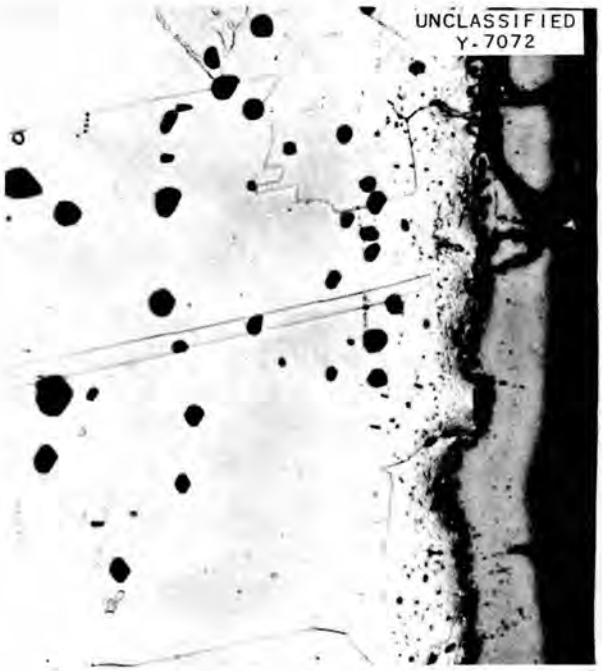

Fig. 23. Voids Formed During Air Corrosion of Inconel at 1200°C. 250X

Fig. 24. Voids Formed During Vacuum Treatment of 80% Nickel–20% Chromium Alloy at 1375°C. Etched with aqua regia. 250X

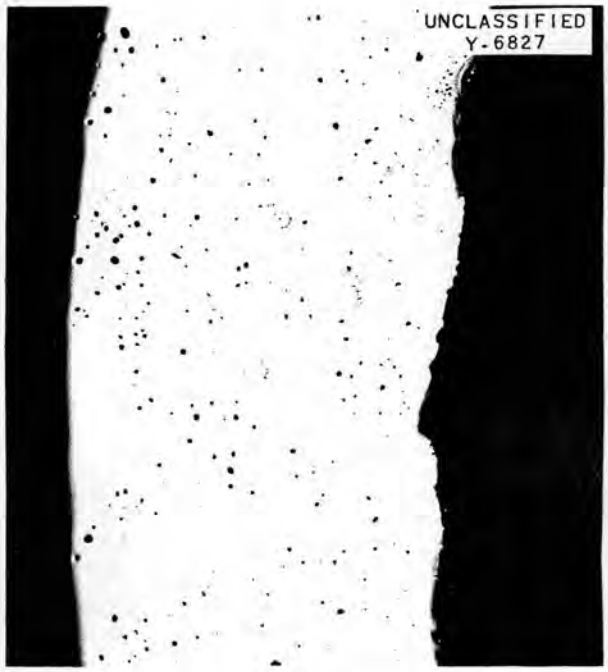

Fig. 25. Fig. 24 at Lower Magnification. 50X

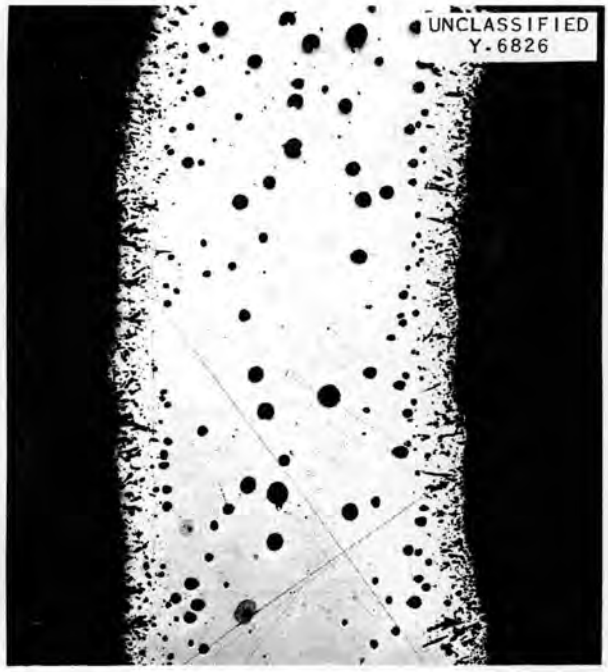

Fig. 26. Voids Formed in Inconel During Vacuum Treatment at 1375°C. 50X

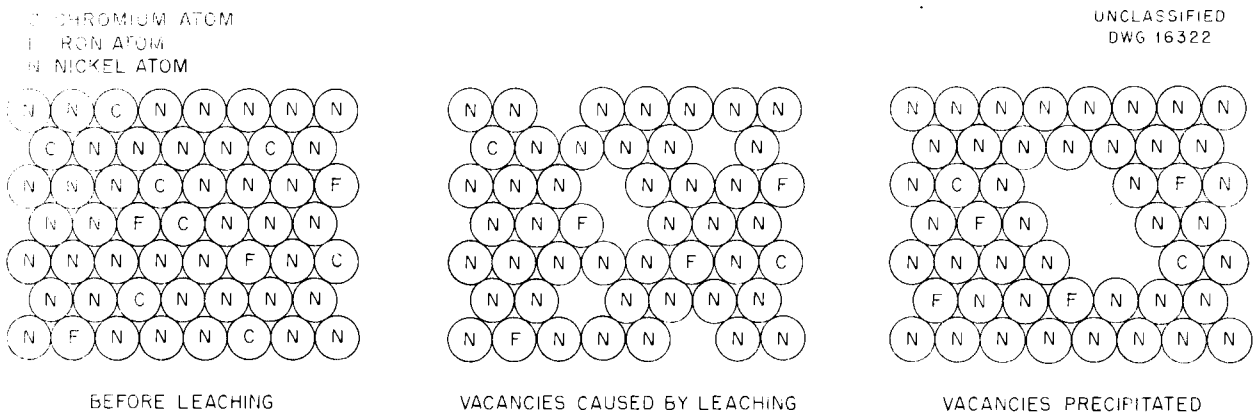

Fig. 27. Sketch Illustrating Formation of Subsurface Voids Caused by Removal of Chromium Atoms.

TABLE 20

TEST CONDITIONS TO DETERMINE EFFECT OF CHROMIUM ADDITION TO FLUORIDE NO. 14 ON ATTACK OF INCONEL

	NO ADDITION	¼% CHROMIUM ADDITION
Test number	SSF-5	SSF-37
Time (hr)	210	200
No. of cycles	55,200	53,500
Hot-zone temperature (°C)	780	785
Cold-zone temperature (°C)	630	637

Liquid Metal Tests. The desirability of lead as a coolant is largely offset by its susceptibility to mass transfer and attack of most commercial, heat-resistant alloys. Sodium, on the other hand, is quite suitable from both standpoints but has unfavorable inflammability characteristics. A logical compromise may be found in the use of lead-sodium mixture. Initial tests in a dynamic system were very encouraging; both corrosion and mass transfer were minimized.

Seesaw tests in which type 310 stainless steel was tested in contact with lead to which 0, 3, and 50 wt % sodium was added were made under the following conditions: temperature, 780°C hot zone, 475°C cold zone; time, 190 hr; number of cycles, 51,000.

Examination of the specimens after test indicated the usual mass transfer in the cold zone of the sodium-free test, reduced mass transfer when 3% sodium was added to the lead, and no mass transfer when 50% sodium–50% lead was used. The attack in the hot zone was reduced from 6 mils in the case of the sodium-free lead to 1 mil in the case of the 50:50 mixture. The type of attack was less serious.

Effect of Temperature on Fluoride Attack of Inconel. Inconel was tested at a series of temperatures for 200-hr periods in molten fluoride No. 14. A rather surprising effect was noted: at the higher temperatures, void formation became less prominent, as shown by Figs. 30, 31, and 32 and by the data of Table 21.

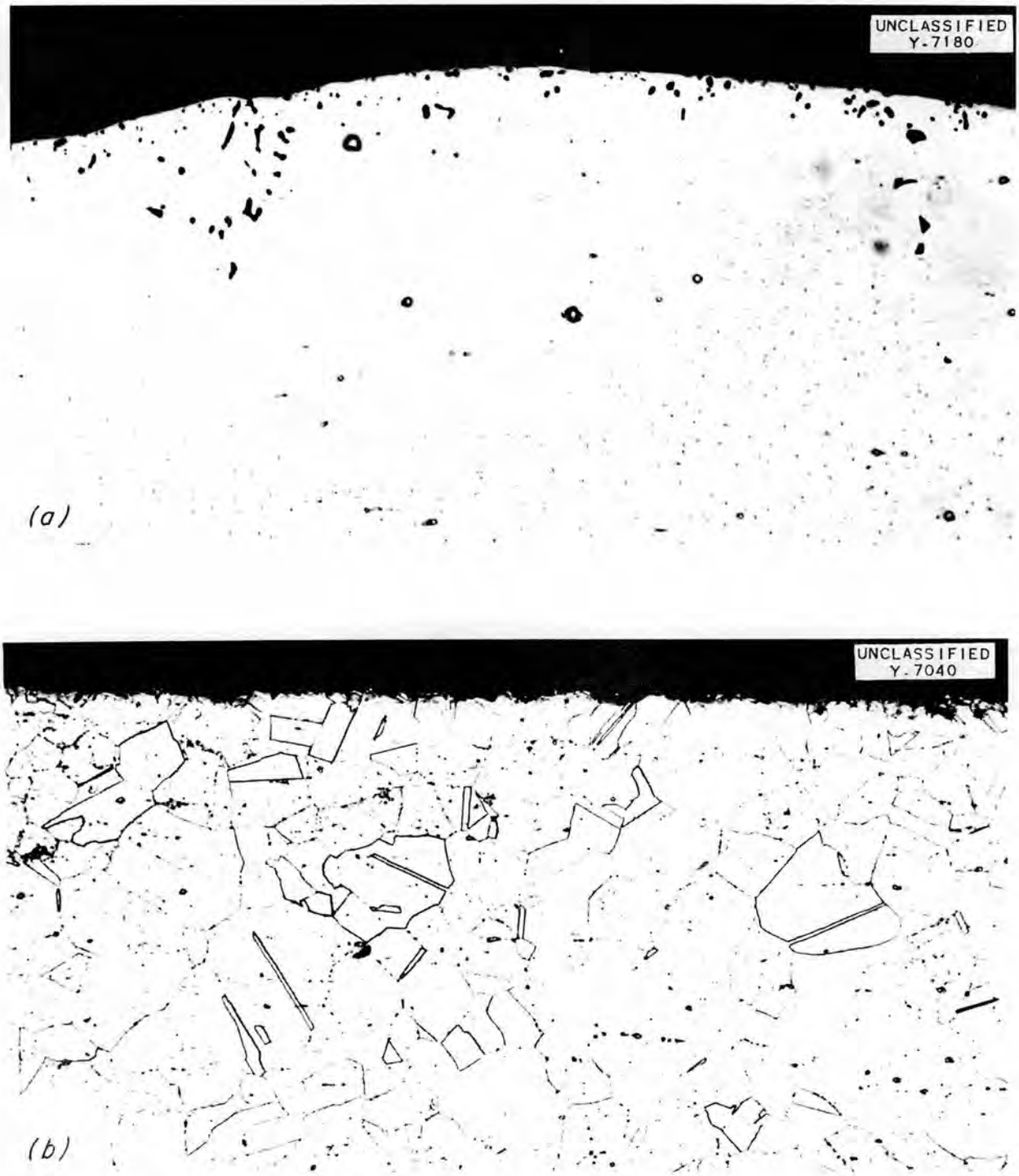

Fig. 28. *a*. Hot Zone of Inconel Seesaw Test Specimen After 200-hr Exposure to Fluoride No. 14. *b*. Same Specimen Tested in Fluoride No. 14 with 0.25% Chromium Added. Etched with aqua regia. 250X

Fig. 29. Cold Zone of Inconel Seesaw Test Specimen; Base Metal Is Intact; White Particles Are Powdered Chromium; Gray Particles Are UO_2. 250X

The analysis of the fluoride bath after test confirmed the observations in Table 21; in the 800°C test, 1800 ppm of chromium was detected in the bath, whereas the fluoride of the 1300°C test yielded only 65 ppm of chromium.

The nature of the film (Fig. 32) detected on the Inconel surface of the high-temperature tests is not known, nor is the full significance of its presence clear at this time.

Fluoride Corrosion of Inconel As a Function of Time. A series of tests was made to determine the extent of corrosion as a function of time. Inconel test specimens were prepared for testing at a series of time intervals ranging up to 3000 hours. The hot zone of the specimen in the seesaw test was about 800°C and the cold zone was about 650°C.

The test data are summarized in Table 22 and plotted in Fig. 33. The data indicate that most of the corrosion occurs in the first 500 hr; beyond this time, the additional amount of attack is quite small.

Effect of Carbon Content on Fluoride Attack. To establish the effect, if any, of carbon content on the corrosion behavior of face-centered-cubic metals in fluoride No. 14, two seesaw test specimens were run simultaneously so that identical time and temperatures would prevail. One specimen was a regular, type 304 stainless steel (containing 0.08% C) and the other was an extra-low-carbon, type 304 stainless steel (0.006% C).

The test conditions for both tubes were the following: temperatures, 720°C hot zone, 600°C cold zone; time, 190 hr; number of cycles, 51,150.

Examination of the tubes after testing gave identical results: 5 mils of void formation in the hot zones of both tubes. No attack or deposition was detected in the cold zones.

Fig. 30. Inconel Tested at Various Temperatures for 200-hr Periods in Fluoride No. 14 Showing Depth of Void Formation as a Function of Temperature. Test temperatures: *a.* 900°C. *b.* 1000°C. *c.* 1100°C. *d.* 1200°C. 250X

Fig. 31. Section of Inconel Tube That Contained Fluoride No. 14 at 1200°C for 200 hr.

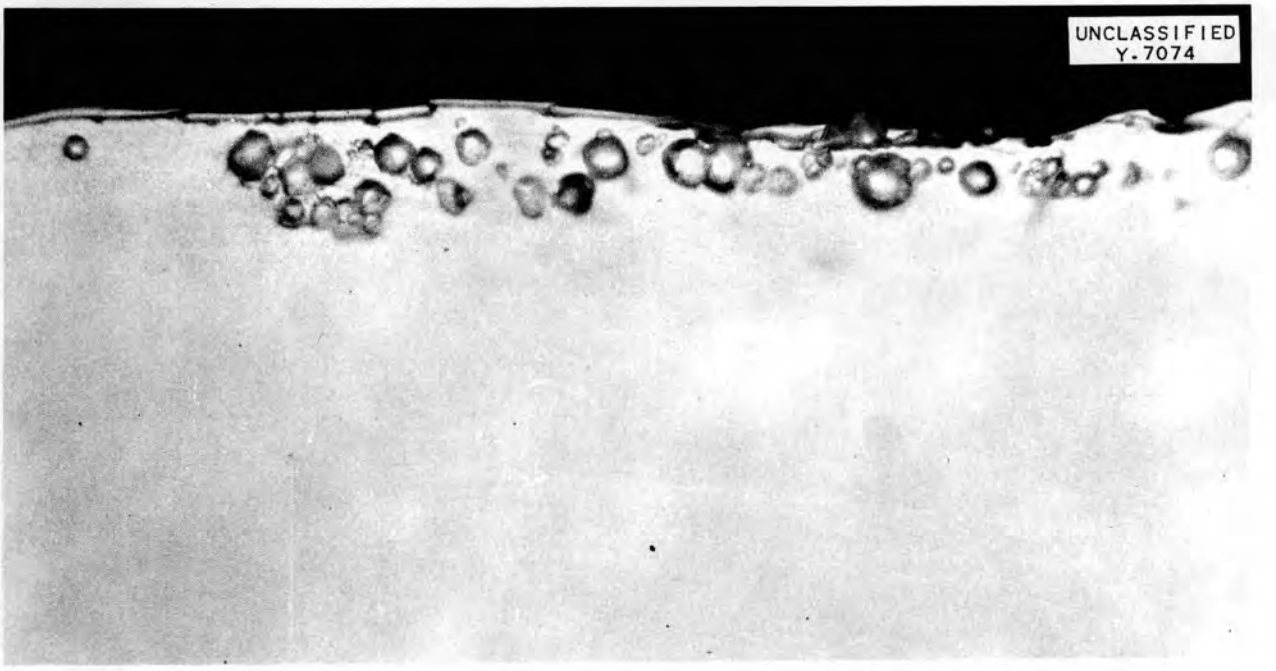

Fig. 32. Magnified View of Metal-Fluoride Interface Shown in Fig. 31. Note formation of brittle layer on surface and subsurface voids beneath. 2000X

TABLE 21

CORROSION OF INCONEL BY FLUORIDE NO. 14 AS A FUNCTION OF TEST TEMPERATURE

TEST TEMPERATURE (°C)	DEPTH OF VOID FORMATION (mils)	THICKNESS CHANGE OF SPECIMEN
800	2	None
900	1.5	None
1000	1	None
1100	1	None
1200	0.5*	None
1300	0.2*	None

*Thin film observed on metal surface; shown in Fig. 32.

TABLE 22

EFFECT OF TIME ON THE DEPTH OF FLUORIDE ATTACK ON INCONEL AS DETERMINED BY THE SEESAW TEST

TEST NO.	TIME (hr)	NO. OF CYCLES	TEMPERATURE (°C)		HOT ZONE DEPTH OF VOID FORMATION (mils)		COLD ZONE
			Hot Zone	Cold Zone	Average	Maximum	
SSF-3	66	18,500	812	618	0.5	1	No evidence of reaction
SSF-4	115	30,200	780	600	1	2	No evidence of reaction
SSF-5	210	55,200	780	630	2	5	No evidence of reaction
SSF-6	500	132,000	750	610	3	7	Metallic deposit, 0.5 mils thick
SSF-8	750	198,000	816	620	3.5	6	Metallic deposit, 0.5 mils thick
SSF-7	3000	786,000	800	560	4	13	Metallic deposit, 0.5 mils thick

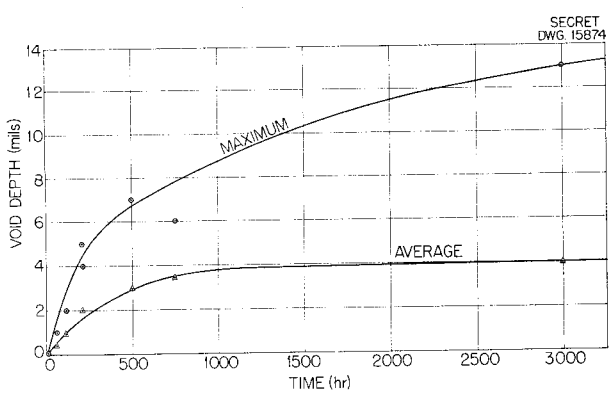

Fig. 33. Corrosion vs. Time for Inconel in Fulinak No. 14 as Determined by the Seesaw Test at 800°C.

PHYSICAL CHEMISTRY

G. P. Smith J. V. Cathcart
W. H. Bridges P. C. Sharrah
N. C. Simpson

Studies are being conducted with the aid of neutron diffraction to determine the structure of liquid metals. A description of the work with liquid lead and liquid bismuth has already been given.[6] Part of the numerical values of this

[6] G. P. Smith, W. H. Bridges, J. V. Cathcart, and P. C. Sharrah, *Metallurgy Division Quarterly Progress Report for Period Ending January 31, 1952*, ORNL-1267, p. 85.

work are contained in the previous report and the recently obtained results are presented in Tables 23, 24, and 25. The positions are summarized in Table 23. Table 24 summarizes the peak positions for the distribution curves. It will be seen from Table 24 that the positions of the concentrations in the distribution curves compare well with those reported by other workers using x-ray techniques. The positions shown for the first concentration were obtained by locating the center of the peak, but the positions shown for other regions of excess on the curves can only be read approximately.

The area under the atomic distribution curve, $4\pi R^2\rho(R)$, between any two values of R gives the number of atoms within that range. It is especially significant to assign the number of atoms represented by the first peak on the curve. This was done by sketching the right hand side of the peak down to the base line in such a manner that the resulting peak was symmetrical. Table 25 shows the values obtained along with those given by others. Also given is the number of atoms from the origin atom out to the distances shown.

Neutron-diffraction studies are now in progress to determine the atomic distribution curves for lead-bismuth alloys with the aid of neutron diffraction. No previous studies of alloy systems have been made using neutron diffraction.

TABLE 23

DIFFRACTION PATTERN PEAKS AND MINIMA IN SIN θ/λ

SUBSTANCE	MAXIMUM	MINIMUM	MAXIMUM	MINIMUM	MAXIMUM	MINIMUM	MAXIMUM
Lead, 350°C	0.180	0.25_0	0.32_5	0.41_0	0.48_5	0.56	0.65
Lead, 550°C	0.175	0.24_5	0.33_0	0.41_5	0.49_0	0.57	0.65
Bismuth, 300°C	0.175	0.26_5	0.33_0	0.42_0	0.49_5	0.57	0.65
Bismuth, 550°C	0.170	0.27_0	0.33_0	0.42_5	0.49_5	0.58	0.65

TABLE 24

ATOMIC CONCENTRATION POSITIONS

Values in parentheses were obtained from the references given

SUBSTANCE	FIRST POSITION (Å)	SECOND POSITION (Å)
Lead, 350°C	3.40	6.6
Lead, 550°C	3.40	6.6
Bismuth, 300°C	3.35	6.8
Bismuth, 550°C	3.35	6.8
Lead, 375°C*	(3.40)	
Lead, 390°C**	(3.4)	(6.4)
Bismuth, 340°C*	(3.32)	
Bismuth, 310°C**	(3.2)	(6.7)

*H. Hendus, Z. *Naturforsh.* 2A, 505 (1947).

**O. Chamberlain, *Phys. Rev.* 77, 305 (1950).

TABLE 25

ATOMS IN FIRST PEAK AND ATOMS TO DISTANCES SHOWN

Values in parentheses were obtained from the references given

SUBSTANCE	PEAK	3.5	4.0	4.5	5.0	5.5	6.0
Lead, 350°C	9.4	5.3	9.3	11.9	14.5	19.1	26.1
Lead, 550°C	9.5	5.1	9.0	11.8	14.6	18.6	25.1
Bismuth, 300°C	7.7	4.6	7.8	11.0	14.5	18.4	23.3
Bismuth, 550°C	7.5	4.6	7.7	10.6	13.9	17.8	23.1
Lead, 375°C*	(8)						
Lead, 390°C**	(12 ± 1)						
Lead ***	(11)						
Bismuth, 340°C*	(7 – 8)						
Bismuth, 310°C**			(8.0)				
Bismuth***	(7-7.5)						

*H. Hendus, *Z. Naturforsh.* 2A, 505 (1947).

**O. Chamberlain, *Phys. Rev.* 77, 305 (1950).

***A. I. Danilova, V. I. Danilov, and E. Z. Spektor, *Doklady Akad. Nauk S.S.S.R.* 82, 561 (1952).

MECHANICAL TESTING

R. B. Oliver D. A. Douglas
J. W. Woods

Uranium Creep Testing. Figure 34 is a tentative design curve for normal uranium that was alpha rolled at 600°C and tested at 500°C in a vacuum. Preferred orientation studies are being made for correlation with this data.

Eight bars from this material have been beta treated for 80 sec at 730°C. Metallographic examination indicates that the treatment was adequate to give complete transformation of the entire test bar. The bars will be tested under the same conditions as the alpha-rolled bars.

Thorium Creep Testing. Table 26 summarizes the present status of the creep- and stress-rupture testing of extruded Ames thorium. The tests were conducted on 0.505-in. round bars at 300°C in vacuum.

The creep rates at stresses of 16,000 psi or less are very favorable, but the initial elongation with slow load rates is large. It is proposed to explore the variables that control the initial elongation.

Inconel Stress-Rupture Tests. Figures 35 and 36 present revisions of the design curves[7] for fine- and coarse-grained Inconel sheets that were tested at 1500°F in argon.

The rupture times reported are substantially shorter than the rupture times for similar tests conducted in air. The creep rates observed in both argon and air compare closely in the lower stress range.

[7]R. B. Oliver, J. W. Woods, and C. W. Weaver, *op. cit.*, ORNL-1227, p. 149.

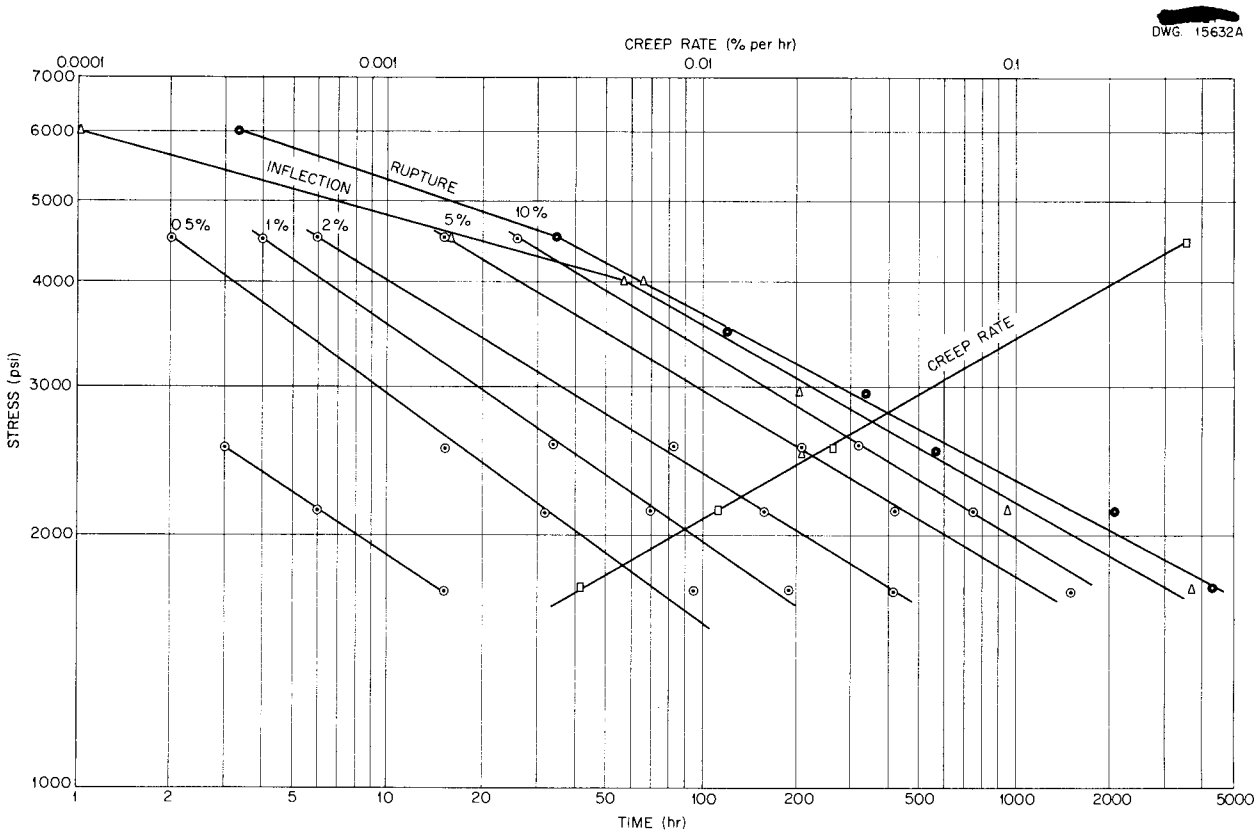

Fig. 34. Creep Rate of Normal Uranium Alpha Rolled at 600°C to $^7/_8$-in. Rod; Test Section 0.505-in. Round by 3-in. Gage Length; Tested in Vacuum at 500°C. Grain size: approximately 0.020 mm in diameter. Times were measured for 0.1, 0.5, 1, 2, 5, and 10% extension, inflection, and rupture points vs. stress. Extension was measured optically.

TABLE 26

RESULTS OF CREEP AND STRESS-RUPTURE TESTING OF EXTRUDED AMES THORIUM

STRESS (psi)	TIME IN TEST (hr)	ELONGATION (%)	CREEP RATE (% per hr)
16,000	5900	4.0	0.00005
17,000	2900	9.7	0.0015
17,500	800	6.7	0.0025
17,800	1100	7.4	0.003
18,000	910 (rupture)	36.5	0.005
18,200	429 (rupture)	34.9	0.0140
18,500	100 (rupture)	33.0	0.060
19,000	45 (rupture)	33.0	0.12

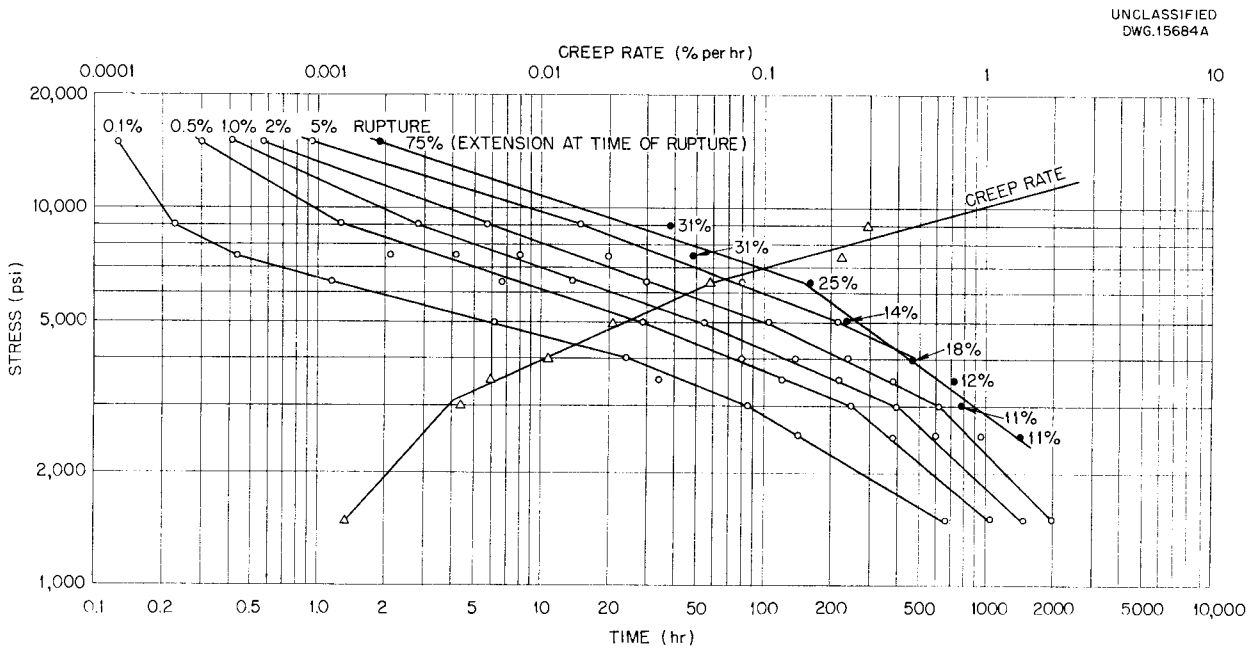

Fig. 35. Creep Rate of Inconel Sheet Cold Rolled at 1650°F and Tested in Argon at 1500°F. Grain size: approximately 90 grains per square millimeter, 0.105 mm in diameter. Times were measured for 0.1, 0.5, 1, 2, and 5% extension and rupture vs. stress. Extension measured optically.

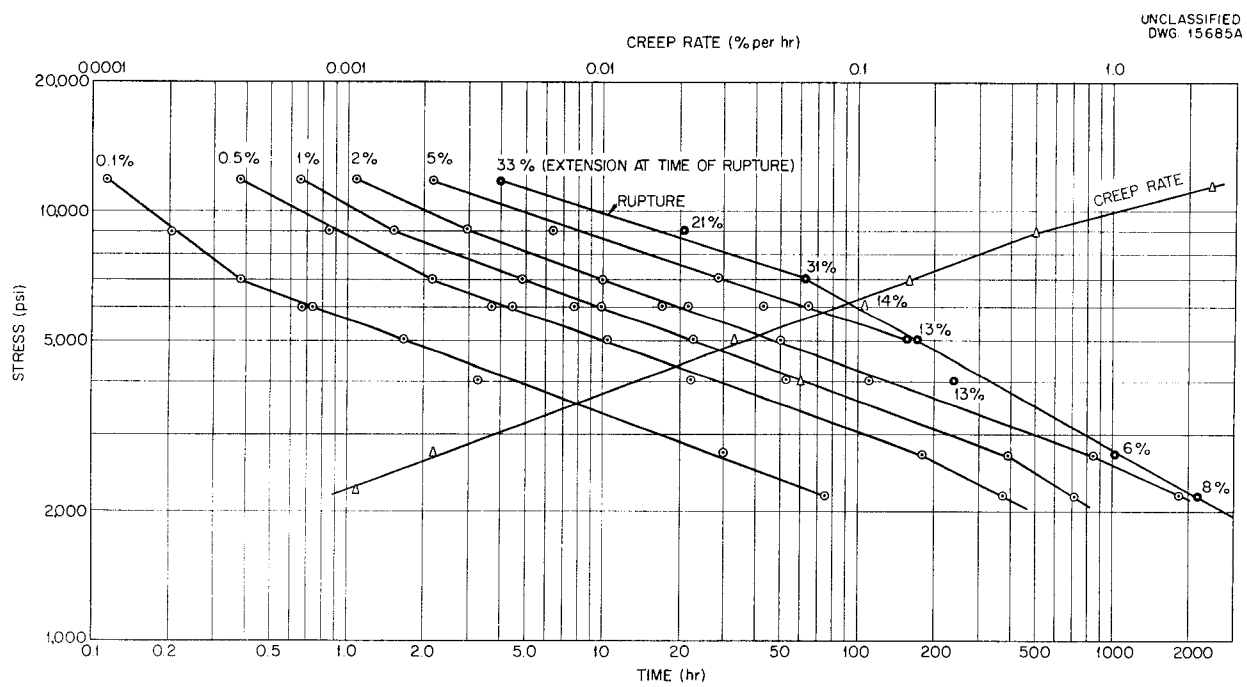

Fig. 36. Creep Rate of Inconel Sheet Annealed for 1 hr at 2050°F and Tested in Argon at 1500°F. Grain size: approximately 15 grains per square millimeter, 0.250 mm in diameter. Times were measured for 0.1, 0.5, 1, 2, and 5% extension and rupture vs. stress. Extension was measured optically.

FABRICATION

E. S. Bomar J. H. Coobs
H. Inouye

ARE Control and Safety Rods. The program for preparation of components to be used in the ARE control and safety rods, based on work outlined in previous reports,[8] has been completed, and the parts have been turned over to the Welding Group for canning. Sixty inserts composed of boron carbide and iron were pressed; 54 were necessary for preparation of three safety rods. Thirty-three cylinders composed of dilute mixtures of B_4C and Al_2O_3 were fabricated for use in two control rods with different B_4C investments. These two rods required the use of 29 inserts. The surplus parts were prepared for use in case of breakage.

Only minor difficulties were encountered in producing the slugs. The first cylinders prepared cracked along their length during the cooling cycle that followed hot pressing. This difficulty was avoided by ejecting the graphite mandrel from the center of the slugs while they were still at temperature. Another difficulty involving differences in expansion coefficients was encountered when the first slug was sealed in a can by brazing. The clearances originally set up were not adequate to allow for the expansion of the inner stainless steel liner when the assembly was heated to 1120°C for brazing. Consequently, the excessive internal loading caused the ceramic cylinder to break. By increasing the inside diameter of the pressed cylinders by 0.015 in., this type of failure was prevented during the canning operation. The per cent of B_4C of the B_4C-Al_2O_3 cylinders was increased to compensate for the decreased volume that accompanied the increase in inside diameter.

Densities of 80% of those of the theoretical mixtures were obtained in pressing full-size parts of the two types of materials. The B_4C-Fe cylinders were pressed with 2500 psi of pressure at 1520 to 1540°C. The Al_2O_3-B_4C inserts were compacted at the same pressure but were heated to 1650°C. In both instances, graphite dies surrounded by bubble-alumina insulation and an inert atmosphere of argon were used.

BRAZING AND WELDING

P. Patriarca G. M. Slaughter

High-Temperature Brazing Alloy Evaluation Program. The static corrosion testing of brazed joints for the high-temperature brazing alloy evaluation program continues. The 16.5% Cr–10.0% Si–2.5% Mn–71.0% Ni alloy developed by the General Electric Co. is attacked rather severely by the fluoride No. 14 bath when brazed both on Inconel and type 316 stainless steel. Figures 37 and 38 are photomicrographs of the corroded joints.

Since A nickel has been found to be relatively unattacked in molten sodium hydroxide, static corrosion T-specimens of this material brazed with several of the promising alloys have been prepared. The samples have not yet been completely examined, but several photomicrographs of the as-brazed joints show excellent wettability and flow characteristics. Some of the more promising alloys in the as-brazed condition are shown in Figs. 39 and 40, which are photomicrographs of T-joints brazed with 60% Pd–40% Ni and Nicrobraz on A nickel.

A few preliminary tensile tests of joints that were butt-brazed with the 60% Pd–40% Ni alloy were considered advisable prior to a more thorough investigation with the high-temperature extensometer that has been ordered. Standard tensile bars, 0.505 in. in diameter, were machined from type 316 stainless steel, butt-brazed, tensile blanks. Three of the bars were tested at room temperature and three were tested at 1500°F. Test bars of type 316 stainless steel that were subjected to heating cycles similar to the brazing cycles were also tested as check samples on the strength of the parent metal.

The average of the tensile strengths of the brazed joints tested at room temperature was 75,400 psi. The average of the type 316 stainless steel tests at room temperature was 82,000 psi, resulting in a brazed joint efficiency of 92%. At

[8] *ANP Project Quarterly Progress Report for Period Ending June 10, 1952*, ORNL-1294, p. 135; *Metallurgy Division Quarterly Progress Report for Period Ending April 30, 1952*, ORNL-1302, p. 78.

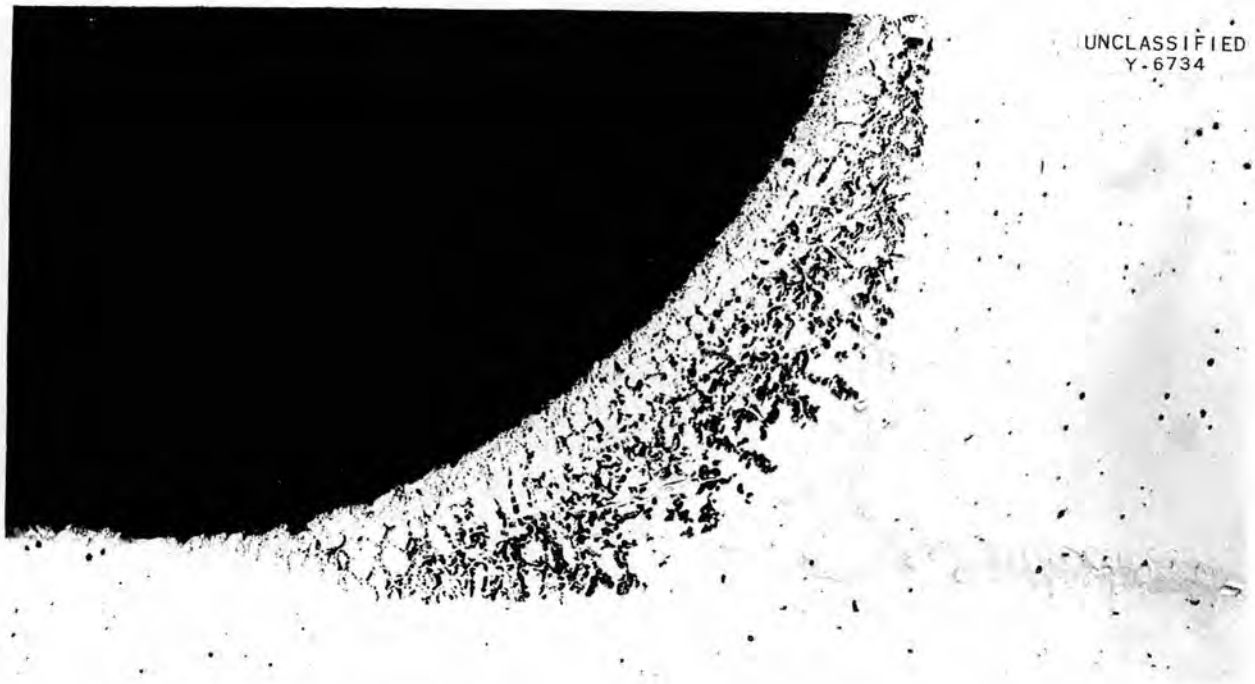

Fig. 37. Inconel Tube-to-Header Brazed with 16.5% Chromium–10.0% Silicon–2.5% Manganese–71.0% Nickel Alloy and Tested in Fluoride No. 14 for 100 hr at 1500° F. Moderate attack can be seen. 75X

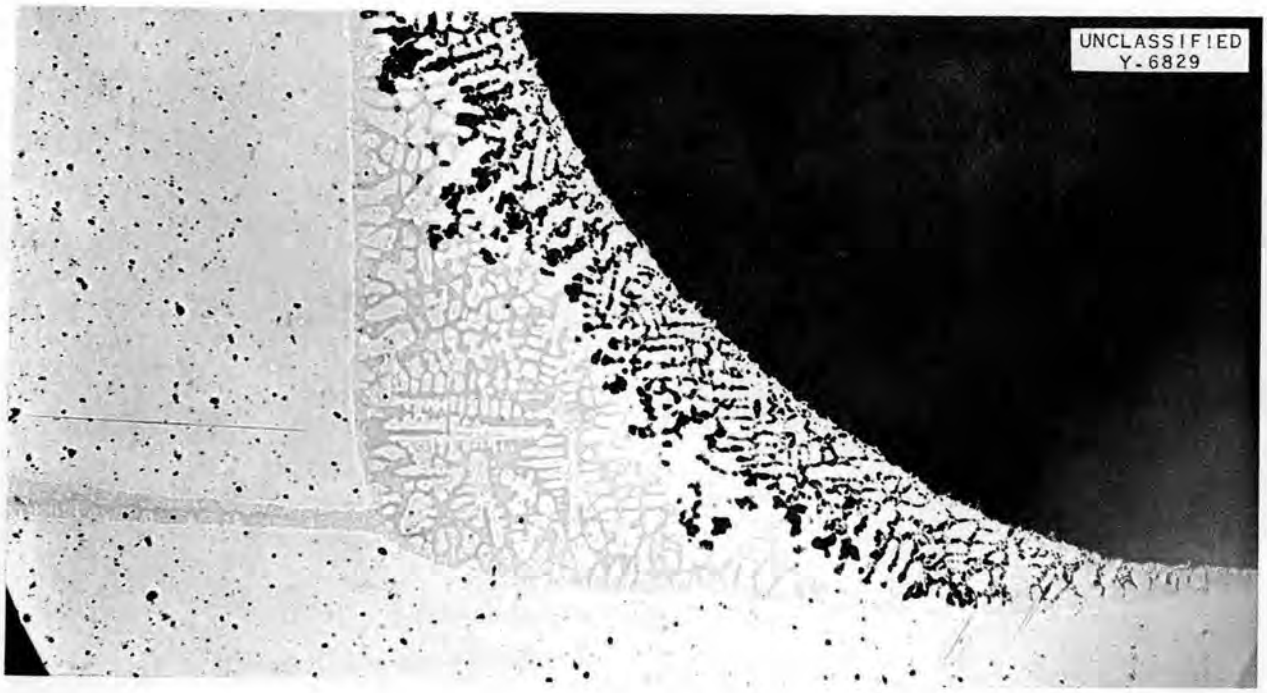

Fig. 38. Type 316 Stainless Steel Brazed with 16.5% Chromium–10.0% Silicon–2.5% Manganese–71.0% Nickel Alloy and Tested in Fluoride No. 14 for 100 hr at 1500° F. Moderate attack on the brazing alloy can be seen. 75X

Fig. 39. A Nickel T Joint Brazed with 60% Palladium–40% Nickel Alloy. Etched with aqua regia. 50X

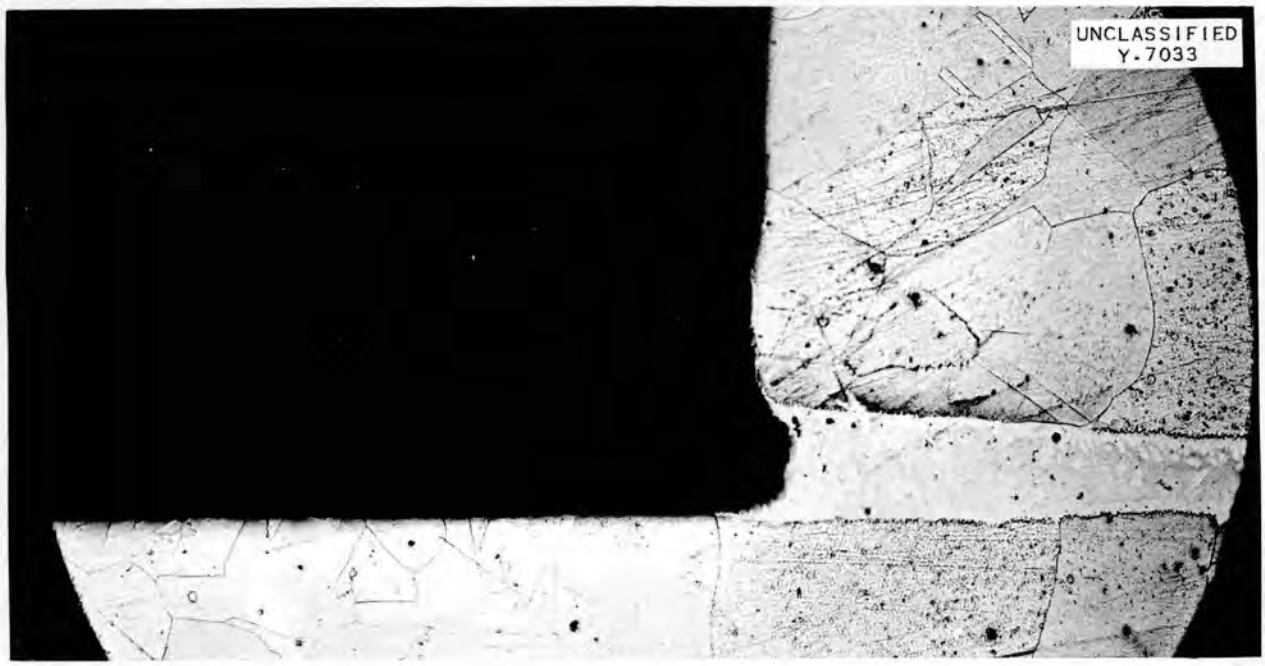

Fig. 40. A Nickel T Joint Brazed with Nicrobraz. Etched with aqua regia. 50X

1500°F the average strength of the butt-brazed specimens was 22,400 psi, whereas the stainless steel check bars pulled at 25,600 psi. The corresponding joint efficiency at 1500°F is therefore 87%. The elongation in a 2-in. gage length was 40% at room temperature and 18.4% at 1500°F for the butt-brazed specimens. For the stainless steel check bars, the elongation at room temperature was 75% and at 1500°F, it was 33%. A photomicrograph showing the type of fracture of the butt-brazed joint at room temperature is shown in Fig. 41. It can be seen that the fracture occurred along the braze metal–base metal diffusion zone. Figure 42, a photomicrograph of the fracture occurring at 1500°F, illustrates a more ragged type of surface. The fracture did not follow completely along the diffusion zone, but in some areas it appeared to occur in the braze metal itself. This data suggest that the 60% Pd–40% Ni alloy is very promising, but it is still extremely desirable to strive for lowering of the melting point by alloying.

Only one brazing alloy has been investigated at present with the more desirable 0.252-in.-dia butt-brazed tensile bars. A high-temperature extensometer designed for use with this size of specimen has arrived, and work on this phase of the brazing alloy evaluation program should proceed much more rapidly. A series of tensile tests at room temperature and at 1500°F was completed for Inconel brazed with the 75% Ag–20% Pd–5% Mn alloy. At room temperature, the average tensile stress of the brazed joint was 55,900 psi, whereas the average elongation in a 1-in. gage length was 9%. At 1500°F, the average tensile stress of the brazed joint was 19,700 psi, whereas the average elongation was 2.5%. These results apparently mean that the brazed joint decreases in strength with increasing temperature more rapidly than does the base Inconel. The elongation of the base metal is quite large at room temperature, whereas at 1500°F there is very little elongation. Tensile bars of the pure Inconel will be tested at these temperatures after undergoing the same

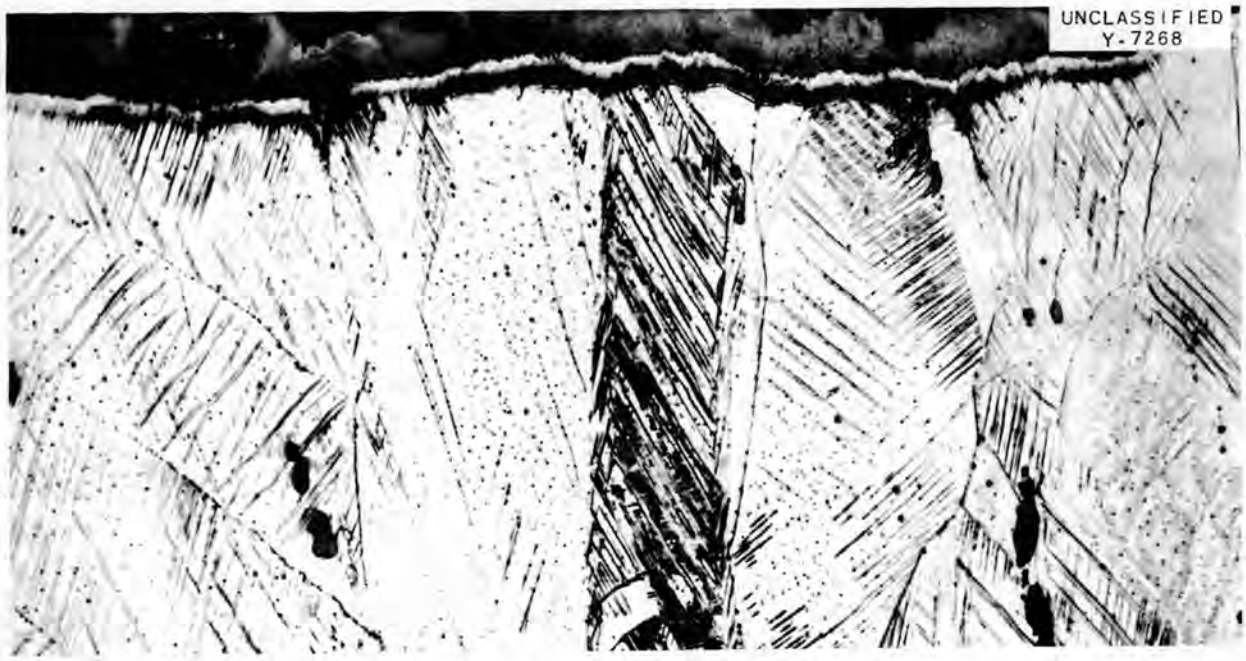

Fig. 41. Room-Temperature Fracture in a Type 316 Stainless Steel Tensile Bar Butt Brazed with a 60% Palladium–40% Nickel Alloy. Along this particular section fracture occurred in the diffusion zone of the brazed joint. No large areas of light-etching braze metal can be seen since these are located on the other half of the tensile bar. Etched with aqua regia. 250X

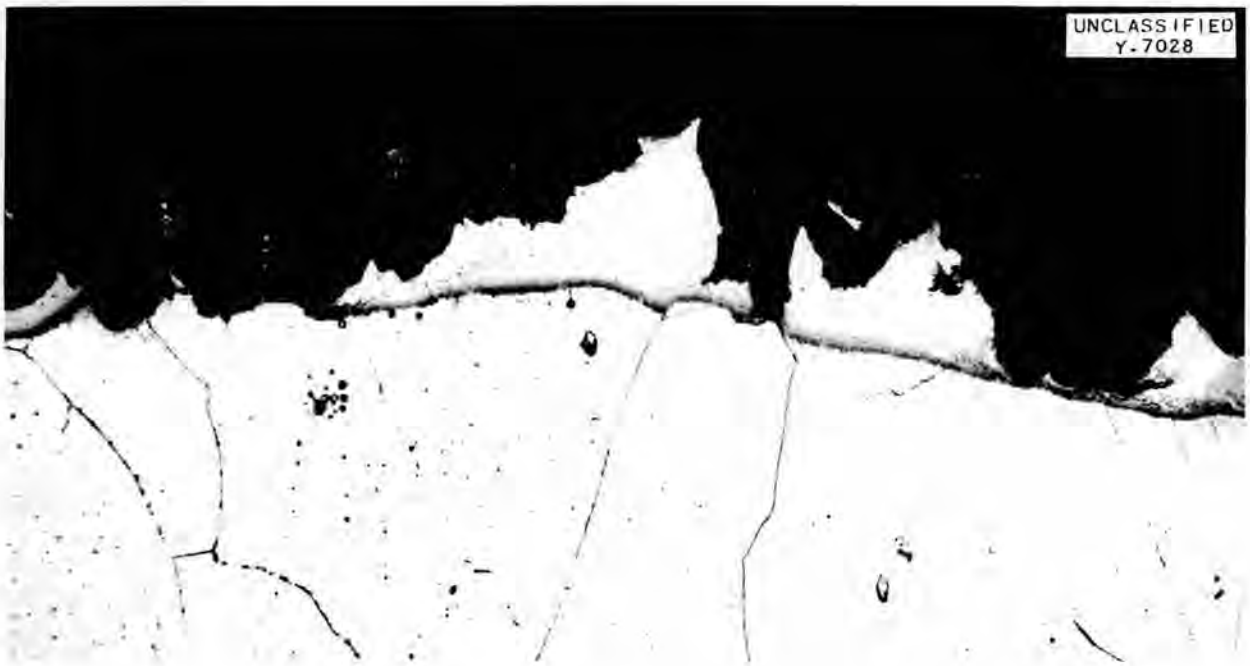

Fig. 42. Fracture of a Type 316 Stainless Steel Tensile Bar Butt Brazed with 60% Palladium–40% Nickel Alloy and Tested at 1500°F. Failure occurred primarily in the diffusion zone, but there was some tendency for failure to occur in the fingers of light-etching braze metal. Etched with aqua regia. 250X

heat treatment as the butt-brazed bars. This should allow the calculation of joint efficiency for comparison purposes. Photomicrographs of fractures at both room and elevated temperatures show evidence of fracture in the diffusion zone between the braze and base metals (Figs. 43 and 44).

Because of the interest shown in the fabrication of molybdenum, a limited program on the brazing of molybdenum with the various high-temperature alloys presently under investigation for the ANP Program was conducted. The wettability characteristics of the various brazing alloys on bright, annealed, molybdenum sheet in a dry-hydrogen atmosphere are listed in Table 27.

A further indication of the strength of brazed joints on molybdenum should be obtained from tensile test specimens that will be prepared in future work. If a small quantity of ductile molybdenum can be obtained, tensile tests will be made on this material, since more reliable data should result.

Service Work. The complicated stainless steel heat exchanger test unit shown in Fig. 45 is typical of the assemblies that can be brazed by the use of canning techniques. Since this test unit is to be a sodium-to-air system, several joints required complete sealing. Nicrobraz powder was placed on all the joints, including approximately 2500 tube-to-baffle plate joints. Good hydrogen flow over the entire assembly was needed for proper flow of the brazing alloy, and it is expected that a series of baffle plates inside the can will be required to attain this flow for similar, but larger, heat exchanger units.

As a service function for the ARE group, 18 boron carbide slugs were canned in stainless steel for a safety rod. Nicrobraz was used as the brazing alloy. Nicrobraz was also used in sealing the ends of a 30-in. control rod containing 15 boron carbide–aluminum oxide slugs for the ARE.

Cone-Arc Welding. The feasibility of applying the cone-arc welding process to fabrication of

Fig. 43. Fracture of an Inconel Tensile Bar Butt Brazed with 75% Silver–20% Palladium–5% Manganese Alloy and Tested at Room Temperature. Fracture occurred largely in the joint diffusion zone. Etched with aqua regia. 250X

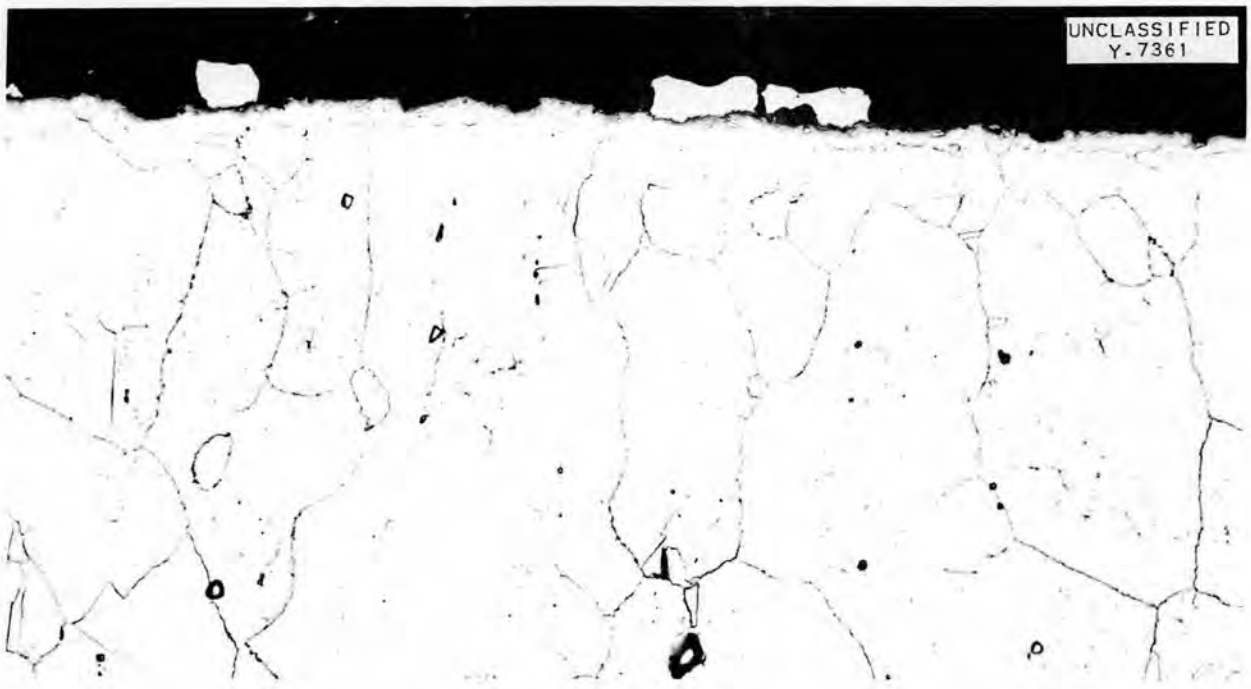

Fig. 44. Fracture of an Inconel Tensile Bar Butt Brazed with 75% Silver–20% Palladium–5% Manganese Alloy and Tested at 1500°F. The diffusion zone appears to be the weakest area in the joint. Etched with aqua regia. 250X

TABLE 27

WETTABILITY CHARACTERISTICS OF VARIOUS BRAZING ALLOYS ON MOLYBDENUM

BRAZING ALLOY	WETTING PROPERTIES
60% Pd–40% Ni	Excellent
Nicrobraz	Fair
16.5% Cr–10.0% Si–2.5% Mn–71.0% Ni	Good
50% Pd–40% Ni–10% Mn	Very good
40% Pd–40% Ni–20% Mn	Good
60% Pd–37% Ni–3% Si	Excellent
73.5% Ni–16.5% Cr–10.0% Si	Excellent
75% Ag–20% Pd–5% Mn	Excellent
64% Ag–33% Pd–3% Mn	Excellent

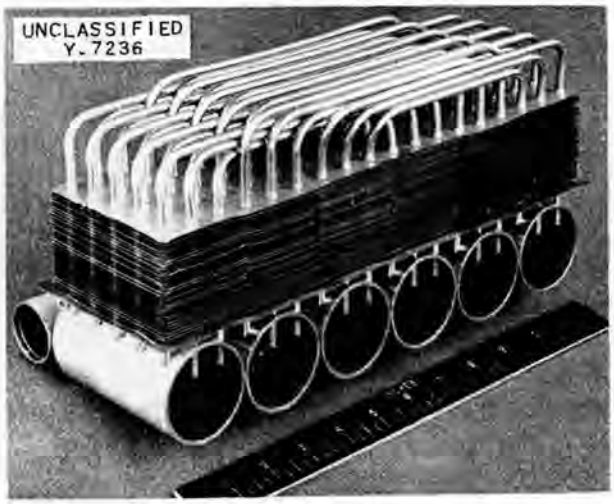

Fig. 45. Typical Heat Exchanger Test Unit Nicrobrazed with the Use of Canning Techniques.

tube-to-header heat exchangers has been experimentally determined in previous studies. It has been recognized, however, that a systematic determination of the behavior of the basic welding variables associated with the cone-arc process would contribute to a better understanding of its possible application and limitations.

The effects of arc-current magnitude and arc-current duration on the parameters D_0, D_I, and P have been determined: D_0 is the outside diameter of the circumferential weld bead resulting from cone-arc welding a tube into a flat header; D_I is the inside diameter of the circumferential weld bead, that is, the available header opening to fluid flow after cone-arc welding a tube into a flat header; and P is the minimum weld penetration and is taken as the shear distance from the weld surface to the beginning of the unwelded root between the tube outside surface and header wall.

A Hathaway S14-C, film type of recording oscillograph was used to record the instantaneous behavior of arc current and arc voltage. A typical oscillographic trace is presented in Fig. 46. It may be noted that the first ten cycles of arc current are transient in nature. This surge current, which is generally in the order of 100% greater than the steady-state value, is a property of the power supply used in this investigation. Elimination of the surge has been accomplished by addition of approximately 0.5 ohms of load. The effect of this surge on the weld parameters D_0, D_I, and P is the subject of current work.

As in previous work, the materials were 0.100-in.-OD, 0.010-in.-wall, type 316 stainless steel tubing and 0.125-in.-thick type 316 stainless steel header sheets, and the header configuration consisted of 19 tube holes drilled one diameter apart at the apex of the equilateral triangle that was the basic pattern. All tubes were set flush with the header surface prior to welding. A series of welds was made under the conditions outlined in

UNCLASSIFIED
DWG. 16374

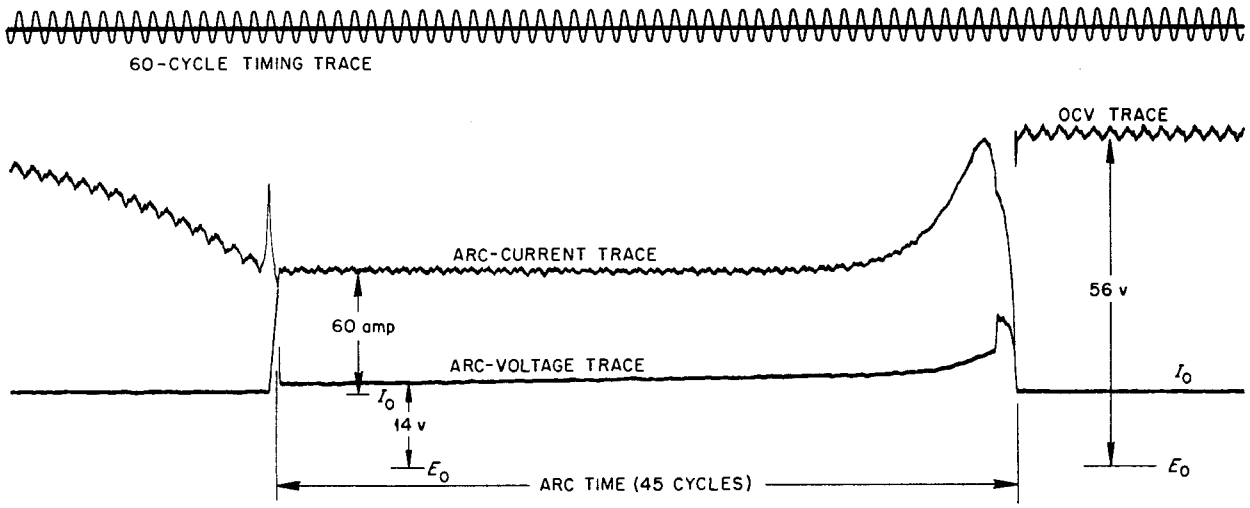

Fig. 46. Typical Cone-Arc Weld Oscillograph.

Figs. 47 and 48. The variables were arc current and arc time.

Examination of Fig. 47 reveals that the predominate effect of increasing arc current is to increase the value of D_0. This, coupled with the relatively small increase in weld penetration, P, and an equally small decrease in D_l, indicates that the major portion of additional energy introduced as increasing arc current served to increase the ineffective weld area. It may be noted, however, that cone-arc welds may be made over a relatively wide range of conditions, which indicates that arc current is not a critical variable requiring precise control within the limits of 55 to 75 amp for the other welding conditions indicated. Operation in the higher current range, however, should be avoided since greater header distortion becomes evident with higher energy input.

The results of a similar study are presented in Fig. 48, in which arc time is used as the variable. The similarity of Figs. 47 and 48 is evident. Analysis of the curves in Fig. 48 reveals that arc time is not a critical variable within the limits of 1.5 to 4.2 sec for the other welding conditions indicated.

Both sets of curves reveal a D_0 overlap range. Increasing heat by increasing arc current or arc time may not only increase distortion but may introduce a condition of nonuniformity of heat flow when the outside diameters of the welds are large enough to overlap onto the next welds. This range should therefore be avoided.

The D_l sensitive range is also a limiting factor in that surface tension and/or gravitational forces acting on the relatively large weld pool will close off the header hole if energy input is excessive.

There is reason to believe that two very important variables to be considered are header hole-to-hole distance and header thickness. It is expected that the criticality of arc current and arc time will increase with a reduction of the hole-to-hole distance and header thickness. Experiments to evaluate these variables will be conducted as part of future work.

In addition to the studies undertaken to evaluate the basic effects of cone-arc welding variables, immediate application of cone-arc welding to fabrication of test assemblies has been necessary

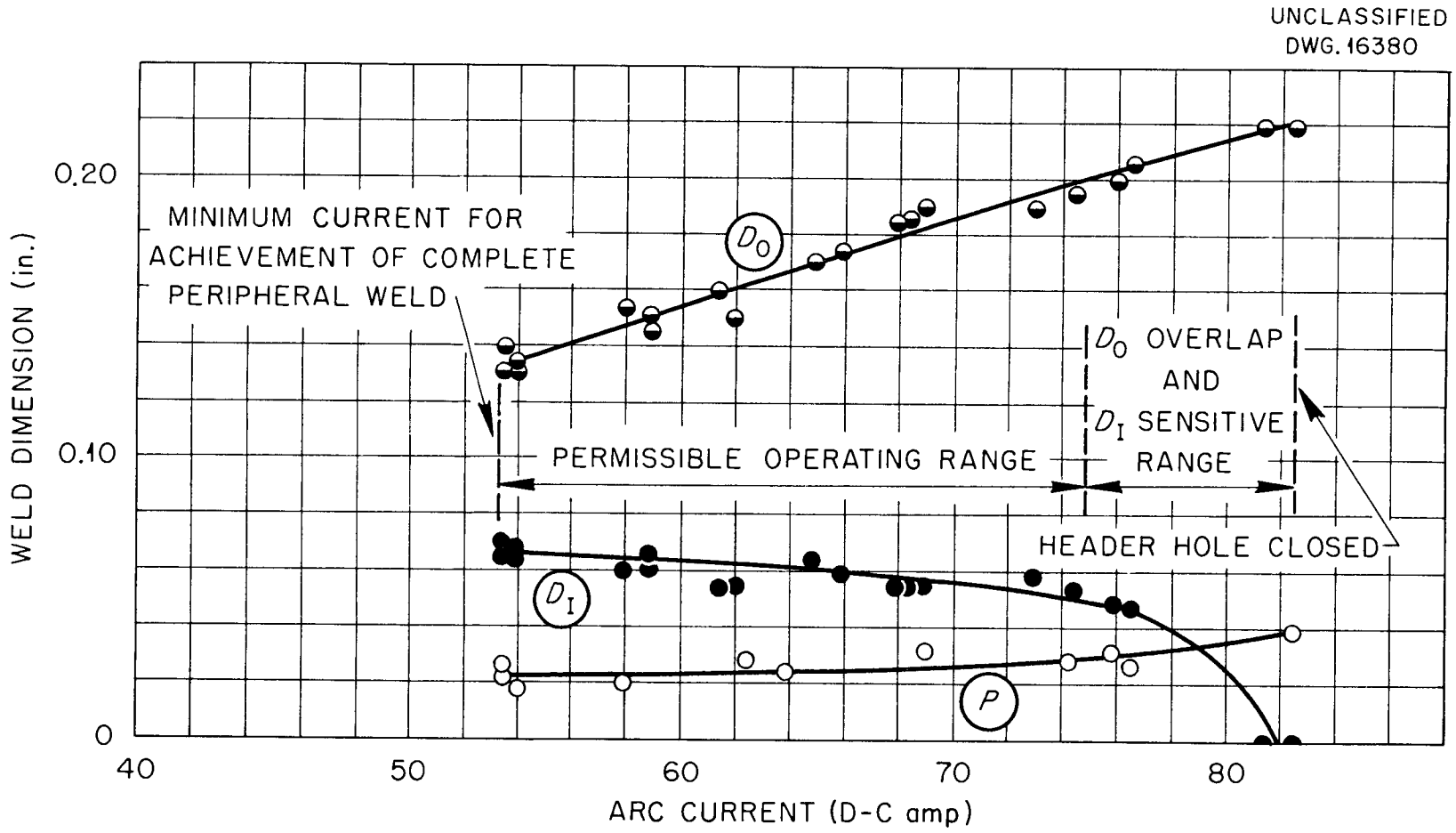

Fig. 47. Effect of Arc Current on Cone-Arc Weld Parameters D_0, D_I, and P.

Material: tubes, type 316 stainless steel, 0.10 in. OD, 0.010-in. wall
header, type 316 stainless steel, 0.125 in. thick
tube hole separation, 0.10 in. (one tube diameter)

Welding conditions: arc time, 1.5 sec
arc distance, 0.05 in.
high-thoria tungsten filament, 0.0625 in. in diameter (pointed)
argon gas flow, 30 cfh

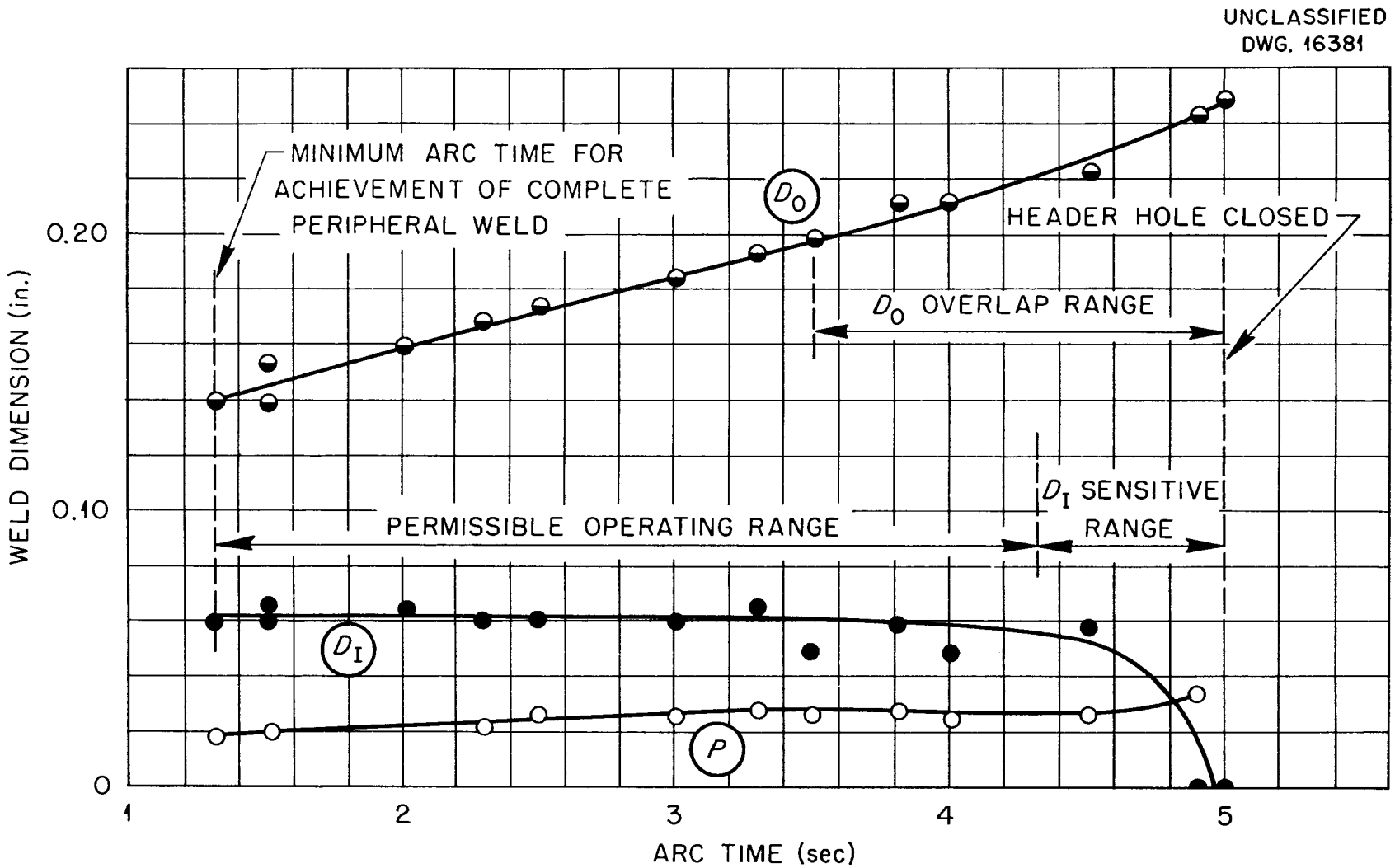

Fig. 48. Effect of Arc Time on Cone-Arc Weld Parameters D_0, D_I and P.

Material: tubes, type 316 stainless steel, 0.10 in. OD, 0.010-in. wall
header, type 316 stainless steel, 0.125 in. thick
tube hole separation, 0.10 in. (one tube diameter)

Welding conditions: arc current, 5.9 amp d. c.
arc distance, 0.05 in.
high-thoria tungsten filament, 0.0625 in. in diameter (pointed)
argon gas flow, 30 cfh

and has received attention. A typical example of a recently fabricated heat exchanger is illustrated in Fig. 49. This photograph shows one end of an Inconel counterflow heat exchanger consisting of 52 tubes, 0.150-in. OD, 0.0250-in. wall, cone-arc welded into a cylindrical Inconel header, 3-in. ID, $^1/_8$-in. wall. A total of 104 welds, the other end of the heat exchanger being identical to the one illustrated, were made under the following conditions:

arc current	102 amp,
arc time	2.0 sec,
electrode	$^3/_{32}$-in.-dia pointed high-thoria tungsten,
arc distance	0.165 in.,
argon flow	30 cfh.

It may be noted that the welds appear to be bright and clean in the as-welded condition, which is a favorable characteristic of all cone-arc welds.

Fig. 49. One End of an Inconel Tube-to-Header Heat Exchanger Consisting of 52, 0.150-in.-OD, 0.0250-in.-Wall, Inconel Tubes Cone-Arc Welded into a $^1/_8$-in.-Thick, 3-in.-ID, Cylindrical, Inconel Header. Photographed as welded.